Synecdoche, Two-Component Systems:
E. coli EnvZ/OmpR as a Model of Transmembrane Communication and Chimeric Biosensor Design

by

Rahmi Yusuf

Student ID: 797155

School of Pharmacy and Biomedical Sciences

The thesis is submitted in partial fulfilment of the

requirements for the award of the degree of

DOCTOR OF PHILOSOPHY

of the University of Portsmouth

January, 2019

Preface

This PhD was fully funded by the Indonesia Endowment Fund for Education (Lembaga Pengelola Dana Pendidikan). The PhD project started at Durham University on October 2014 (Scholarship reference no.: S-1997/LPDP.3/2014) and completed at the University of Portsmouth from October 2015 (Scholarship reference no.: S-4833/LPDP.3/2015).

The project was supervised by Dr Roger R. Draheim and Dr Ivor Ebenezer.

Experiments were conducted at the School of Pharmacy and Biomedical Sciences, and within the remit of the Institute of Biological and Biomedical Sciences, University of Portsmouth.

Rahmi Yusuf

Abstract

This thesis tells the story of my doctoral research in chronological order; a story that is divided into four acts.

The first act is the prologue, which narrates my exploration into the world of two-component signalling—a system familiar amongst bacteria, but one that gradually disappears further down the phylogenetic tree, which is the main reason that this system would be an excellent novel antibiotic target. Dubbed as the canonical two-component system (TCS) due to it being the most well-understood of its kind, EnvZ/OmpR still raises questions regarding several aspects of its signalling mechanism, one of which regards its transmembrane domain, and that is empirically addressed in this thesis.

The second act addresses the interaction between the transmembrane helices of EnvZ and its correlation to signal output quantified by *ompC* and *ompF* transcription. Using sulfhydryl-reactivity experiments, our studies showed that the most prominent structural shifts occurred at the second transmembrane domain, following a non-piston model of movement, whereas shifting in the first transmembrane domain mainly occurred near the periplasmic region, implying possible interaction with other periplasmic protein controlling EnvZ sensory mechanism. Results presented here provide insight into the question of what role the transmembrane domains play in the signal transmission process within sensor histidine kinases.

The third act addresses my attempt to create a chimeric receptor by fusing the sensory region of *S.* Typhimurium magnesium sensor, PhoQ, with the catalytic region of a well-characterised EnvZ. Results showed that simply inserting the gene into our backbone, pRD400, and aromatically tuning the receptor were not enough to completely restore the sensory function of the PhoQ-native domain. A different approach to plasmid design was undertaken using the Standard European Vector Architecture (SEVA) platform, which allowed for better control of receptor expression as demonstrated by immunoblotting

results. Further analysis on signal output still needs to be performed to assess if expression of the chimeric receptor using the SEVA backbone could restore the sensory function, and produce a dose-response signal output, which would be the ideal signal pattern required if this chimera were to be used in a high-throughput screening platform.

The fourth and final act concludes the story of transmembrane signalling and chimera design, and furthermore lays out plans on how the projects are or could be expanded within the research group, particularly which questions still need to be answered: the nature of interdomain interaction during EnvZ signalling, and how to optimise the design of the PhoQ-EnvZ chimera.

Keywords: EnvZ/OmpR two-component system, EnvZ transmembrane signalling, chimeric two-component system, SEVA platform

Declaration

Whilst registered as a candidate for the above degree, I have not been registered for any other research award. The results and conclusions embodied in this thesis are the work of the named candidate and have not been submitted for any other academic award.

Word Count: 35,901

Contents

List of Figures

List of Abbreviations

Amp	Ampicilin
CA	Catalytic
CCW	Counterclockwise
CFP	Cyan Fluorescence Protein
CGMD	Coarse Grained Molecular Dynamics
CW	Clockwise
DBD	DNA-binding domain
DHp	Dimerisation and Histidine phosphotransfer
DNA	Deoxyribonucleic acid
DPPC	Dipalmitoylphosphatidylcholine
FBDD	Fragment-based Drug Discovery
HK	Histidine Kinase
HPt	Histidine Phosphotransferase
HTS	High-Throughput Screening
IG	Intergenetic region
IPTG	Isopropyl β-D-1-thiogalactopyranoside
MCP	Methyl-accepting Chemotaxis Protein
MDR	Multidrug resistance
MGD	Minimum Glycosylation Distance
NavZ	NarX-EnvZ
NEM	N-ethylmaleimide
NMR	Nuclear Magnetic Resonance (Spectroscopy)
OD	Optical Density
OM	Outer Membrane
ORF	Open Reading Frame
OST	Oligosaccharyltransferase
PDR	Pandrug resistance
PhonZ	PhoQ-EnvZ

RBS	Ribosome Binding Site
RD	Receptor domain
REC	Receiver domain
RNA	Ribonucleic acid
RR	Response Regulator
SBVS	Structure-based Virtual Screening
SDM-PCR	Site-Directed Mutagenesis - Polymerase Chain Reaction
SDS-PAGE	Sodium Dodecyl Sulfate - Polyacrylamide Gel Electrophoresis
SEVA	Standard European Vector Architecture
SHK	Sensor Histidine Kinase
Sm	Streptomycin
Sp	Spectinomycin
SPI	Salmonella Pathogenicity Island
Taz	Tar-EnvZ
TCS	Two-Component System
TM	Transmembrane
TMD	Transmembrane Domain
XDR	Extensively drug resistance
YFP	Yellow Fluorescence Protein

List of Bacterial Strains and Plasmids

***Escherichia coli* Strain**	**Function or Feature**
K-12 MG1655	F- λ- *ilvG rfb50 rph1*
MDG147	MG1655 Φ(*ompF*$^{+}$-*yfp*$^{+}$) Φ(*ompC*$^{+}$-*cfp*$^{+}$)
EPB30	MDG147 *envZ::kan*
MC1061	F- *hsdR2*(rK^{-} mK^{+}) *mcrA0 mcrB1*
DH10B	Electrocompetent cell
Plasmid	**Function or Feature**
pEB5	Δ*envZ*
pRD400 (pEnvZ-V5)	pEnvZ with linker (GGSSAAG)and V5 tag
pRY100 (pPhonZ-V5)	pRD400 *envZ::phonZ*
pSEVA434	Sm/Sp^{R}, pBBR1 ori, *lacI* promoter
pSEVA434-EnvZ-V5	*envZ-V5*$^{+}$
pSEVA434-PhonZ-V5-WeakRBS	phonZ^{+}, RBS (TCACACAGGACTACTAG)
pSEVA434-PhonZ-V5-MediumRBS	phonZ^{+}, RBS (TCACACAGGAAAGTACTAG)
pSEVA434-PhonZ-V5-StrongRBS	phonZ^{+}, RBS (AAAGAGGAGAAATACTAG)

Acknowledgements

My journey to the prestigious PhD title started in early 2012, just when I was about to complete my masters in Biomedical Engineering in Karlsruhe, Germany. I sent out at least two dozen applications per semester, all exclusively in Europe and only to those offering full funding, and eventually lost count of how many rejections I received by the time I admitted defeat and returned to Jakarta a year later. My religious parents, as any other spiritual person in Indonesia, would say, ''God wants you to wait for something better.'' So I decided to give it a break, look for a research job or intern or whatever (not in a position to be picky) and deal with the agony of PhD applications another day.

Fast forward to October 2014 in Durham, England, having heard my fellow doctoral awardees of the LPDP scholarship complain about how they hardly ever got to see their supervisors, how lonely they felt in their group, or how they were always left to figure things out on their own (research related or not), I started to see the value of what those Indonesians believe in. If there's anything I had never experienced in the Draheim group, it would be the feeling of abandonment. Research related or not, whenever I had something to say or complain about there's always someone who listened. Roger, Rob, Than and Fadhael, that's the closest to a compliment that you guys will ever get from me. You see, Reader, we're not a group that grandiosely praise one another, at least not before drinks are served…a fifth round. On that note, Ivor, you're awesome. Thank you for the support.

When not in the lab, I'm lucky enough to be surrounded by great friends whose struggle on their own doctoral research made me feel better sometimes (haha). Arianna, Gina and Kim, I missed out on a lot of parties (on purpose) with companies I didn't enjoy but I would never miss out on a house party with you guys whom I would never get bored of. That's when you know that an introvert LOVES you.

When not in the lab or in Portsmouth, I'm lucky to have a very supportive family. Mom & Dad, I appreciate your faith in me during the 10 years that I spent being an unemployed, non-tax paying human who couldn't even afford health insurance. I'm finally done! You can stop worrying about me and focus on the two other children now. Don't

hold your breath on grandchildren though; I still want to be a scientist. Little sister, we still have more countries to visit. Little brother, without you, we'd be a boring, left-brain dominant family.

Not to forget the hand that feeds: Terima kasih kepada Lembaga Pengelola Dana Pendidikan (LPDP), Departemen Keuangan, Republik Indonesia atas penganugerahan Beasiswa Pendidikan yang telah membiayai pendidikan doctoral saya selama empat tahun belakangan ini. Terima kasih juga atas pemberian insentif dana publikasi internasional untuk dua publikasi pertama saya. Semoga bermanfaat bagi bangsa, mengharumkan nama Indonesia dan membanggakan bagi LPDP. Terima kasih atas dukungan dari tim pengurus LPDP yang telah membantu saya dalam menangani segala proses administrasi, khususnya ketika saya berpindah universitas. Saya tidak mungkin sukses tanpa kalian semua. Semoga LPDP terus berjaya! (Rahmi Yusuf, PK-17, Tim Salman)

On a slightly weird note, I would like to thank Steven Spielberg. Yes, THE Steven Spielberg, for making the masterpiece that is Jurassic Park. Seven-year-old me saw this film at a movie theatre in a forgettable shopping mall in Cleveland, Ohio. The cinematic experience, however, was truly unforgettable, and was implanted in my brain for many years to come. Since then I have grown up wanting to become an array of Jurassic Park-inspired professions, from Archaeologist, Film-maker, Philanthropist (still might happen), and eventually a Biologist. So I guess in a way, you initiated this whole thing.

Last but not least, thank YOU for reading my thesis. I worked really hard on it. You're either my supervisors, my viva examiners, a new student continuing my research who gave up trying to read my lab notes, or just an extremely bored individual. But thanks anyway.

Rahmi Yusuf

Act I:
Prologue

Chapter 1: A Brief History of the Two-Component System

1.1 Signalling Systems across the Three Domains of Life

One way that organisms adapt to their environment is by employing proteins to tackle extracellular challenges, thus prompting the emergence of a large collection of proteins with various functions. These proteins interact with each other in order to achieve a unified goal, *i.e.* a system. Following this logic, the most basic systems would consist of two components, which are then simply called 'two-component systems' (TCSs), where one component ("the sensor") detects an input signal and then transmits the information to the second component ("the effector"), which is responsible for controlling the production of a corresponding output. In a bacterial cell, two proteins, the histidine kinase (HK) and the response regulator (RR), serve as these components (1). ***Figure 1.1*** illustrates this basic signal processing scheme involving one sensor and one effector in an HK-RR two-component system.

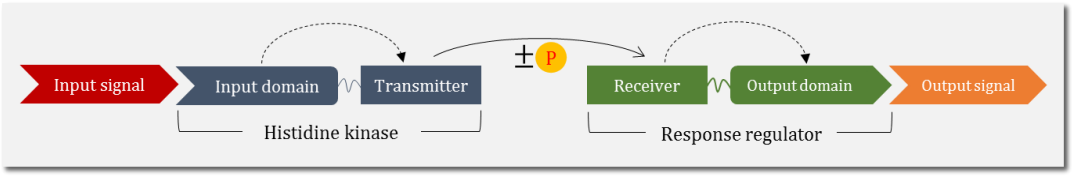

Figure 1.1. Interaction between units and modules in a bacterial two-component system signal processing.
The system consists of two modules: the histidine kinase (HK) and the response regulator (RR). The HK contains an input domain, which detects or interacts with the input signal, prompting activation/phosphorylation of the transmitter unit of the kinase, which then transfers the signal to the receiver unit of the RR, prompting its output domain to coordinate the expression of an appropriate output. *Image adapted from (1).*

As the natural environment evolved over time, organisms were compelled to adapt to the changes by evolving their intracellular systems, hence increasing the complexity of the two-component systems, by recruiting additional units (or 'domains') to play different roles in signal transfer between the two original members of the system. In many cases, a new unit becomes so well integrated into the system, it physically links itself to the histidine kinase, thus adding more domains to the receptor. For simplicity, the diversity of signalling systems could be classified into two types based on the amount of players involved in signal processing: the phosphotransfer and the phosphorelay (2). A phosphotransfer system follows the traditional pattern of the TCS, having a single protein accepting an input signal, and another producing an output, whilst a signal entering a phosphorelay system is passed on from one discrete protein to another before reaching the final effector protein (***Figure 1.2***). For this reason, phosphorelay systems are not synonymous with two-component systems simply because they are composed of more than two units.

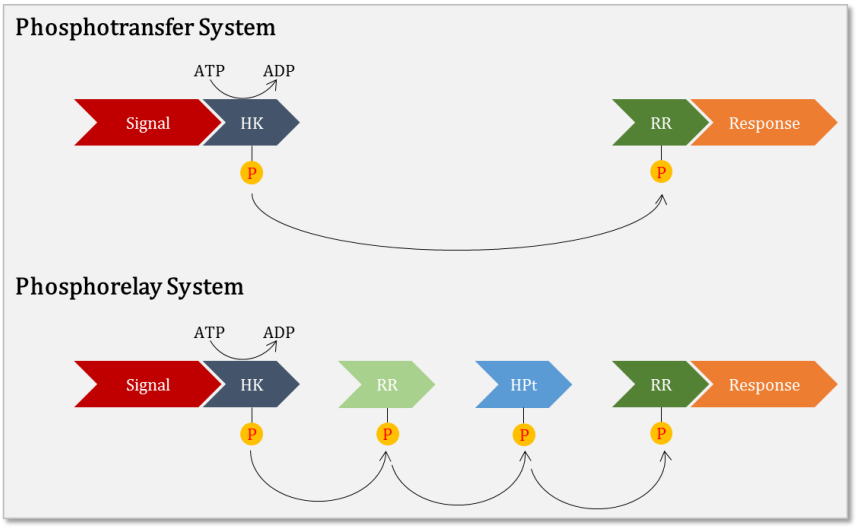

Figure 1.2. Difference in signal processing between a phosphotransfer and phosphorelay system.
In a phosphotransfer system, an HK detects, processes, and then transfers an incoming signal directly to its cognate RR. As the name suggests, a signal entering a phosphorelay system goes through a 'relay' as other proteins, such as other RRs or histidine phosphotransferases (HPt), become part of the system. *Image adapted from (2).*

Based on the source of the signal, HKs are either extracellular (or periplasmic)-sensing, membrane-sensing, or cytoplasmic-sensing (***Figure 1.3***). The most common type of HKs is membrane-bound and periplasmic-sensing, and EnvZ best represents this group. This receptor typically has a sensory domain exposed to the periplasm, which makes it ideal for sensing solvents, and a kinase domain located in the cytoplasm, separated by two or more transmembrane (TM) domains, thus stressing the importance of TM domains in its signal transfer ***(Figure 1.3-A)***. The second type of HK is membrane-bound and membrane-sensing. Similar to the first type, this type also has two or more TM domains; however, their TM domains act as the sensor, and the linkers between TM domains are much shorter ***(Figure 1.3-B)***. Membrane-sensing HKs normally receive their signal from within the membrane (mechanical stress or membrane-bound enzymes) or at the membrane interface (3). The third type (and second most common) HKs are cytoplasmic-sensing and either membrane-bound or soluble ***(Figure 1.3-C)***, which normally detects signals in form of cytoplasmic solutes or metabolic proteins (3).

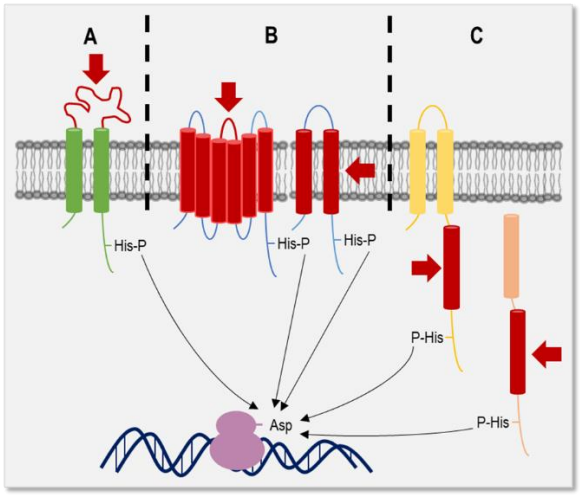

Figure 1.3. Three different types of HKs based on the type of sensor regions.
Periplasmic sensing for membrane-bound HKs **(A)**, a combination of periplasmic and transmembrane sensing or transmembrane sensing alone for membrane-bound HKs **(B)**, and cytoplasmic sensing for either membrane-bound or soluble HKs **(C)** provide varying options for TCS sensor detection. The red arrows represent input signal, while the sensory part(s) of the receptors is coloured in red. *Image adapted from (3).*

Parallel to the evolution of organisms from unicellular to multicellular, selective pressure from the environment pushes canonical systems to increase in complexity and form phosphorelay systems. For this reason, phosphotransfer systems or TCSs are rarely found in mammals. Eukaryotic kinase sensitivity greatly increases as the receptors become more saturated, therefore allowing them to interact with a vast array of downstream targets, contrary to bacterial kinases, which favour the creation or evolution of new TCSs and preserving exclusivity of existing HK-RR pairings over crosstalk between two existing TCSs, *i.e.* between an HK of one system and an RR of another (4). For complex cellular functions, however, this restriction is often compensated by transcriptional cross-talk between two or more TCSs, which allows them to cooperatively control multiple gene transcriptions involved in certain pathways. The cross-talk between PhoQ/PhoP, EnvZ/OmpR and SsrA/SsrB to control the expression of proteins that construct the type III secretion system in *S.* Typhimurium is an ideal model for this type of interaction, and will be discussed further in Chapter 8.3.

For bacterial kinases, restricted partnership between HK and its cognate RR is controlled as increase in sensor kinase saturation is balanced by the decline in unphosphorylated RRs, while the total RRs in the cell (phosphorylated and unphosphorylated) remains relatively constant throughout the signalling process. Nonetheless, an exception to this rule applies to several bacterial TCSs, in which elevated level of RR are expressed to maintain a particular level of phosphorylated RR, allowing new RRs to interact with a larger variety of downstream targets. The fitness requirement of a TCS drives evolutionary pressures that ultimately result in either isolation of an HK-RR pair or expansion of HK-RR interface and functionalities (4,5). ***Figure 1.4*** shows how a simple phosphotransfer system evolves into more complex phosphorelay systems, while maintaining conserved patterns, by recruiting intermediary proteins, as the complexity of the input signal and required output increases.

Statistical analysis of evolutionary changes in HK and RR residues revealed that the ability of cognate HK-RR pairs to recognise each other is determined by a specific set of amino acids located on each protein defining the molecular recognition pattern

of each TCS pair, and *in vitro* manipulation of these clusters in a certain HK has been shown to render the protein able to interact with a non-cognate RR, and vice versa (6). On the other hand, cross regulation between two or more TCSs, possibly mediated by connector proteins, allows the bacterial cell to regulate more complex and highly controlled processes, *e.g. Salmonella* PhoQ/P and PmrB/A working together to regulate resistance against polymyxin B, or *E. coli* EnvZ/OmpR and CpxA/R connected by protein MzrA to maintain integrity of outer membrane proteins (7,8).

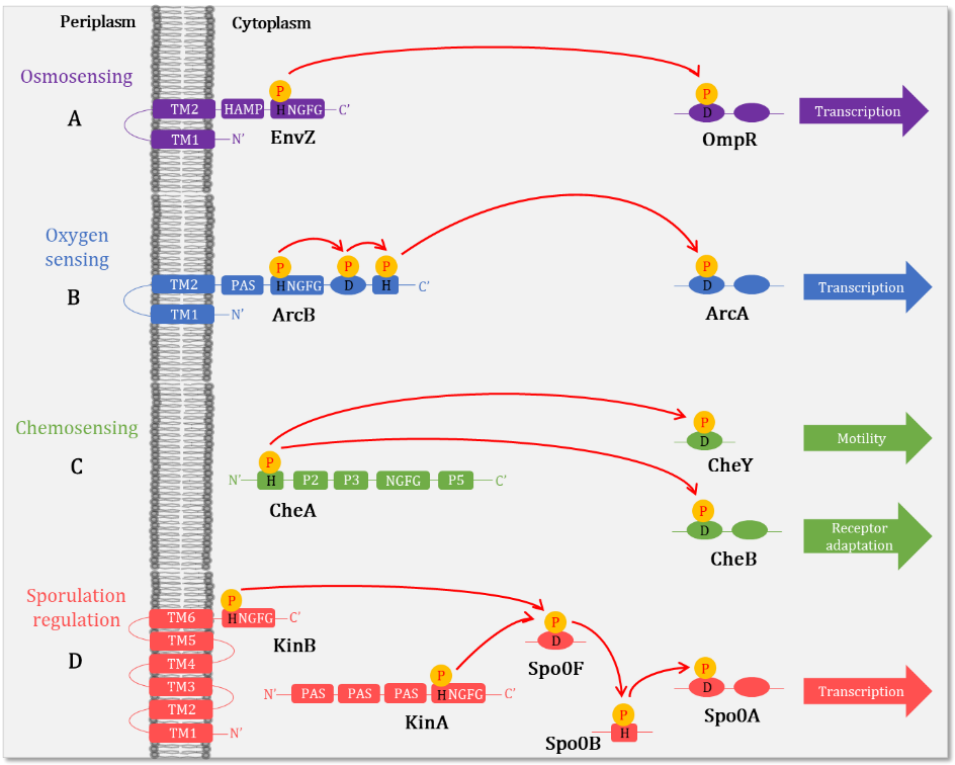

Figure 1.4. Different examples of phosphotransfer and phosphorelay systems which best represent the variety of HKs and RRs in bacterial cells along with domain organisation.
From the canonical system to the most complex: **(A)** EnvZ/OmpR of *E. coli*, which controls osmotic shifts, has the simplest modules of a TCS; **(B)** also having a membrane-bound HK and a transcription factor RR, E. coli oxygen sensor AcrB/AcrA, contains a PAS (Per-Arnt-Sim) domain, which acts as the sensor, as well as a fused RR domain and a HPt domain (9); **(C)** the *E. coli* chemoreceptor CheA consists of 5 domains (P1-P5) interacting with two competitive RRs, CheY and CheB (9); **(D)** sporulation in *Bacillus subtilis* depicts one of the most complex organisation of a phosphorelay system, with the first HK having 6 transmembrane domains and the second HK having 3 PAS domains, together controlling the RR Spo0F, which controls DNA-binding RR Spo0A via single domain His-containing Spo0B (9). *Image adapted from (9).*

Figure 1.4 maps out domain organisations of various HK and RR. Overall, several conserved motifs are found in all systems: the phosphor-binding histidine residue at the dimerization domain and NGFG motif in the catalytic domain of the HK, as well as the phosphor-binding aspartate residue in the receiver domain of the RR. Therefore, basic layout of a phosphotransfer system is represented by *E. coli EnvZ/OmpR*, as EnvZ represents the most common group of histidine sensor kinase and OmpR represents the largest family of response regulators ***(Figure 1.4-A)***. To adapt with the multitude of environmental stimuli, phosphotransfer systems evolved with the addition of new domains to the basic template, such is the case with the *E. coli* oxygen sensor ArcB/A ***(Figure 1.4-B)***, which contains a sensing domain called the PAS (Per-ARNT-Sim) domain, which was originally found in *Drosophila* proteins period and single-minded, and the vertebrate aryl hydrocarbon receptor nuclear transporter, and is well spread out in all three domains of life (10). Cytoplasmically located, PAS domains are known to perceive changes in oxygen, light, redox potential, as well as the overall energy level of the cell, hypothetically by monitoring protein motive force or similar parameters, suggesting that this sensor detects environmental stimuli that enters the cell; not surprisingly, this motif is also commonly found being involved in plant chemotaxis, control of insect circadian rhythms and vertebrae ion channels (10,11). Fused into the sensor and conserved domains, ArcB became a phosphorelay HK as a RR and HPt are fused into the main body of the HK.

More complex expansions are observable in bacterial systems controlling chemotaxis, notably the *E. coli* CheA/Y ***(Figure 1.4-C)***. Within these systems, CheA, the chemosensor, or specifically the methyl-accepting chemotaxis protein (MCP), couples with CheW to form a stable complex of a HK equivalent (12,13). With the help of MCP enzymes CheB and CheR, which further modifies CheA by controlling cycles of (de)methylation via direct interaction with the adaptor region of the receptor (14), this HK then interacts with its cognate RR, CheY, to control the "run or tumble" cycle of cell motility (12,13). To further increase the speed of signal regulation, an additional protein, CheZ, is found in enteric bacteria to be involved in signal removal by destabilising CheY-P; this system, however, was not found in other

chemotactic bacteria and archaea (15). ***Figure 1.5*** overviews the versatility of the chemosensory system in relation to the myriad of adaptor proteins that control the range of signal response by CheA. Due to this wide dynamic range, chemoreceptors provides an excellent scaffold to design chimeric biosensors, allowing access to numerous biochemical functions and pathways (16).

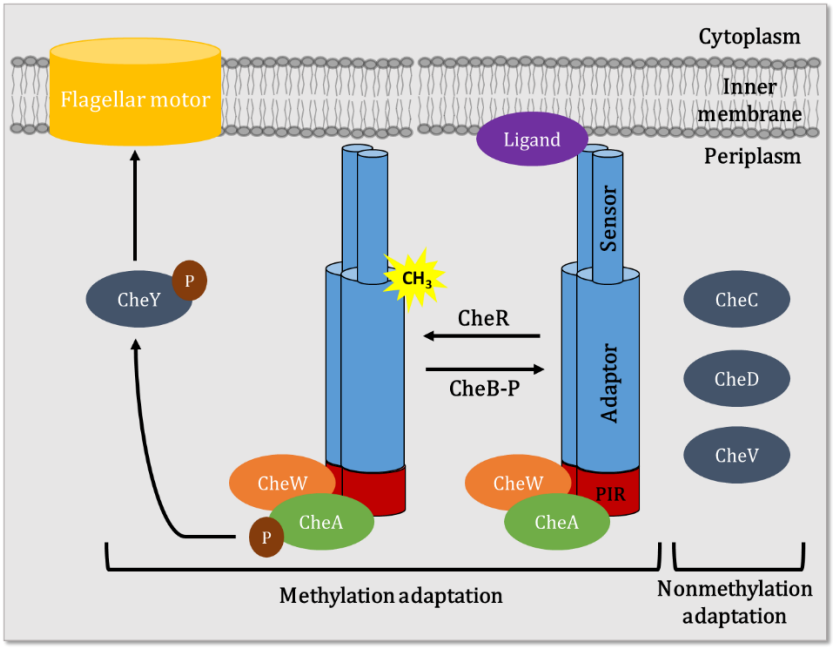

Figure 1.5. Schematic of signal transduction in soluble chemoreceptors.
The domain organisation of chemoreceptors or methyl-accepting chemotaxis proteins (MCPs) consists of a variable sensory domain and a conserved methyl-accepting (MA) domain, further differentiated into the adaptor region, which binds with CheR or CheB, and the protein interaction region (PIR), where CheW/CheA interact with the chemoreceptor (14). Methylation adaptation is orchestrated by CheR and CheB, as they control CheA (de)phosphorylation, which in turn controls flagellar rotation via CheY. Nonmethylation adaptation, well characterised only in *B. subtilis*, is conducted by CheV proteins, which are chimeras of CheW-REC, allowing for more robust chemoreceptor-kinase control, or CheC together with CheD, which increase CheA activity via direct interaction at the methylation region (14,15). *Image adapted from (14).*

The intricate process of sporulation in *B. subtilis* is controlled by multiple HKs interacting with more than one RR ***(Figure 1.4-D)***. The main RR of this system, Spo0A, is both transcriptional activator and repressor of various sporulation genes, as it receives cues from the phosphorelay intermediates, Spo0F and Spo0B, which function as physiological adaptors to integrate the many signals that initiate sporulation (17,18), such as those coming from the Kin HKs. Membrane-bound HK, KinB, and soluble HK, KinA, positively regulates the system, whilst another HK, KinC, signals Spo0A to control *abrB*, which expresses a sporulation-repressing protein, AbrB (17).

As expected, sequence homology studies revealed that TCS genomes are found in all three domains of life, although the more complex the organism, the more its system deviates from the typical HK-RR TCS architecture. In eukaryotic organisms, the signalling system becomes so evolved that their origins in bacteria could not be clearly traced. Nonetheless, certain proteins, *e.g.* the Ser/Thr/Tyr kinases, might indicate an ancestral relationship with prokaryotic TCS.

Solely for this reason the bacterial TCS makes for a perfect antimicrobial target, as the side-effects on humans and other mammals could be minimised. ***Figure 1.6*** depicts the distribution of TCS genes in bacterial cells (19). *E. coli* has almost an equal amount of HK and RR, implying minimum occurrence of cross-talk between two systems, allowing for relatively good isolation of a TCS during *in vivo* studies.

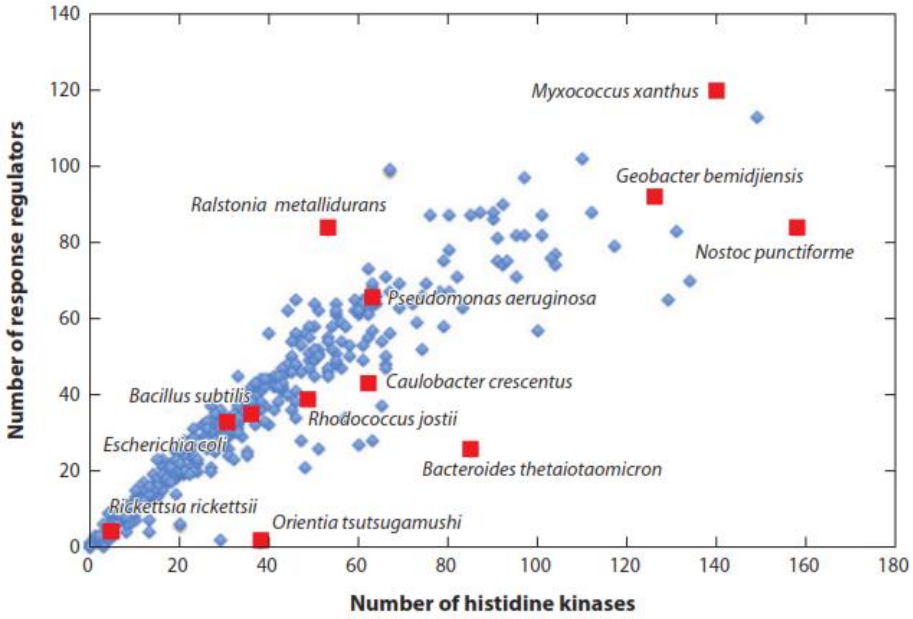

Figure 1.6. Scatterplot depicting the amount of TCS genes in various microbes.
Generally the ratio of HK:RR is 1:1, unless certain RRs in the cell receives signal from a multitude of HKs. The red squares mark examples of well-studied species. *Image taken from (19).*

1.2 *Escherichia coli*: The "Poster Child" of Bacterial Systems

Due to its ease of maintenance, short duplication time and fully sequenced genome, *Escherichia coli* or *E. coli* has become an invaluable tool in biomedical research. A huge number of Nobel-winning discoveries in molecular biology attributed their accomplishments to this Gram-negative, facultative anaerobic, rod-shaped bacterium.

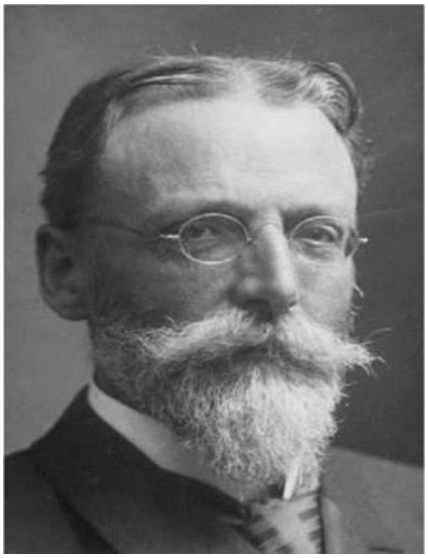

Figure 1.7. Dr Theodor Escherich (1857–1911)

In 1885, four years after being awarded a doctorate in medicine, at the young age of 28, Dr Theodor Escherich (***Figure 1.7***), a German-Austrian paediatrician and bacteriologist, noticed a disturbing trend of infants dying of diarrhoea. As he believed that microorganisms were the main cause of these diseases, he began to investigate the microbes present in human faecal matter, especially those in children. Using Christian Gram's new staining method, as well as various cultivation techniques he learned from Robert Koch himself, his quest eventually led to the discovery of a rod-shaped bacterium (20), which he named *Bacillus coli*; 'bacillus' is Latin for 'wand' or 'little staff' and 'coli' refers to 'colon', where it is commonly found. A year later, Escherich published this findings in a 177-page postdoctoral thesis, titled "Die Darmbakterien des Säuglings und Ihre Beziehungen zur Physiologie der Verdauung" ("The Intestinal Bacteria of the Infant and Their Relation to the Physiology of Digestion") (20).

A decade later, as Dr Escherich became Professor of Paediatrics at the Karl-Franzen University of Graz, *Bacillus coli* was reclassified into the genus Escherichia, to honour its founder, and the family Enterobacteriaceae (for coliforms and enterics), thus its nomenclature was changed to *Escherichia coli.* Over the last 100 years, *E. coli* has been extensively studied, its genome sequenced and manipulated, and as more strains of *E. coli* became associated with various case studies, they have

been serologically classified into different groups based on their O (lipopolysaccharide), K (capsular) and H (flagellar) antigens (21).

Being genetically versatile in its nature, *E. coli* became the primary source of information for all things bacteria, as well as providing molecular biologists a tool to perform DNA manipulations for various purposes. Dr Escherich's original strain of *E. coli* (NCTC 86) contains a 5,144,392 bp circular containing 4805 open reading frames (ORF), of which 8.62% encoded conserved hypothetical proteins and 11.32% were associated with mobile elements or phage related (22). The common non-pathogenic *E. coli* strain K-12 MG1655, which has been used as a starting template for many laboratory-made mutants, shares a common backbone with Escherich's strain as it was isolated from diphtheria patients without diarrhoea and UTIs, supporting the scientist's claim of a commensal *E. coli* as part of the normal microbiota (22).

Roughly 1.5% of the total ORFs in the *E. coli* genome encode two-component proteins (19), and a large number of these proteins are also found in other microbes. Coupled with its favourable characteristics as a model organism in general, the *E. coli* K-12 MG1655 strain would make an ideal model to study two-component systems. This study utilises this strain to explore the signalling features of the EnvZ/OmpR TCS, which is considered the canonical and most well-understood TCS.

1.3 Filling in The Gaps of EnvZ/OmpR Signalling

1.3.1 The Histidine Kinase, EnvZ

The *E. coli* EnvZ/OmpR TCS is the main focus of this thesis project. Every aspect of this TCS has been dissected throughout the years, and most of its features have been determined, therefore making it an excellent model to create synthetic signalling systems for various purposes. The first part of this thesis project concentrates on answering questions still relatively neglected in EnvZ/OmpR signalling, which is the role of transmembrane domain in EnvZ signal transduction.

The EnvZ/OmpR TCS responds to changes in extracellular osmolarity and responds by expressing protein channels, called porins, to counter the increase in osmotic pressure. Porins controlled by OmpR, namely OmpC and OmpF have been associated with resistance to antibiotics, bile salts and bile acids. Studies with *ompC* deleted mutants have shown decreased susceptibility to carbapanems and cephalosporins, as well as serum resistance (23), while an earlier publication regarding the role of porins in antibiotic resistance described that bacteria are able to increase resistance by regulating OmpC and OmpF expression, or by reducing permeability of certain porins via mutation (24). Similarly, studies conducted on *E. coli* (25) and *S. enterica* serovar Typhi (26) have shown that modulation of porin levels would allow enteric bacteria to maintain resistance to bile salt and survive in the gastrointestinal environment (27).

The HK of the system, EnvZ, is a multidomain osmosensor transmembrane protein build up by 450 amino acid residues, which is divided into these domains (***Figure 1.8***): a cytoplasmic N-terminal end (residues 1-15), two transmembrane helices (TM1, residues 16-47; TM2, residues 163-179), a periplasmic domain (residues 48-162) and a cytoplasmic C-terminal end (residues 180-459) (28), which has been furthermore distinguished into linker domains A (dimerization and histidine-containing residues 223-289) and B (catalysis-assisting and ATP-binding residues 290-450) (29). Later on, a domain termed HAMP (found in histidine kinases, adenylyl cyclases, methyl-accepting chemotaxis protein, and phosphatases) connecting TM2 and the histidine-kinase domain has been identified (30).

Figure 1.8. Schematic map of domain organization of EnvZ in strain *E. coli* K-12.
Domains consist of transmembrane (TM) 1 and 2, HAMP (the linker), dimerisation and histidine phosphotransfer (DHp) and catalytic domain (CA). Conserved residues

of the HK core are the H, which binds with phosphate, N, D, F and G boxes (31). *Image adapted from* (31).

The sensory mechanism of EnvZ has been subject to much debate. The cytoplasmic domains near the C-terminus of this receptor has been associated with osmosensing, specifically in the 17-amino acid region flanking the His-243 autophosphorylation site (32). Not only do amino acid substitutions greatly influence kinase activity, but this region has also been shown to be very dynamic under low osmolarity ("stretch-relaxation" model), with NMR structures showing high rates of exchange (32,33).

Interaction with stimulus itself has been thought to be non-ligand binding, due to the versatility of EnvZ to sense increase of osmolarity caused by a variety of substrates, but rather via mechanosensing ion channels (34). Foo *et al.*, 2015 hypothesised that upon increase in extracellular osmolarity, EnvZ concentrates the cytoplasm by stimulating water efflux, thus dramatically increasing spheroplast volume, which then triggers mechanical stress to the TM domains of the receptor. This stress would likely induce a conformational change in the periplasmic domain and/or cytoplasmic domain of EnvZ via allosteric interaction, thus allowing the receptor to take on its "high-osmolarity" form (as opposed to the "low-osmolarity" form), which translates to a certain signal output (35).

Formerly called the 'linker' domain, the HAMP domain is predicted to be involved in propagating signal from TM2 to the histidine-containing domain by controlling structural changes in downstream domains, and possibly aligning two EnvZ molecules in a dimer (36–38). Furthermore, due to its interspecies homology, could be used as a fusion point to design functional chimeric receptors (37).

The transmembrane domains, while not involved in stimulus sensing, are proved to be directly involved in signal transfer. Tokishita *et al*, 1992 studied the *in vitro* effect of amino acid substitutions at the TM domain of EnvZ on porin expression, *i.e.* OmpC and OmpF. Substitution of Pro-41 to Ser

in TM1 locked EnvZ in high osmolarity conformation, resulting in accumulation of OmpR-P and subsequent overexpression of OmpC, despite changes in extracellular osmolarity; conversely, substitution of Arg-180 to Cys in TM2 reduced OmpR phosphorylation, thus increasing OmpF expression over OmpC (39). Furthermore, studies elucidating the relationship between EnvZ transmembrane conformation and signal output using in vivo disulphide cross-linking experiments has been reported (40,41). These results hinted towards the relationship between TM structure and signal output, furthermore opening the possibility of controlling signal output via manipulation of transmembrane structure, giving rise to the development of a stimulus-independent signal output modulation technique, named "aromatic tuning", in which alteration of the position of aromatic residues in the TM domains is conducted to achieve a desirable signal OmpC to OmpF ratio (42).

Several models hypothesising the movements of TM helices have been proposed ***(Figure 1.9)***. A combination of empirical data and molecular dynamics have been widely used to deduct this pattern of movement.

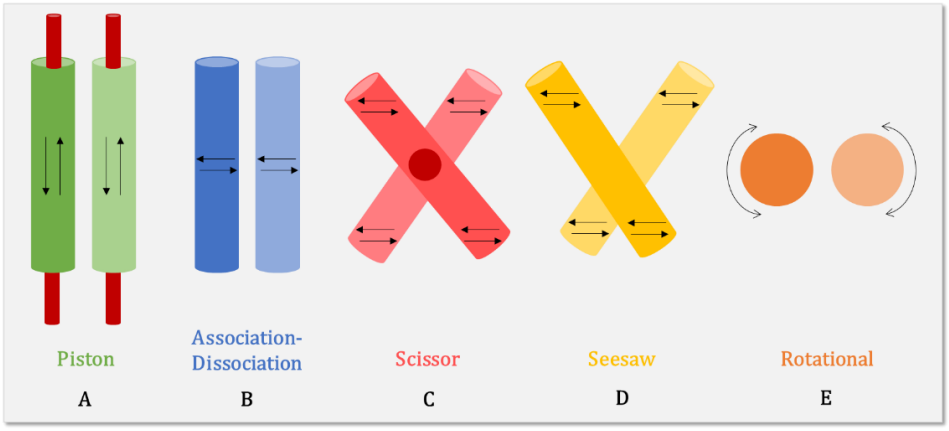

Figure 1.9. Postulated models of transmembrane signalling for ligand-binding receptors.
Models here present the possible interaction within transmembrane domains of a histidine kinase (between TM1-TM1' or TM2-TM2'). In the piston model, the transmembrane helices move vertically parallel against the membrane **(A)**; in the association-dissociation model the transmembrane helices move closer or further

apart to one another within the membrane plane **(B)**; in the scissor model the transmembrane helices tilts closer or further against a central axis **(C)**; in the seesaw model the transmembrane helices flips between an open and closed conformation **(D)**; in the rotational model the transmembrane helices rotates around a longitudinal axis **(E)** (40,43).

1.3.2 The Response Regulator, OmpR

The second component of the two-component system is the response regulator (RR), which typically consists of two weakly interacting domains, namely the (N-terminal) regulatory and (C-terminal) effector domain, respectively responsible for regulating (de)phosphorylation and binding with a macromolecule to produce a response, bridged by a tightly wounded polypeptide linkage, which is loosened upon phosphorylation, compelling dimerisation between the RR and the targeted macromolecule (44,45).

The receiver (REC) domain of RR is a highly conserved $\alpha_4\beta_5\alpha_5$ domain and acts as a receiver of signal from its cognate HK, specifically at its D (aspartate) box, which is part of the domain's active site. Conserved residues in this domain is also responsible for regulating the phosphorylation and (auto)dephosphorylation cycle of protein, thus this domain is also known as the regulator domain. Upon phosphorylation, subtle repositioning of Phe/Tyr and and Ser/Thr in the backbone occurs as these residues are directed towards the active site (46,47). This domain is arguably the most important part of a RR, despite its involvement with the effector domain determining its specific function within a TCS pathway, as removal of the receiver or regulator domain has been shown to render the RR partially or completely inactive (47). In addition to conserved residues rearrangement, divalent cation, especially Mg^{2+}, adjacent to the phosphorylation site is also required to mediate interaction with phosphoryl groups (46,48), whereby this ion interacts with conserved Asp residue, a backbone carbonyl group and two water molecules within the six coordination positions of the metal ion. Upon phosphorylation, a water molecule and the phosphoryl group swap an oxygen

atom, and the metal binding affinity of the RR presumably increases due to adjacent hydrophobic amino acid residues (48).

The most prominent classification of RRs is a categorisation based on the function of its effector domain, as this is the variable component of the RR (***Figure 1.10***). The largest class of two-domain RR has its effector domain act as transcriptional regulator for a wide range of effector proteins, from essential growth factors to virulence factors; all RRs in this class binds DNA with the exception of two RRs found to interact with RNA, whereas the second largest RR class are enzymatic, catalysing reactions such as methylesterases, histidine kinases, serine/threonine protein kinases and protein phosphatases (46,48,49). The third class of RR interacts with other proteins and is found in genomes of most alpha-proteobacteria. Furthermore, each RR class is distinguished into families based on structural similarities or patterns (48,49).

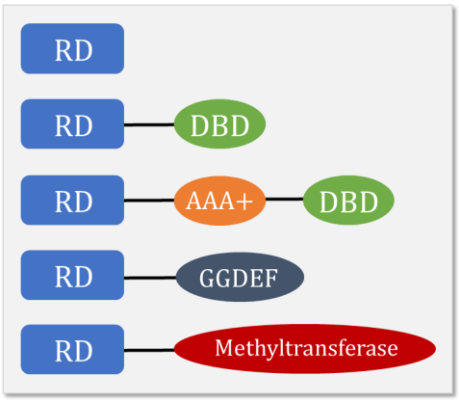

Figure 1.10. Different classes of response regulators (RRs) based on domain organization.
The conserved receiver domain (RD) exists either on its own, or with a DNA-binding domain (DBD), with a combination of an AAA+ (an ATPase) and a DBD, with a GGDEF domain (involved in cyclic di-GMP synthesis), or with a CheB-like methylatransferase domain (19). *Image adapted from (19).*

OmpR is the cognate response regulator of EnvZ. Located in the cytoplasm, this 27 kDa protein (125 aa N-terminal joined by a short linker, optimally between 13-15 aa residues (50) with 100 aa C-terminal) is the most well-characterised RR in the OmpR/PhoB subfamily (51,52), which shares a

conserved DNA-binding domain. OmpR is phosphorylated by EnvZ at its highly conserved phospho-accepting aspartate, Asp57, which along with other surrounding conserved residues play an important role in regulating the phosphorylation-dephosphorylation switch of the RR. *In vivo* quantitative analysis of OmpR phosphorylation has revealed that both EnvZ phosphatase activity and OmpR autodephosphorylation are required to maintain a fine balance between OmpR and OmpR-P (53). At low extracellular osmolarity, OmpR-P is kept at roughly 5% of total OmpR, while at higher osmolarity OmpR is never completely phosphorylated even under full activation of the system, thus allowing a wider gradient of response (53).

OmpR acts as a transcription factor controlling expression levels of *ompF* and *ompC*, genes encoding porins OmpF and OmpC respectively. The C-terminal of OmpR has been shown to interact with DNA, with a highly conserved winged helix-turn-helix binding motif (54), at the *ompF* and *ompC* promotors, while the N-terminal was theorised to interact with other proteins, *i.e.* EnvZ and RNA polymerase; close proximity between RNA polymerase and OmpR binding sites suggests possible protein-protein interaction (55). It was eventually discovered that the C-terminal domain of this RR interacts with the C-terminal domain of the α-subunit of RNA polymerase (56,57).

When overexpressed, OmpR has been found to function as a multimer, most likely during DNA binding, possibly having different conformations at low and high osmolarity (58,59). The concentration of OmpR has been shown to be significantly greater than OmpR-binding sites in the DNA, allowing for saturation of the binding sites at substoichiometric conditions of OmpR phosphorylation (53,60). Furthermore, OmpR dimerisation as well as stabilisation of the dimer is required upon binding with DNA and is increasingly achievable at the presence of DNA, thus highlighting the importance of dimerisation in OmpR signalling, making it a potential target for novel antibiotics (53).

1.4 The Two-Component System as a Novel Antibiotic Target

Prior to the widespread use of commercial antibiotics, a selective number of bacteria species have been found to be either intrinsically resistant, or possess resistance genes, due to the bacteria itself being the agent producing the antibiotic. The use of heavy metals to treat disease may have presented the first human-made environmental pressure for pathogenic microbes to develop resistance (61). Within the first decade of the 20th century, the antisyphilitic drug, arsphenamine (Salvarsan™ or compound 606) developed in the lab of Paul Ehrlich, was introduced to the German market, followed by widespread use in Europe in the subsequent years, which eventually uncovered the severe toxic effects of this drug in human (62). The word 'antibiotic', however, was coined by Selman Waksman several decades later (in 1941), to describe small compounds produced by microbes to inhibit the growth of other microbes (63). Ampicillin, the first systematically used antibiotic, ultimately replaced arsphenamine upon its discovery in September 1928 by Alexander Fleming and mass production campaign in the 1940's by Howard Florey and Ernst Chain (64), which lead to the 1945 Nobel prize in Medicine to these three scientists. Ehrlich's and Fleming's antibiotics, as well as their method of discoveries, *i.e.* large-scale and systematic screening (high-throughput screening in today's terms) and the use of inhibition zone respectively, signal the beginning of the 'modern antibiotic era' (64).

Within half a century following the introduction of ampicillin to the market, a wide array of antibiotics was rapidly discovered and introduced, and further classified into different structural classes, each targeting different parts of the bacterial cell. In general, antibiotics currently available functions either as bacteriostatic or bactericidal agents (65,66). Having a short doubling time, bacteria are able to accumulate mutations faster than other organisms, arguably shortening their evolution timeline as well. Any direct threat to bacteria survival would drive them to mutate and develop resistance. Coupled with horizontal gene transfer, resistance genes spread easily from species to species. Consequently, throughout the course of history, resistance genes or resistant strains were discovered nearly as fast as the introduction of the corresponding novel antibiotic, furthermore escalated by

the uncontrolled use of antibiotics in farming (64,67). Unfortunately, the last class of antibiotic was discovered in the 1980's, thus it is only a matter of time when all antibiotics used today would be obsolete—a situation that the modern media have labelled as 'the antibiotic apocalypse'.

The issue of antimicrobial resistance has captured the attention of government and health-related organisations across the globe. The European Centre for Disease Prevention and Control (ECDC) and the Centers for Disease Control and Prevention (CDC) created standardised terms to define different types of antibiotic resistance: multidrug-resistance (MDR) is resistance to at least one agent in three or more antimicrobial categories, extensively drug-resistance (XDR) is resistance to at least one agent in all but two or fewer antimicrobial categories, and pandrug-resistance (PDR) is resistance in all agents in all antimicrobial categories (68,69). In its 68th World Assembly, WHO recognised the severity of this issue by conceptualising five strategic objectives to combat MDR. One of the five objectives is the improvement of our understanding of antimicrobial resistance through research, including but not limited to understanding how resistance develops (70).

In addition to much needed government regulations to control antibiotic use, amongst the proposed solution is "antibiotic cycling", *i.e.* periodic replacement of front-line drugs with other structurally similar classes of compounds. However, this proves to be merely a short term solution as resistance genes are reselected when previous drugs are reintroduced (71). One recent example of such a case occurred upon the introduction of a novel fifth-generation cephalosporin of the β-lactam class, ceftaroline, in 2010 (72), which was followed by the isolation of resistant staphylococcus strain just a year after (results published in 2014) (73).

The most effective solution to the antimicrobial crisis is to create novel classes of antibiotics hitting either previously unexploited targets, or unexploited mechanisms regulating existing targets, due to the lack of resistance already developed (74). The bacteria two-component systems, particularly those involved in virulence expression, has been proposed as novel targets for a new antibacterial class (75,76). ***Figure 1.11*** illustrates possible interaction between inhibiting compounds and components of a classical two-component system.

Both natural and synthetic inhibitors of two-component systems have been identified. Oleic acid has been found to inhibit KinA phosphorylation in the sporulation regulation of *B. subtilis*, whereas bromoacetosyringone has been found to inhibit gene expression by a two-component system in *Agrobacterium tumefaciens* responsible for plant wound infection and tumor growth; both compounds do not affect bacterial growth (76). A number of synthetic compounds have also been identified as potential inhibitors, either by structure-based virtual screening (SBVS) or *in silico* screening, fragment-based drug discovery (FBDD), or high-throughput screening (76–79), furthermore solidifying the promising future of the two-component system as a potential antibiotic target.

Having obtained the understanding of how two-component signalling works allowed us to go a step further and create a functional synthetic biosensor for the purpose of high-throughput screening (explained in detail in Act III). One of the bottlenecks during synthetic receptor creation is controlling signal output to ensure that the receptor has a wide dynamic range. Aromatic tuning, discussed in the next chapter, could provide a solution to this issue.

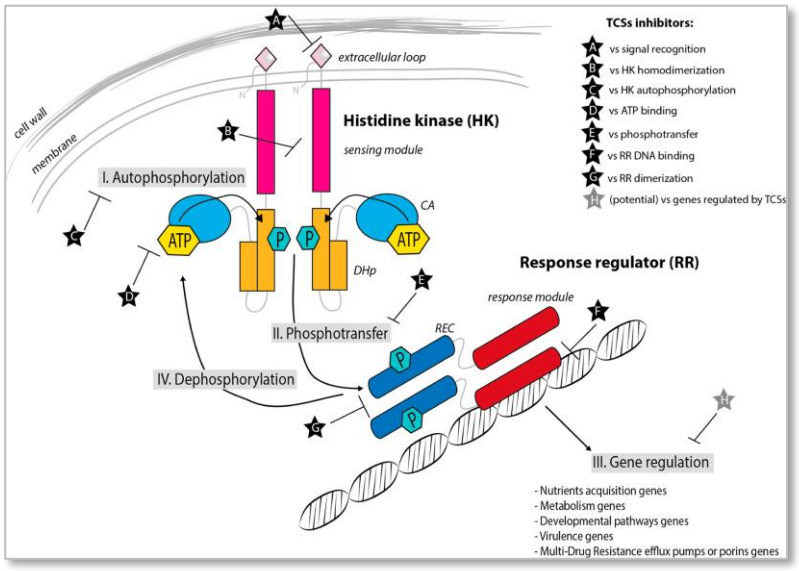

Figure 1.11. Predictions of possible targets of two-component system inhibitors.
Targets within the system are marked with stars. Inhibitors could either work on the histidine kinase side—signal recognition **(A)**, homodimerization **(B)**, autophosphorylation **(C)**, ATP binding **(D)**, or phosphotransfer **(E)**—or on the response regulator side—DNA binding **(F)**, dimerization **(G)**, or gene regulation **(H)**. *Image taken from* (79).

Chapter 2: Stimulus-Independent Modulation of the Two-Component System

2.1 Disclaimer

One of the biggest challenges in TCS research is controlling the signal output of the system, whether in a wild-type or synthetic system, especially in one such as EnvZ/OmpR where the direct physical interaction between input signal and receptor remains unknown. However, as evidence has been presented that structural conformation of transmembrane domain(s) correspond to a specific signal output, modulation of TCS output could then be conducted simply by moving aromatic residues in the TM domain, circumventing the need for an input signal; this method has been referred to as "aromatic tuning". This chapter was adapted from our publication (Yusuf and Draheim, 2015) that highlighted the practical use of this technique in synthetic microbiology.

2.2 Introduction

Two-component signalling circuits (TCSs) are a ubiquitous mechanism by which bacteria sense, respond and adapt to external stimuli. TCSs facilitate responses to a wide range of environmental parameters, such as ambient temperature, availability of nutrients or external osmolarity (80). Medically relevant multiorganism phenomena including quorum-sensing (81) and host-pathogen interaction are also governed by TCSs (82). Furthermore, these systems control essential agricultural and environmental processes such as chloroplast synthesis (83) and nitrogen fixation (84), which is involved in root nodule formation. More than 400,000 open reading frames (ORFs) believed to encode TCSs have been sequenced and annotated suggesting that these systems control a large number of processes that could be harnessed by synthetic microbiologists (85,86). Based on this premise, engineering TCSs with novel functionality is a very active field (87), especially because it has been recently shown that these modified systems can be systematically transferred to mammalian cells (88). However, rationally designing

TCSs, either by moving intact components from one microorganism to another or by forming chimeric components from the domains of two different proteins, can result in aberrant signal output or loss of stimulus-perception, or both (89). Here, an aromatic tuning methodology that has been established to circumvent these issues and is generally applicable to both native and rationally designed TCSs is described.

2.3 Biophysical and Biochemical Underpinnings of Aromatic Tuning

Aromatic tuning was conceived based on studies with peptides that possess an aliphatic core of Ala-Leu repeats flanked by Trp (WALP) or Tyr (YALP) residues ***(Figure 2.1-A)***. When these WALP (90) and YALP (91) peptides were mixed with various synthetic bilayers of an appropriate thickness they were shown to adopt a transmembrane α-helical confirmation based on circular dichroism (CD), ^{2}H NMR and ^{31}P NMR spectroscopy. Initially, hydrophobic mismatch, or differences between the length of the aliphatic core of these peptides and the thickness of the hydrophobic bilayer core was considered to be the crucial determinant in how α-helical peptides interact with the surrounding lipidic environment (90). Subsequently, it was shown that the contribution of interfacial anchoring, *i.e.* interactions between Trp residues flanking the aliphatic core and the polar/hydrophobic interfaces near the boundaries of a lipid bilayer, can dominate over the effects introduced by hydrophobic mismatch alone (92). Although this was only explicitly demonstrated for Trp residues, it was proposed that Tyr residues would also facilitate interfacial anchoring due to possessing similar physiochemical properties (92). This elegant series of biophysical experiments is summarized in ***Figure 2.1-A***. Addition of WALP or YALP peptides possessing a shorter distance between their flanking aromatic residues than the thickness of the hydrophobic core between the interfacial regions of a synthetic bilayer to which they are added results in induction of inverted hexagonal (H_{II}) phases that can be detected by ^{31}P NMR and sucrose density centrifugation (90–92). Conversely, when the distance between the aromatic residues was larger than the thickness of the hydrophobic core, the acyl chains within the bilayer became more ordered as determined by ^{2}H NMR,

demonstrating that the membrane is slightly expanding to accommodate these "longer" peptides (91,93). In essence, these experiments demonstrate that amphipathic aromatic residues, namely Trp and Tyr, possess affinity for the interfacial regions where the polar phospholipid headgroups attach to the hydrophobic acyl chains.

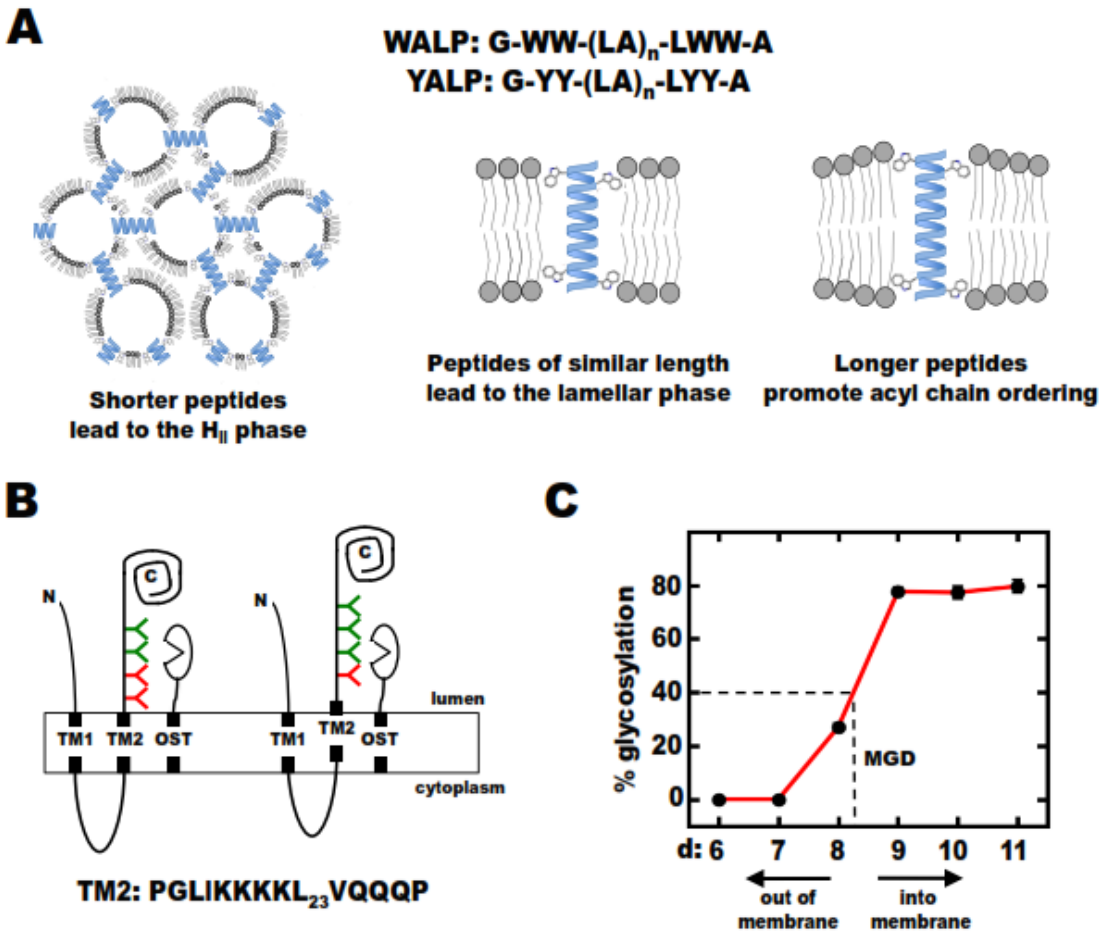

Figure 2.1. Schematic summary of the biophysical and biochemical evidence supporting the affinity of amphipathic aromatic residues for polar/hydrophobic interfaces.

(A) Mixing peptides consisting of a poly-Ala-Leu core of different lengths flanked by Trp residues (WALP peptides) with synthetic bilayers of different thicknesses demonstrates the affinity of the Trp residues for the polar/hydrophobic interfaces (90,91). When the distance between the Trp residues was sufficiently shorter than the distance between the polar/hydrophobic interfaces, the lipids adopted an inverted hexagonal (H_{II}) phase to accommodate interactions between the Trp residues and the interfacial regions (left panel). When the distance between the flanking aromatic residues was increased so that it matched the distance between the interfacial regions, a standard lamellar phase was observed (centre panel). As the distance between Trp residues was increased, the acyl chains became more

ordered suggesting a slight expansion of the bilayer to accommodate these "larger" peptides (right panel). Tyr-flanked peptides (YALP peptides) demonstrated similar effects (90,91). In essence, these results demonstrate that the aromatic residues found at the polar-hydrophobic interface are important for governing how the WALP/YALP peptides were positioned within the membrane. **(B)** Glycosylation-mapping analysis employs a Lep model protein with two TM helices (94). Segments to analysed are inserted at TM2 and a glycosylation-accepting site is positioned between 6 and 11 residues away from the luminal boundary of TM2. Glycosylation-accepting sites shown in green are distal enough to become glycosylated while those in red are not. Proximity of an accepting site to the active site of oligosaccharyltransferase (OST) correlated with the extent of glycosylation. Therefore, repositioning of TM2 will change these relative positions and hence the extent of glycosylation. **(C)** A schematic demonstrating calculation of minimum glycosylation distance (MGD). MGD simply indicates the number of residues required for half-maximal glycosylation. In this example, MGD is approximately 8.2. Repositioning of TM2 into the membrane will increase MGD, while outward displacements of TM2 result in a reduction of MGD. Previous changes in MGD have demonstrated that moving Trp residues about the luminal end of TM2 resulted in bidirectional, *i.e.* into and out of the membrane, displacement of the TM helix (95). These two sets of experimentation strongly suggested that moving aromatic residues within a full-length protein could alter how individual helices were positioned within the membrane. In the case of Tar, it was hypothesized that the signalling helix (TM2) could be repositioned within the membrane by moving the aromatic residues normally found at the cytoplasmic polar-hydrophobic interface (96).

From a biochemical perspective, another methodology, known as glycosylation mapping, also demonstrated the contribution of aromatic residues to positioning α-helices within a lipid bilayer (94). Glycosylation mapping utilizes the luminally positioned endoplasmic reticulum enzyme oligosaccharyltransferase (OST) to add a glycan to the Asn residue in Asn-Xaa-(Ser/Thr) glycosylation acceptor sites. In this manner, OST acts as a molecular ruler because each acceptor site will be glycosylated to an extent that correlates with the distance between the active site of OST and the acceptor site. In ***Figure 2.1-B***, the red acceptor sites are not far enough from the lumenal membrane to become glycosylated, whereas the green sites are distal enough to become glycosylated. From this information, minimum glycosylation distance (MGD), or the distance required to attain half-maximal glycosylation, can be determined as schematically shown in ***Figure 2.1-C***. These MGDs can then be compared between segments to determine whether any helix repositioning occurred. Upon comparison, a decrease in MGD suggests that luminal boundary of

TM2 has been displaced into the lumen, while an increase in MGD demonstrates that the TM2 boundary has been repositioned into the membrane ***(Figure 2.1-C)***. By creating a series of TM segments that are identical except for the position of the flanking aromatic residues at one end can be assessed for changes in MGD that can be assigned to the repositioning ability of those aromatic residues.

Changes in MGD have been reported when Trp residues are moved throughout the C-terminal half of a poly-Leu transmembrane segment (95), thereby demonstrating that directional repositioning of the TM segment is due to the affinity of Trp residues for the polar/hydrophobic interfaces ***(Figure 2.1-B)***. In a slightly modified version of this assay that considers all possible positions within the TM helix, Tyr residues where shown to possess character similar to Trp residues (97). Taken together, before aromatic tuning was conceived, previously existing biophysical and biochemical evidence suggested that Trp and Tyr residues possess affinity for the polar/hydrophobic regions located within membranes and suggested that moving them within an intact membrane-spanning protein could reposition individual TM helices.

2.4 Aromatic Residues at The Ends of Tar TM2 Govern Its Position in The Membrane

With the aforementioned biophysical and biochemical evidence suggesting that moving flanking aromatic residues could reposition a TM helix within an intact protein, it was necessary to select an initial bacterial membrane-spanning receptor in which to examine the role of these residues in governing signal output. The aspartate chemoreceptor of *E. coli* (Tar) was chosen because it governs a well-characterized downstream signalling pathway. It is important to note that Tar is not a canonical sensor histidine kinase (SHK), requires CheW and CheA to form functional intracellular signalling complexes, and controls flagellar rotation rather than gene transcription ***(Figure 2.2-A)*** (98–102). When aromatic tuning of Tar was originally undertaken, the mechanistic models for transmembrane signalling were based upon piston-type displacements of the second transmembrane helix (TM2) (96,103–107). This model proposes that displacement of TM2 toward the cytoplasm occurs upon binding of cognate ligand, *i.e.* aspartate, to the periplasmic domain

(Figure 2.2-B). Binding of aspartate results in squelched CheA kinase activity, which, in turn, reduces the intracellular level of phospho-CheY that promotes counterclockwise (CCW) flagellar rotation *(Figure 2.2-B)*. Phospho-CheB, also phosphorylated by CheA, is the active form of the methylesterase and is also found in reduced intracellular levels upon binding of aspartate to Tar. This results in an increase in the extent of methylation within the cytoplasmic domain of Tar, which allosterically counteracts the effect of aspartate binding and leads to restoration a normal flagellar rotational bias *(Figure 2.2-C)*. One advantage to initially employing this signalling circuit was that each of these activities could be independently assessed to determine whether changes in Tar signal output has occurred. For example, it is possible to monitor CheA kinase activity *in vitro* without the complicating effects of covalent methylation (96,99,103). Likewise, the extent of methylation can be examined *in vitro* in the absence of CheA kinase activity (106). Finally, flagellar rotation can be examined in vivo, which will allow for determination of when signal output from Tar is biased beyond the compensatory range of methylation (96,103).

Armed with these outputs to monitor changes in Tar signaling, initial arginyl- and cysteinyl-scanning mutagenesis of Tar TM2 from *Salmonella enteritica* serovar Typhimurium was performed and resulted in several mutations that highlighted the importance of aromatic residues in governing helix position within the cytoplasmic membrane (106). Large changes in signal output consistent with a displacement of TM2 toward the periplasm, similar to those observed in the apo conformation of Tar, namely increased CheA kinase activity and decreased methylation, were observed when either Phe-189 or Trp-192 was replaced with an Arg residue at the periplasmic end of TM2. This was also seen when Phe-189 was replaced with a Cys residue. Conversely, reduced kinase activity and increased levels of covalent methylation, both consistent with the aspartate-bound confirmation of Tar, were observed when Trp-209 was replaced with Arg (106). Independently, the importance of Trp-192 and Trp-209 in maintaining baseline signal output from *E. coli* Tar was demonstrated when they were substituted for alanyl residues (103). In the case of the Tar W192A variant, the receptor was undermethylated and exhibited higher signal output,

consistent with apo state and displacement of TM2 toward the periplasm. In contrast, the W209A mutant was overmethylated and possessed reduced signal output, suggesting a displacement of TM2 toward the cytoplasm as proposed to occur within the aspartate-bound confirmation. In summary, these results demonstrate that aromatic residues within TM2 of Tar are critical for maintaining normal signal output and suggest that they govern the baseline position of the helix within the membrane to an extent that could be employed to manipulate Tar signal output.

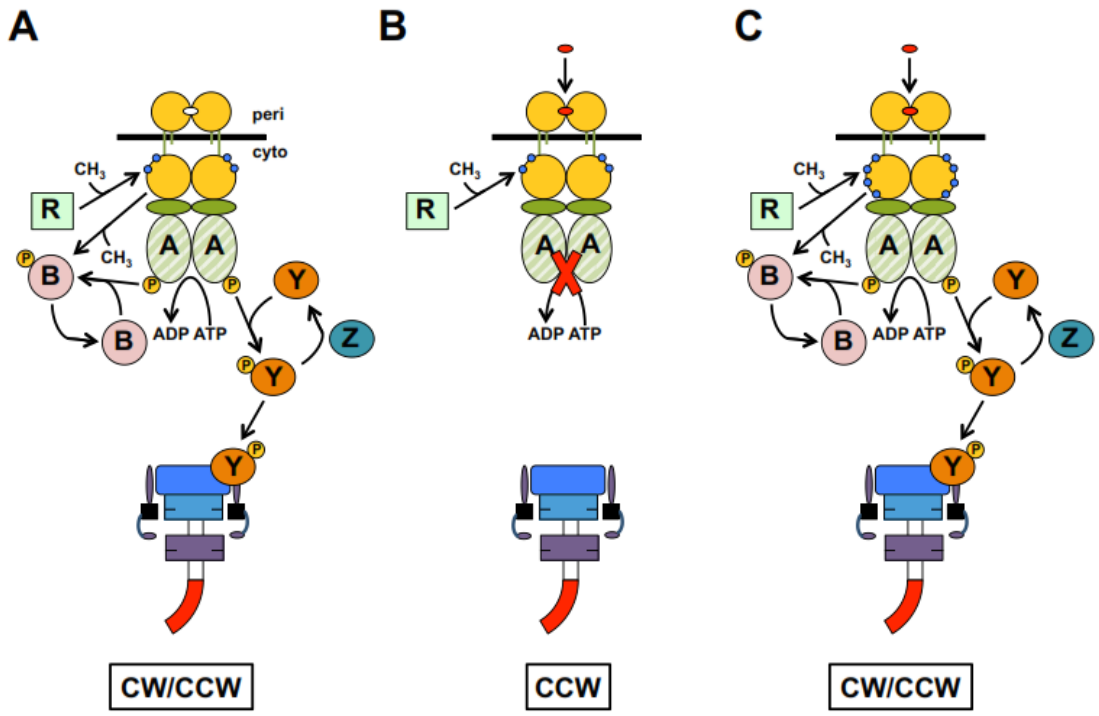

Figure 2.2. The chemotactic circuit underlying control of flagellar rotation.
(A) In the absence of chemoeffectors, baseline CheA activity maintains phspho-CheY levels that produce the three-dimensional random walk underlying canonical bacterial chemotaxis. **(B)** Binding of attractant (red oval in the periplasm; peri) to the chemoreceptor, *i.e.* aspartate to Tar, abolishes CheA activity, thereby decreasing intracellular phospho-CheY levels. This also results in reduced methylesterase activity due to reduced CheB-P levels. Transmembrane communication (across the black line) is believed to occur via a piston-type displacement of TM2 toward the cytoplasm (cyto; center panel). **(C)** Adaptive methylation (blue dots in the cytoplasm) due to reduced CheB-P levels, restores the ability of the chemoreceptor to stimulate CheA activity when it is occupied by an attractant ligand (100). In summary, this circuit was an excellent initial target for aromatic tuning because binding of attractant leads to displacement of TM2 toward the cytoplasm, reduced CheA kinase activity and increased levels of covalent modification. Conversely, displacements of TM2

toward the periplasm are consistent with increased CheA activity and reduced levels of covalent modification. In addition, signal output from Tar that is biased beyond the compensatory extent of methylation can be detected by monitoring rotation of individual flagella.

2.5 Incremental Tuning of Tar Signal Output

Based on the contributions of the individual aromatic residues to maintenance of signal output and the biophysical and biochemical data described above, it was originally hypothesized that aromatic tuning would displace TM2 of Tar within the membrane in a step-wise manner (96). To examine this hypothesis, a series of Tar receptors was created in which the Trp-Tyr tandem found at the cytoplasmic end of TM2 was moved up to three residue steps in either direction ***(Figure 2.3-A)***.

Previous results show that the intracellular concentration of CheY-P governs the clockwise flagellar (CW) rotational bias ***(Figure 2.3-B)***. Therefore, Tar signal output could be estimated from the aromatically tuned variants by monitoring flagellar rotation. To accomplish this, individual flagella from single *E. coli* cells were monitored for 20 seconds and classified into one of five categories that represent increasing levels of intracellular CheY-P: those rotating exclusively CCW, flagella rotating mostly CCW with occasional switching to CW rotation, flagella rapidly switching between CCW and CW with no inherent bias, flagella rotating mostly CW with occasional switching to CCW rotation, and finally those that rotate exclusively CW (96). When flagella from cells expressing the aromatically tuned variants described in ***Figure 2.3-A*** were analysed, a clear shift from a majority of CCW to CW rotational bias was observed as the aromatic residues were moved from WY-3 toward WY+3 ***(Figure 2.3-C)***. This indicates that the signal output from the minus-series of tuned Tar variants (*i.e.* WY-3 to WY-1) was so far biased toward reduced signal output that the compensatory action of covalent methylation failed to completely overcome this signalling bias. Conversely, the WY+2 and WY+3 variants were biased toward increased signal output to the extent that methylation could also not compensate. As expected, in the absence of receptor (-ctrl), only CCW rotation was observed ***(Figure 2.3-C)***. It is also important to note that, as predicted,

overmethylation of Tar was observed for the minus-series (WY-3 to WY-1) of receptors, while undermethylation was seen for the plus-series (WY+1 to WY+3) of aromatically tuned variants (96). When taken together, these results demonstrate that signal output from Tar is modulated in an incremental manner when the aromatic residues were moved at the cytoplasmic end of TM2.

While these results served as an interesting foray into aromatic tuning, they do not empirically demonstrate that moving the aromatic residues at the cytoplasmic end of TM2 results in a physical repositioning of the helix. Therefore, two subsequent studies, one computational and one biophysical, were performed to assess repositioning of Tar TM2 upon moving the Trp-Tyr tandem. Coarse-grained molecular dynamics (CG-MD) simulations that were employed to examine the ability of aromatic tuning to displace Tar TM2 in the presence of an explicit membrane and solvent demonstrated that moving the Trp-Tyr residue was sufficient to induce small TM2 displacements of up to 1.5 Å (108). In addition, the glycosylation-mapping assay described above ***(Figure 2.1-B* and *C)*** was performed in order to determine whether moving the Trp-Tyr pair at the end of TM2 would yield analogous results in a biological membrane. Assuming that the region in Lep that contains the glycosylation-accepting site is in an extended conformation, a shift in MGD of 0.5 residues as seen for the Tar constructs corresponds to a shift in the positioning of the TM2 helix of 1.6-1.7 Å (109), in close agreement with the CG-MD results described above (108). Furthermore, within both the CG-MD simulations and MGD analysis, similar patterns of displacement were observed. A grouping of the minus-series of receptors with similar displacements toward the cytoplasm (WY-3 through WY-1), a baseline position for the wild-type (WY 0), two receptors that are slightly displaced toward the periplasm (WY+1 and WY+2) and a larger shift toward the periplasm for the WY+3 variant was observed with both techniques. Therefore, this combination of *in vivo, in vitro* and *in silico* results demonstrate that repositioning the Trp-Tyr tandem at the cytoplasmic end is sufficient to generate a physical displacement of TM2 and the resulting modulation of Tar signal output in an incremental manner.

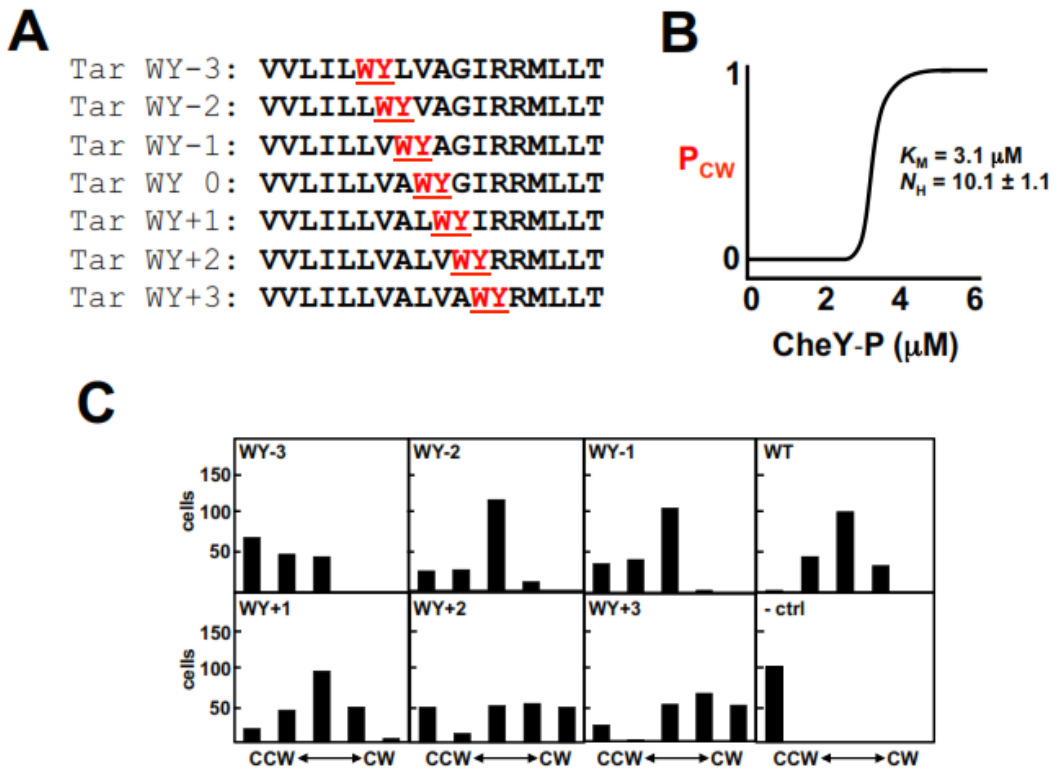

Figure 2.3. Incremental tuning of signal output from the aspartate chemoreceptor of *E. coli* (Tar). **(A)** At the C-terminal end of Tar TM2, a Trp-Tyr (red) was moved about its original position at the cytoplasmic polar/hydrophobic interface (96). **(B)** The intracellular level of CheY-P governs the probability of clockwise flagellar rotation (PCW). Previous results demonstrate that increased intracellular CheY-P levels lead to an enhanced probability of CW rotation. In these experiments, a sharp transition was observed, *i.e.* a Hill coefficient of more than 10 (110). **(C)** Rotation of a single flagellum from roughly 200 independent *E. coli* cells expressing one of the aromatically tuned variants were analysed and classified into one of five categories (from left to right): rotating exclusively CCW, rotating primarily CCW with occasional reversals, rapidly switching between both rotational directions (CW/CCW), rotating primarily CW with occasional reversals and those rotating exclusively CW. As Tar signal output increases, the number of cells in each category shifts from CCW toward CW rotational bias. In summary, the lowest overall signal output was observed from cells expressing the WY-3 variant, while the greatest was observed from cells expressing the WY+2 or WY+3 variants. Therefore, in the case of Tar, the absolute vertical position of the aromatic residues correlates with signal output (96).

2.6 Non-Incremental Tuning of EnvZ Signal Output

In order to determine whether aromatic tuning would work within a canonical SHK, its effectiveness was examined within the major *E. coli* osmosensor (EnvZ), where a rotation of TM2 was initially proposed as the mechanism of transmembrane communication (111–115). More recently, a regulated folding/unfolding model on the region connecting the sensor and output domains (116) has been suggested, in which SHKs are modular proteins composed of individually folding domains that each contribute a distinct functionality. Regulated unfolding suggests that the effector domain within an SHK is maintained in an inactive conformation by a rigid connection between the stimulus perception and effector domains. Upon perception of stimulus, this connection disengages allowing the effector domain to adopt an active conformation (116). This region connecting the TM to the cytoplasmic domain in bacterial receptors is colloquially referred to as a "control cable" because its residue composition governs coupling of signal transduction between adjacent domains (96,103,117–124).

EnvZ is a canonical SHK that responds to changes in the extracellular osmolarity of inner-membrane impermeable compounds by modulating the intracellular level of phosphorylated OmpR ***(Figure 2.4-A)*** (125–128). In a laboratory environment, EnvZ signal output is modulated by simply adding sucrose to the bacterial growth medium. Subsequently, phospho-OmpR regulates the transcription of a number of genes, including those encoding two outer membrane porins, OmpF and OmpC. At low intracellular levels of phospho-OmpR (OmpR-P), transcription of ompF is upregulated, whereas at higher levels of OmpR-P, transcription of ompF is repressed and transcription of ompC is activated. This results in a predominance of OmpF at low osmolarity and OmpC at higher osmolarities ***(Figure 2.4-B)*** (129–131). The easily controllable nature of the input stimulus, *i.e.* addition of sucrose, and the well-characterized transcriptional output made the EnvZ/OmpR osmosensing circuit an ideal choice for examining aromatic tuning within an SHK.

To analyse steady-state signal output from EnvZ/OmpR osmosensing circuits containing aromatically tuned receptors, a two-color fluorescent reporter strain was

employed. This E. coli strain possesses transcriptional fusions of *cfp* to *ompC* and of *yfp* to *ompF* within its chromosome ***(Figure 2.4-B)*** (132). Quantifying the ratio of CFP to YFP fluorescence provides a rapid and sensitive measure of the ratio of *ompC* to *ompF* transcription, which estimates the intracellular level of phosphoylated OmpR. Therefore, the ratio of CFP to YFP can be employed to estimate signal output from the aromatically tuned EnvZ variants. To confirm this, we previously demonstrated that the transcription of CFP and YFP behaved as expected upon addition of sucrose to the growth medium ***(Figure 2.4-C)*** (86).

Due to the proposal of non-piston signalling mechanisms, it was difficult to predict what pattern of signal outputs would be observed upon aromatic tuning of an SHK. In the case of EnvZ, a Trp-Leu-Phe triplet was moved from five residues into the membrane (WLF-5) through two residues out of the membrane (WLF+2) in single residue steps ***(Figure 2.4-D)***. In this case, the surface of TM2 that the aromatic residues reside upon was found to be the major determinant of EnvZ signal output rather than their absolute vertical position as was the case with Tar ***(Figure 2.4-E)*** (86). These results clearly demonstrated that even though a different mechanism of transmembrane communication has been proposed, aromatic tuning remained successful in modulating signal output. Similar results were obtained with a Trp-Tyr-Ala triplet that is more similar to the Trp-Tyr tandem employed during tuning of Tar suggesting that in the case of EnvZ, the composition of the residues that are moved is not a major determinant in the pattern of signal output (86). However, additional experimentation is required to support the concept that disturbance of a particular helical surface is the cause of changes in EnvZ signal output. It should also be noted that these different patterns of signal output modulation are not surprising given that the concept of various signalling mechanisms being employed by different subclasses of bacterial receptors has been recently put forward (133–135). Therefore, regardless of whichever signalling mechanism is employed by a receptor aromatic tuning may be successful in modulating signal output.

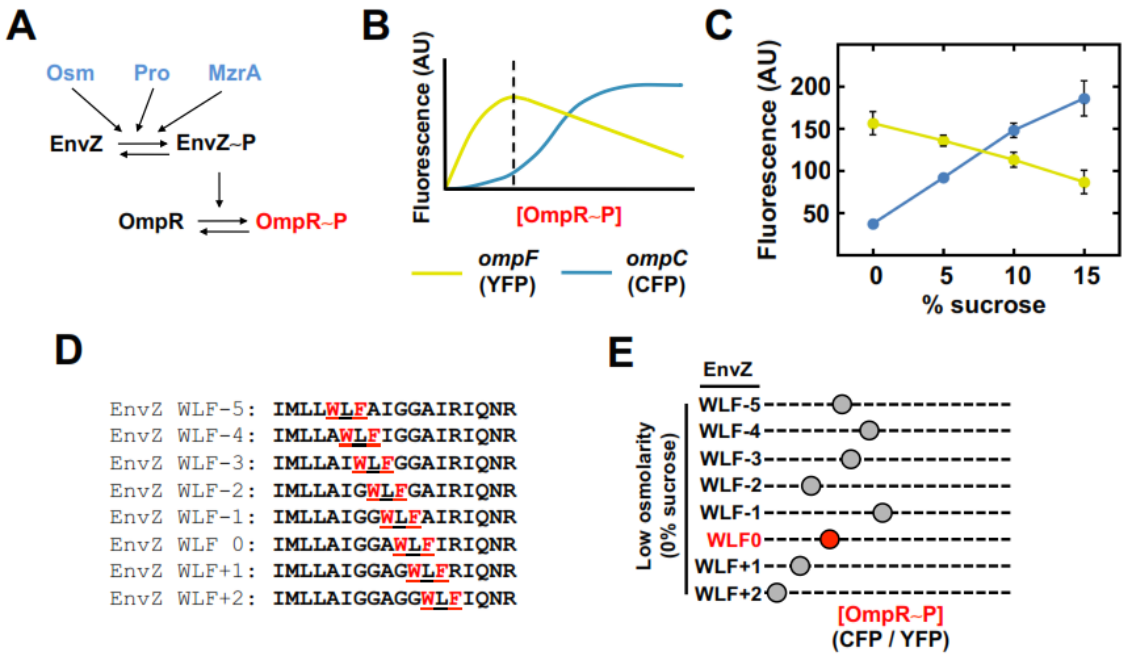

Figure 2.4. Non-incremental tuning of signal output from the major osmosensor of *E. coli* (EnvZ). **(A)** EnvZ is bifunctional and possesses both kinase and phosphatase activity. The ratio of these activities is modulated by several factors including the presence of extracellular osmolarity (34,136), procaine (137) or MzrA (8,138). OmpR serves as the cognate RR of EnvZ and the intracellular level of phosphorylated OmpR (OmpR-P) in governed by EnvZ activity. **(B)** OmpR-P levels control transcription of *ompF* and *ompC* which can be monitored by employing an E. coli strain that contains a transcriptional fusion of *yfp* to *ompF* (yellow) and of *cfp* to *ompC* (blue) (86). Intracellular levels of OmpR-P can thus be estimated by monitoring the CFP/YFP ratio (red). **(C)** Experimental results demonstrating that increasing sucrose levels in the growth medium resulted in increasing levels of CFP, decreasing levels of YFP and an increase in the CFP/YFP ratio. The black dashed line in ***Figure 2.4-B*** represents signal output from this strain upon growth in medium with no additional sucrose. **(D)** When aromatic tuning was performed in EnvZ, a Trp-Leu-Phe triplet (red) was repositioned within the C-terminal region of TM2. **(E)** The gray-filled circles on the dashed lines indicate the estimated OmpR-P levels in cells expressing one of the aromatically tuned variants. Aromatic tuning in EnvZ resulted in a pattern of signal output that did not correlate with the absolute vertical position of the aromatic residues, as was the case with Tar, but rather appeared approximately helical in distribution suggesting that the surface of TM2 that the residues were located upon was of greater importance (109). However, the key outcome is that aromatic tuning was still successful with respect to modulating EnvZ signal output in a stimulus-independent manner.

Glycosylation mapping experiments with TM2 of EnvZ demonstrated that moving the Trp-Leu-Phe triplet resulted in almost no change in MGD. An exception was observed for WLF-3, which is most likely a specific case where the positive charge within the side-chain of Arg-182 would not be able to interact with the headgroups of the membrane any longer due to it being displaced very far out of the membrane. Therefore, in the case of most aromatically tuned EnvZ segments, changes in MGD are very small and not steadily increasing in contrast to what was observed with the aromatically tuned Tar TM2 segments (109). Initial CG-MD analysis with these aromatically tuned EnvZ segments also does not support incremental displacement (B. Hall, MRC Cancer Unit, personal communication).

2.7 Employment of Aromatic Tuning Within a Wide Variety of Membrane-Spanning Receptors

Aromatic tuning was successful in modulating signal output from both Tar and EnvZ, however, a difference in the pattern of signal outputs was observed (86,96). This pattern of signal outputs shows that even through aromatic tuning did not displace the TM2 helix of EnvZ (109), it was still effective in modulating signal output from the full-length receptor in vivo. Aromatic tuning has also been successfully employed in two different Tar-EnvZ chimeric receptors (Lehning and Draheim, unpublished observations), when a Trp-Tyr tandem was used, and within a NarX-Tar chimera (Reinhard and Draheim, unpublished observations), when a single Trp residue was moved.

Published sequence alignments demonstrate that aromatic residues are often found at the cytoplasmic end of the final transmembrane helix within bacterial membrane-spanning receptors (103,139) suggesting that aromatic tuning could be useful for research groups working with other two-component circuits. It is important to note that the majority of aromatically tuned Tar, EnvZ and chimeric receptor variants retain the ability to respond to stimulus suggesting that their signal output is biased but not locked in either a stimulus-deprived or a stimulus-saturated conformation. In this regard, aromatic tuning is advantageous compared to deletion

of entire SHKs (140) or substitution of the conserved His residue involved in autophosphorylation and phosphotransfer because these methods may result in complete loss of kinase or phosphatase activity, which has been shown to result in non-physiological cross-talk between various two-component signalling pathways within a cell (141,142). Thus, by apparently biasing, rather than abolishing activity and stimulus-perception, aromatic tuning represents a significant improvement over previous attempts at stimulus-independent modulation of signal output. Even though these initial attempts have been successful, it remains important to note that we have only observed aromatic tuning in membrane-spanning receptors that possess two TM helices. However, we have concluded based on previous studies that in the case of SHKs containing only two TM helices, that aromatic tuning will facilitate stimulus-independent modulation in the majority of cases. Furthermore, we are currently expanding our range of targets to include SHKs that possess more than two TMs such as AgrC from Staphylococcus aureus that has recently been shown to possess seven TMs (143).

In addition to rectifying issues with signal output or stimulus-perception, we believe that aromatic tuning has other potential uses. For example, the input stimulus has been identified for only a small fraction of SHKs, thereby making it challenging to investigate downstream signalling pathways without extensive mutagenesis and subsequent screening for changes in phenotypic output. Aromatic tuning could be employed to circumvent these limitations and allow manipulation of signal output from a specifically targeted SHK. One potential use would be the rapid assignment of downstream physiological and developmental processes to particular SHKs. Each SHK within an organism could be independently subjected to aromatic tuning and subsequent monitoring for the phenotype of interest. If the appearance of the phenotype correlated with aromatic tuning of a particular SHK, this would suggest that the desired phenotype is governed by the aromatically tuned receptor. In addition to assignment of phenotypes to specific SHKs, aromatic tuning could be employed to facilitate induction of medically relevant bacterial phenotypes in the absence of complex host-pathogen interactions, thus reducing the burden of complex interkingdom laboratory model systems. Finally, aromatic tuning of individual SHKs

could be coupled with pre-existing transcriptional reporter libraries (144) rather than observable phenotypes, to rapidly unravel the signalling pathways governed by each SHK. This would facilitate rapid and cost-effective organism-level signal pathway mapping.

Chapter 3: Project Goals

Taking into consideration the information elaborated in Chapter 1 and 2, here several approaches to solve questions still lingering in EnvZ signalling, specifically regarding the role of its transmembrane domain, is proposed. Furthermore, an exploration of how the system could be used to solve a current issue in Microbiology, in this case the urgent need for new antibiotics, is presented.

3.1 Hypotheses

1. The transmembrane domains of EnvZ employ a specific pattern of movement as they transfer signal from the periplasm to the dimerization/histidine-phosphotransfer domain.
2. EnvZ is a versatile receptor that could be used as a template to create synthetic receptors for various purposes.

3.2 Aims

1. To connect the relationship between input signal (osmotic shifts) and the signal output by mapping the movement of individual EnvZ transmembrane helices.
2. To design the chimeric magnesium sensor, PhoQ-EnvZ (PhonZ), that is able to produce a dose-responsive steady state signal.

3.3 Objectives

Act II: EnvZ Transmembrane Signalling Study

1. Constructing a library of single-Cys containing EnvZ in EPB30 cell lines;
2. Mapping the movement of transmembrane helices during signalling and tracking the corresponding the signal output;

3. Analysing the typical pattern of movement of transmembrane helices with respect to its position in the membrane in the presence and absence of stimulus.

Act III: Construction of Functional Chimeric Receptor, PhoQ-EnvZ (PhonZ)

4. Designing the *phonZ* gene by fusing genes encoding the sensory part of PhoQ with the catalytic part of EnvZ, and then inserting this new gene fragment in EPB30/pRD400 to enable quantification of signal output;
5. Characterising PhonZ receptor expression via immunoblotting analysis and signal output via fluorescence analysis;
6. Aromatically tuning the PhonZ receptor to achieve a dose-response signal output with a wide dynamic range.

Act II:
The Pas de deux of Transmembrane Helices

Chapter 4: Background

As mentioned in Chapter 1.3, the role of transmembrane helices during EnvZ signalling has been subject of much debate. Here, our approach in investigating this matter is explained.

4.1 Redefining the EnvZ/OmpR System

The *E. coli* strain used in this study is EPB30, which contains chromosomal *envZ* deletion and reporter proteins *cfp* and *yfp* fused into *ompC* and *ompF*, respectively ***(Figure 4.1)***. EPB30 was generated by deleting *envZ* from MDG147, whereas MDG147 was generated by introducing translational fusions of fluorescence protein genes *cfp* to *ompC* and *yfp* to *ompF* in the chromosome of the commonly used laboratory wild-type strain, K-12 MG1655 (132). The use of plasmid pEnvZ (145) allows for IPTG inducible expression of EnvZ, in addition to growth in ampicillin-resistance selective media. Modifications to this plasmid including a seven-residue linker (GGSSAAG) and a C-terminal V5-tag to the *envZ* gene resulted in plasmid pRD400 (86). ***Figure 4.2*** highlights important features within pRD400 that were relevant to this project.

Chromosomal fusion of genes encoding the fluorescence proteins CFP and YFP to porin genes, *ompC* and *ompF*, respectively, allows direct quantification of EnvZ/OmpR signal output with respect to porin levels controlled by OmpR ***(Figure 4.1-A)***. Ideally, an increase in external osmolarity would result in increase of cyan fluorescence protein (CFP) and decrease of yellow fluorescence proteins (YFP) ***(Figure 4.1-B)*** as OmpF dominates at low osmolarity and OmpC dominates at high osmolarity.

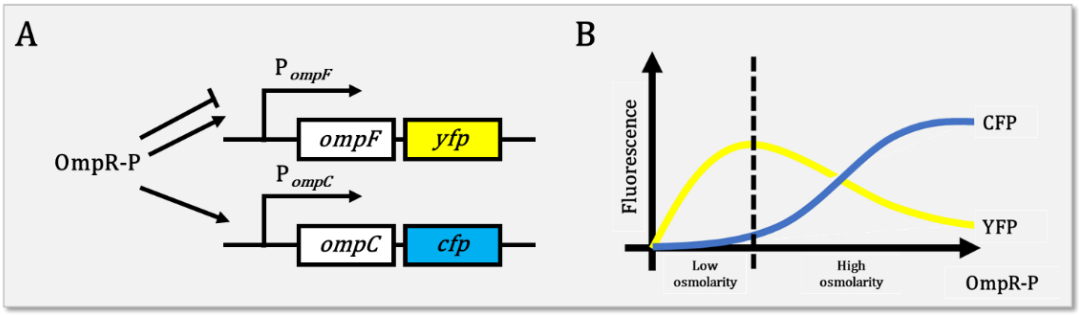

Figure 4.1. Translational fusion of fluorescence protein genes *yfp* and *cfp* to *ompF* and *ompC* within *E. coli* strain K-12 MG1655.
These outer membrane porin genes are controlled by phosphorylated OmpR **(A)**, which results in this steady state pattern of YFP and CFP levels **(B)**.

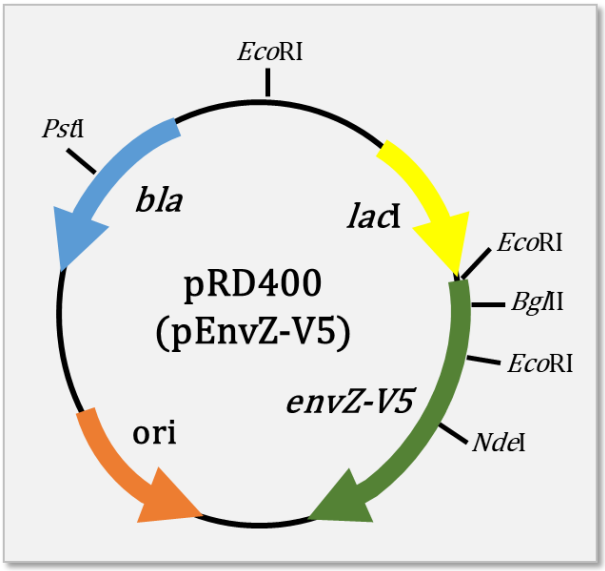

Figure 4.2. Schematic map of pRD400 containing an IPTG-inducible envZ gene with the V5-epitope tag.
The important features used in this project highlighted in coloured arrows: envZ-V5 (green) fused to the lac operon (yellow), ampicillin resistance (blue) and the origin of replication (orange).

To summarise our synthetic system, ***Figure 4.3*** depicts the EnvZ/OmpR two-component system as it works within EPB30/pRD400. EnvZ controls the level of intracellular OmpR-P as it follows the fluctuation of extracellular osmolarity. (Auto) phosphorylated EnvZ maintains a low level of OmpR-P under low osmolarity to ensure constant presence of OmpF on the outer membrane. The promotors of porin genes *ompF* and *ompC* consist of four binding sites for *ompF* with decreasing affinity (F1 > F2 > F3 > F4) and three binding sites for *ompC* with decreasing affinity (C1 > C2 > C3), with F-binding sites having higher affinity than C-binding sites (146).

Under low osmolarity, OmpR-P binds to F1, F2 and F3 sites of the *ompF* promoter, causing high expression of OmpF and YFP. C1 has a higher affinity to OmpR-P than F4, therefore a low amount of the transcription factor would bind to C1, resulting in low expression of OmpC and CFP. When osmolarity is high, OmpR-P would bind to all sites on the *ompF* promoter and all sites on the *ompC* promoter. OmpR-P on F4 would loop and bind with OmpR-Ps on F2 and F3, thus repressing *ompF* transcription (147). Meanwhile, *ompC* and *cfp* are highly transcribed.

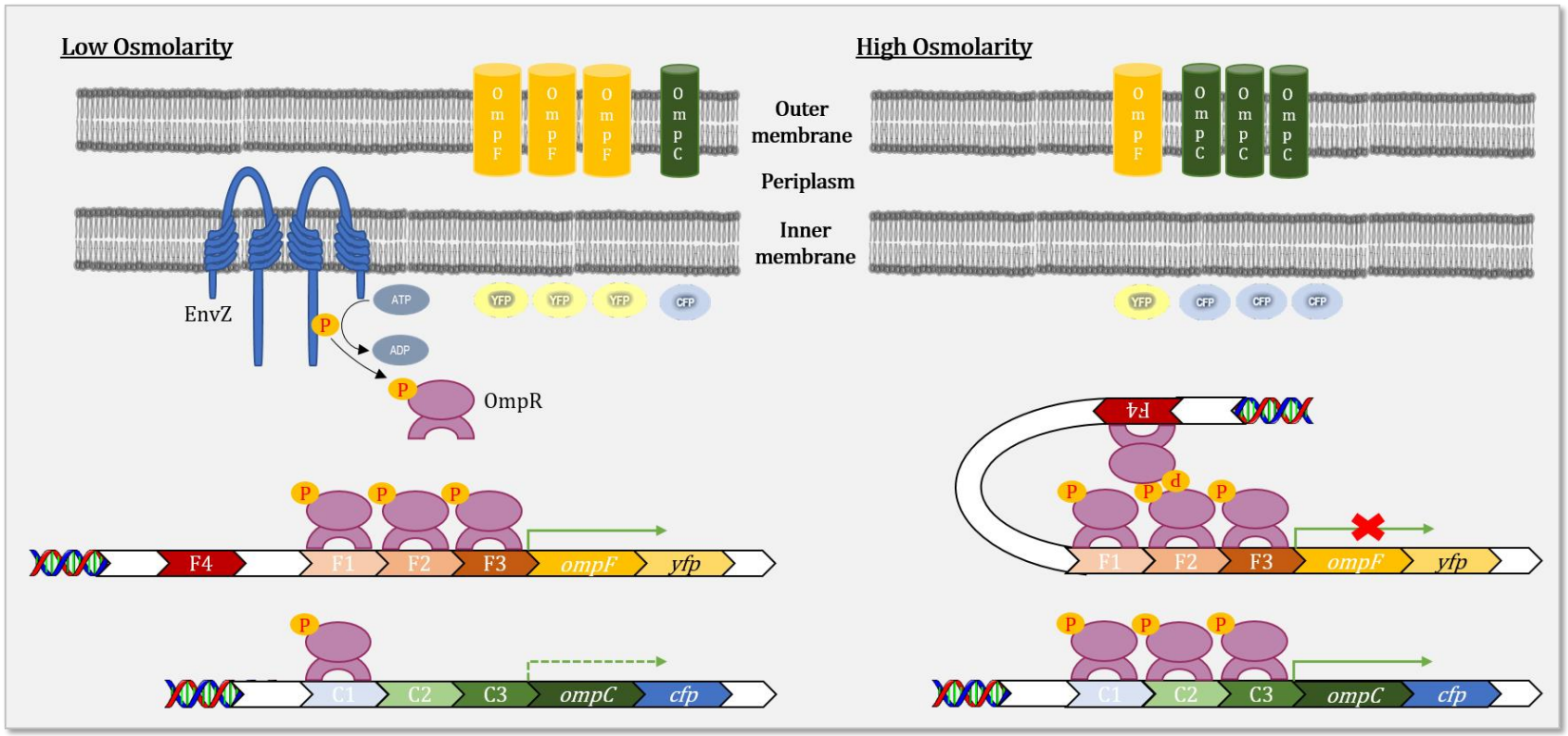

Figure 4.3. The EnvZ/OmpR system within EPB30/pRD400 when grown in low and high osmolarity media.
EnvZ autophosphorylates and transfers the phosphate to OmpR. Under low osmolarity, OmpR-P binds to the F1, F2 and F3 binding sites of the *ompF* promoter, prompting high levels of OmpF on the membrane and subsequently, YFP. Some OmpR-P bind to C1 of the *ompC* promoter, producing low expression of OmpC and CFP. As osmolarity increases, more OmpR-P is formed, which eventually bind to all sites of the *ompF* promoter, creating a loop which represses *ompF* transcription. Meanwhile, OmpR-P also binds with all sites of the *ompC* promoter, thus increasing the level of OmpC and CFP. *Image adapted from* (59,146,147).

4.2 Mapping Patterns of Helical Interaction via Sufhydryl Reactivity Studies

The first part of the work presented in this thesis addressed the relationship between EnvZ transmembrane structure and signal output by creating a library of EnvZ containing single-Cys positioned along the transmembrane domains to map out movements in the domains as osmolarity changes. The transmembrane region selected to be replaced by cysteine residues is shown in ***Figure 4.4***, while the process of selection for these residues are explained in detail in the Chapter 5.2.

Disulphide cross-linking to analyse conformational changes of transmembrane helices have been employed numerously in the past to track the relative movement of helices within the TM domain. Protein structure, correlation between the movements of transmembrane helices and signalling output have been observed and used to predict models representing those movements (40,148–150).

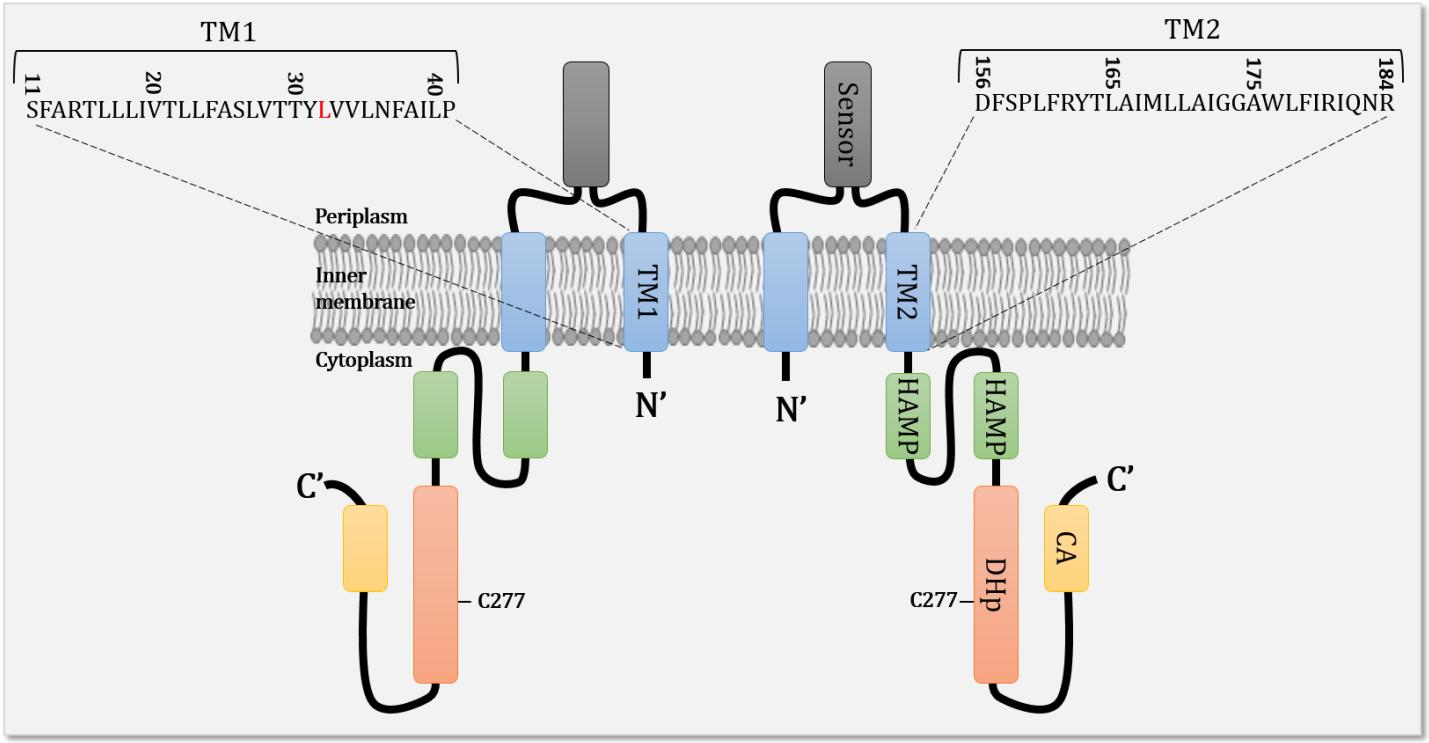

Figure 4.4. Schematic map of EnvZ domains highlighting residues being modified during the Cysteine crosslinking experiment.
The focus of the experiment was the interaction between the transmembrane (TM) helices, specifically residues 11 to 41 at TM1 and 156 to 184 at TM2. Native Cys residue at position 277 was replaced by Ala. Leu at position 32 (TM1) was unable to be replaced by Cys, therefore expression and signal output analysis of the mutant EnvZ-V5-L32C was not presented in our results.

Chapter 5: Materials & Methods

This chapter explains the techniques used to study transmembrane signalling of EnvZ, starting from domain characterisation to the use of sulfhydryl-reactivity combined with immunoblotting to analyse receptor movement, or with fluorescence spectrophotometry to analyse signal output.

5.1 Bacterial Strains and Plasmids

Escherichia coli strain DH10B (New England Biolabs) or MC1061 [F- *hsdR2*(rK$^-$ mK$^+$) *mcrA0 mcrB1*] (151) was used for all DNA manipulations, while strain K-12 MG1655 (F- λ- *ilvG rfb50 rph1*) (152) was used to control for light scattering and cellular autofluorescence. *E. coli* strains MDG147 [MG1655 Φ(*ompF*$^+$-*yfp*$^+$) Φ(*ompC*$^+$-*cfp*$^+$)] (132) and EPB30 (MDG147 *envZ::kan*) (153) were used for analysis of steady-state signal output from osmosensing circuits. Plasmid pRD400 (86) retains the IPTG-based induction of EnvZ originally present in plasmid pEnvZ (145) while also encoding a seven-residue linker (GGSSAAG) (154) and a C-terminal V5 epitope tag (GKPIPNPLLGLDST) (155). As the C-terminus of bacterial receptors can be sensitive to the presence of an epitope tag, we previously ensured that the addition of a V5-epitope tag did not alter the signaling properties of EnvZ (86,156). Plasmid pEB5 (157) served as an empty control vector that does not express EnvZ.

5.2 Selection of Residues Comprising TM1 and TM2 of EnvZ

The primary sequence of EnvZ (NP_417863.1) from *Escherichia coli* K-12 MG1655 was subjected to a full protein scan with DGpred using a minimal window of 9 residues and a maximal window of 40 residues (97). This software searched for putative TM helices by employing a sliding window of variable lengths and calculating the ΔGapp for transmembrane insertion throughout the length of the sequence and suggested that residues between Phe-12 and Val-34 comprise TM1, whilst Leu-160 and Ile-181 comprise TM2. Alternatively, a software package that identifies TM helices with a Markov model (TMHMM v2.0) (158) was employed and

suggested that the residues between Thr-15 and Phe-37 compose TM1, whilst Leu-160 and Ile-179 compose TM2. In both cases, a motif commonly found within TM helices that consisted of positively charged residues and adjacent aromatic resides bracketing a core of aliphatic residues was found within the putative TM segments (159). Based on these observations and to maximize the probability of including all residues within the TM domains, we elected to target all residues between positions 11 to 41 for TM1 and 156 to 184 for TM2 in the creation of a library of single-Cys-containing EnvZ receptors.

5.3 Analysis of EnvZ Signal Output *In Vivo*

Bacterial cultures were grown as described previously (86) with slight modifications. Briefly, MDG147 or EPB30 cells were transformed with pRD400 expressing EnvZ that contains a Cys residue at the desired position or pEB5, as required. Fresh colonies were used to inoculate 2 ml overnight cultures of minimal medium A (160) supplemented with 0.2% glucose. Ampicillin, sucrose and IPTG were added where appropriate. Cells were grown overnight at 37 °C and diluted at least 1:1000 into 7 ml of fresh medium. When the final bacterial cultures reached an OD600nm ~ 0.3, chloramphenicol was added to a final concentration of 170 μg/ml to inhibit protein synthesis. Fluorescent analysis was immediately conducted with 2 ml of culture. All fluorescence measurements were performed with a Varian Cary Eclipse (Palo Alto, CA). CFP fluorescence was measured using an excitation wavelength of 434 nm and an emission wavelength of 477 nm, while YFP fluorescence was measured using an excitation wavelength of 505 nm and an emission wavelength of 527 nm. These values were corrected for differences in cell density by dividing the fluorescent intensities by OD600nm and for light scattering/cellular autofluorescence by subtracting the CFP and YFP fluorescence intensities determined for MG1655/pEB5 cells.

5.4 Analysis of Sulfhydryl Reactivity *In Vivo*

Cells were grown as described above with minor modifications. Upon reaching an OD600nm ~ 0.3, cells were subjected to between 10 and 250 M molecular iodine (as required) for between 1 and 10 min (as required) while incubating at 37°C. The reaction was terminated with 8 mM N-ethylmaleimide (NEM) and 10 mM EDTA. Cells were harvested by centrifugation and resuspended in standard 6X non-reducing SDS-PAGE buffer supplemented with 12.5 mM NEM. Cell pellets were then analysed on 10% SDS/acrylamide gels. Standard buffers and conditions were used for electrophoresis, immunoblotting and detection with enhanced chemiluminescence (161). Anti-V5 (Invitrogen) was used as the primary antibody, while peroxidase-conjugated anti-mouse IgG (Sigma) was employed as the secondary antibody. Digitized images were acquired with a ChemiDoc MP workstation (Bio-Rad), analysed with ImageJ v1.49 (162) and quantified with QtiPlot v0.9.8.10.

Chapter 6: Identification of transmembrane helix 1 (TM1) surfaces important for EnvZ dimerisation and signal output

6.1 Disclaimer

This chapter is adapted from (Heininger et al., 2016), which summarises the work focusing on the signalling mechanism of the first transmembrane domain (TM1) of EnvZ. Roger R. Draheim conceptualised the project and designed the framework of the experiments. Annika Heininger, then at the Institute of Biochemisty, Goethe University Frankfurt, created the single-Cys-containing EnvZ library, optimised the cell collection and protein analysis technique, and finally collected signal output data via fluorescence spectrophotometry. I continued the project by collecting and analysing immunoblotting data of the single-Cys library (plus further optimisation of the techniques used when necessary), and Robert J. Lawrence assisted in collecting additional data required after submission.

6.2 Introduction

Multidrug resistance (MDR) is a frequent problem associated with nosocomial infections that limits therapeutic options (163). In Europe, antibiotic-resistant infections kill nearly 25,000 patients and represent a total expenditure of approximately 1.5 billion € per year (164). Surprisingly, given the seriousness of these issues, our understanding of several key molecular mechanisms involved in conferring MDR to Gram-negative bacteria remains inadequate. The outer membrane (OM) is the first line of defence for Gram-negative bacteria and serves as a major barrier that restricts access of antibiotics to the cytoplasm. The OM is impermeable to large, charged molecules and influx is largely controlled by porins, which are water-filled open channels that span the outer membrane (165–167). β-lactams and fluoroquinolones are prominent groups in our current antibacterial arsenal and porins serve as their major pathway for entry into the cell (168). Thus, it should not be surprising that expression of these porins is often altered in clinical isolates that exhibit MDR (169–175). This is highlighted by a study of *Klebsiella*

pneumoniae isolates collected from different patients undergoing antibiotic treatment. In all isolates, modified outer membrane permeability was observed. In most cases, OmpK35, which belongs to the OmpF porin family that has a larger channel size, was replaced with OmpK36, which belongs to the OmpC family and possesses a smaller channel size (166).

EnvZ of *Escherichia coli* is a canonical sensor histidine kinase (SHK) that responds to changes in the extracellular osmolarity of inner-membrane impermeable compounds such as sucrose, or the presence of certain lipophilic compounds, *e.g.* procaine, by modulating the intracellular level of phosphorylated OmpR, its cognate response regulator (RR) **(*Figure 6.1-A*)** (34,126–128). Subsequently, phospho-OmpR regulates the transcription of a number of genes, including those encoding two major outer membrane porins, OmpF and OmpC. At low intracellular levels of phospho-OmpR (OmpR-P), transcription of *ompF* is upregulated, whereas at higher levels of OmpR-P, transcription of *ompF* is repressed and transcription of *ompC* is activated. This results in a predominance of OmpF at low osmolarity and OmpC at higher osmolarities **(*Figure 6.1-B*)** (130,131,176). Most porins involved in antibiotic transport by Gram-negative bacteria belong to these classical OmpF and OmpC families (166). Dramatic modification of the ratio of porin expression, also known as porin balance, which can occur during antibiotic treatment, strongly suggests that the underlying mechanisms of porin regulation by EnvZ need further characterisation.

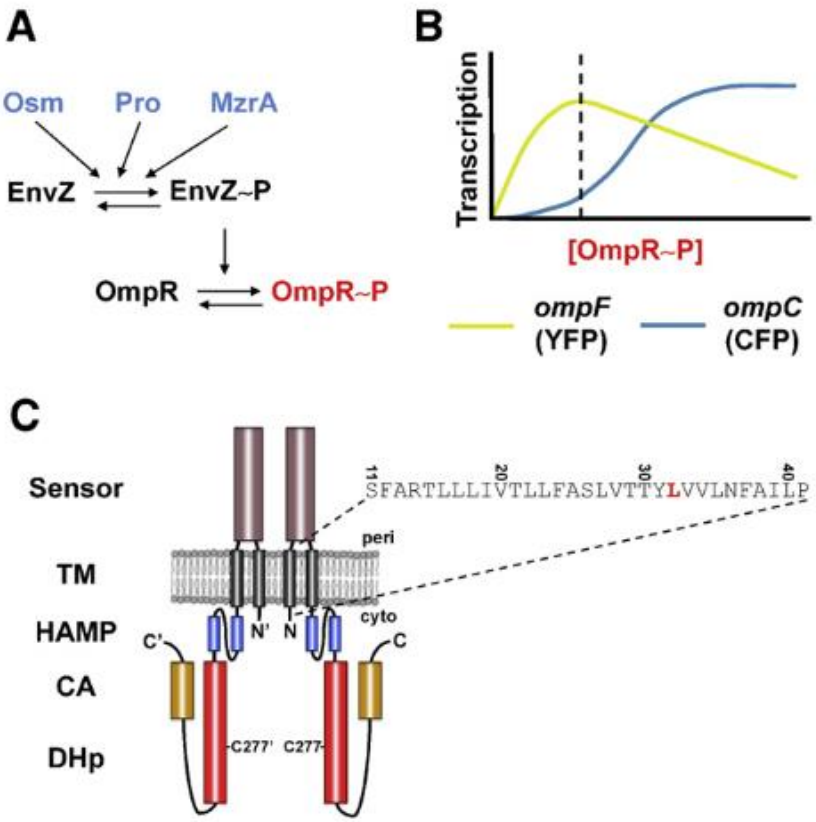

Figure 6.1. The EnvZ/OmpR osmosensing circuit regulates porin expression.
(A) EnvZ is bifunctional and possesses both kinase and phosphatase activity. The ratio of these activities is modulated by presence of extracellular osmolarity (34,126), procaine (137) or MzrA (8,138). OmpR serves as the cognate response regulator (RR) of EnvZ and thus the intracellular level of phosphorylated OmpR (OmpR-P) is governed by EnvZ activity. **(B)** OmpR-P levels control transcription of *ompF* and *ompC*, which can be monitored by employing MDG147 (132) or EPB30 (153) cells that contain a transcriptional fusion of *yfp* to *ompF* (yellow) and of *cfp* to *ompC* (blue). This allows the intracellular levels of OmpR-P (red) to be estimated by monitoring the CFP/YFP ratio. The dashed line represents the baseline level of OmpR-P from EPB30/pRD400 cells expressing wild-type EnvZ grown under the low-osmolarity regime (0% sucrose). **(C)** EnvZ functions as a homodimer with a cytoplasmic N-terminus, the first transmembrane helix (TM1, grey), a large periplasmic domain (brown), the second transmembrane helix (TM2, grey), a membrane-adjacent HAMP domain (blue) and the cytoplasmic domains responsible for dimerisation and histidylphosphotransfer (DHp, red) and catalytic ATPase activity (CA, orange). The residues subjected to Cys substitution are highlighted. Leu-32, indicated in red, could not be substituted for a Cys residue. In addition, the location of the original Cys residue at position 277 is provided.

The molecular mechanisms of perception and response to various classes of stimuli by EnvZ have long been studied but remain somewhat unclear and occasionally contradictory. Detection of and allosteric processing of intracellular osmolarity is perhaps the most well-characterised cognate stimulus of EnvZ. A recent "stretch-relaxation" model has been proposed, in which increased intracellular osmolarity promotes a more folded conformation due to increased stabilisation of intra-helical hydrogen bonding (32,33). This conformation facilitates enhanced rates of autophosphorylation and phosphotransfer to OmpR. The authors also demonstrate that the cytoplasmic domain of EnvZ ($EnvZ_c$) alone is sufficient for osmosensing *in vivo*, leading to a proposal that the periplasmic and transmembrane (TM) domains are unnecessary for osmosensing (32,33). However, two other research narratives suggest roles for the periplasmic or TM domain of EnvZ during detection and response to MzrA, a protein that interacts with the periplasmic domain of EnvZ, and procaine or other lipophilic compounds that potentially interacts with the transmembrane domain of EnvZ. A "gearbox"-type model proposes that a rotation of the second transmembrane helix (TM2), which physically connects the stimulus-perceiving periplasmic domain to the cytoplasmic HAMP domain and domains required for intracellular signalling, is responsible for transmembrane communication (114,115). This model is supported by experimentation with various chimeric receptors composed of the periplasmic and TM domains from the aspartate chemoreceptor of *E. coli* (Tar) and the cytoplasmic domains of EnvZ, respectively, in which modulation of EnvZ signal output upon addition of aspartate, the cognate ligand of Tar, has been demonstrated (89,177). Additionally, recent studies have identified MzrA (modulator of EnvZ and OmpR protein A), a small inner membrane protein that interacts with the periplasmic domain of EnvZ *in vivo* resulting in increased EnvZ signal output (8,138). Although porin expression in *E. coli* cells lacking (Δ*mzrA*) or overexpressing MzrA was drastically different than in wild-type cells, modulation of porin expression due to changes in extracellular osmolarity still occurred in the absence or during overexpression of MzrA. Therefore, these results suggest that MzrA and osmosensing act independently to modulate signal EnvZ output (8,138). Based on these different models of

transmembrane communication, it remains important to better understand the role of the TM domain during stimulus processing by EnvZ in order to predict how porin balance can be targeted for direct manipulation in bacteria exhibiting MDR.

Here, we focused on the TM domain due to its possible interaction with procaine or other lipophilic compounds. In addition, the TM2 domain resides between the periplasmic domain responsible for interaction with MzrA and the cytoplasmic domain responsible for intracellular signal transduction. Furthermore, several dynamic roles for TM1 and/or TM1' have been observed. For example, a rotation between TM1 and TM1' within McpB, a major chemoreceptor within *Bacillus subtilis*, was seen upon addition of arginine, its cognate stimulus (178). Also, comparison of the *apo* and ligand-bound conformations of the periplasmic domains of the nitrate/nitrite sensor NarX and the TMAO-binding TorT-TorS complex suggest that TM1 plays an active role in transmembrane communication (179,180). Finally, a scissors-type model has recently been proposed in cation-/antimicrobial peptide-binding PhoQ, which also involves dynamic movement by TM1 (135). In order to generate a more complete understanding of the organisation of TM domain and its role during stimulus perception and processing, we created a library of EnvZ receptors that each contain a single Cys substitution between positions 11 and 41 and thus encompass the entire region expected to comprise TM1. We demonstrated that placing a Cys residue N- and C-terminal to an internal core of 18 residues resulted in increased EnvZ signal output. Within this internal core, a surface of three adjacent residues (positions 23, 27 and 30) was identified as being intolerant of Cys substitution, in which EnvZ adopted an increased steady-state signal output. We also mapped the surface responsible for TM1 dimerisation, which was found to be composed primarily of residues 19, 23, 26, 30, and 34. Interestingly, we did not observe any significant differences in the apparent TM1-TM1' interface when cells were grown under either the low- or high-osmolarity regime. We conclude by examining these results within the context of various models of transmembrane communication by sensor histidine kinases.

6.3 Results

6.3.1 Overview of Sulfhydryl-reactivity Analysis

One of our primary interests is to determine how the transmembrane (TM) domain of EnvZ allosterically processes and couples different sensory inputs into a single unified output. To determine which residues of EnvZ compose TM1, we subjected the primary sequence to a full protein scan with DGpred (97), which suggested that residues Phe-12 to Val-34 comprise TM1. We also employed TMHMM v2.0 (158), which suggested that the residues between Thr-15 and Phe-37 compose TM1. These results are similar to previously proposed TM1 composition (181,182), therefore, we employed sulfhydryl-reactivity experimentation between residue positions 11 and 41 in order to ensure that the entire first transmembrane helix (TM1) was encompassed.

Sulfhydryl-reactivity possesses several distinct advantages. Firstly, it is well-characterised and has been employed on many soluble and membrane-spanning proteins and higher-order complexes (183). Based on these previous results, we have been able to compare our results with those from other membrane-spanning receptors. Secondly, these reactions can be performed *in vivo*, which allows EnvZ to remain within its native environment while retaining the ability to adjust extracellular osmolarity. In addition, this leaves all accessory proteins, such as MzrA, present and modulatable within the host cell membrane. Finally, the use of an *in vivo* methodology allowed us to monitor signal output with a dual-colour fluorescence-based system that we, and other groups, have previously employed to determine which surfaces of TM1 are intolerant of Cys substitutions (86,132,157). In summary, the *in vivo* nature of this assay facilitated mapping of the TM1-TM1' interface under different osmotic conditions, which is an important first step toward understanding how EnvZ processes different allosteric signal inputs into a single uniform modulation of bacterial porin balance.

6.3.2 Creation of a Cysteine-less EnvZ (Cys-less)

Wild-type EnvZ from *E. coli* contains a single cysteine residue at position 277 (***Figure 6.1-C***). Pre-existing Cys residues would make it significantly more difficult to interpret the results of *in vivo* disulphide-mapping experimentation, therefore, we created a cysteine-less (Cys-less) version of EnvZ. The native Cys-277 codon was converted to a methionine (C277M) because a previous sequence analysis determined that a Met residue was the second most common, after Cys, at position 277 within EnvZ proteins from other organisms (184). A Ser residue was also chosen (C277S) because it was shown to not affect the biochemical activities of the purified cytoplasmic domain from *E. coli* ($EnvZ_c$) (185). Finally, as a small non-polar residue, an Ala (C277A) was also selected for analysis. All substitutions were made using standard site-directed mutagenesis techniques and expressed from pRD400 (86), which results in the addition of a seven-residue linker (GGSSAAG) and a C-terminal V5 epitope (GKPIPNPLLGLDST) that have previously been used within bacterial receptors, including Tar and EnvZ, resulting in minimal effect to steady-state signal output (86,96,103,121–123,154,156).

To measure steady-state signal output from EnvZ/OmpR osmosensing circuits possessing the Cys-less variants, two-colour fluorescent reporter strains were used. MDG147 is a derivative of *E. coli* strain K-12 MG1655 that possesses transcriptional fusions of *cfp* to *ompC* and of *yfp* to *ompF* within its chromosome. This allows the ratio of CFP to YFP fluorescence (CFP/YFP) to provide a rapid and sensitive measure of the ratio of *ompC* to *ompF* transcription, which estimates the intracellular level of phosphoylated OmpR (***Figure 6.1-B***) (86,132,157). MDG147 cells harbouring the empty vector pEB5 (157) were grown in glucose minimal medium under either the low- (0% sucrose) or high- (15% sucrose) osmolarity regime and both CFP and YFP fluorescence were measured. As previously observed, an increase in CFP fluorescence along with a concomitant decrease in YFP fluorescence, resulting in an increased CFP/YFP ratio, was observed when MDG147/pEB5 cells were grown under the high-osmolarity regime (***Figure 6.2-A*** and ***Figure 6.2-B***) (86,132).

To assess whether plasmid-based complementation could produce similar steady-state signal output, EPB30 (MDG147 *envZ::kan*) cells (153) were complemented with the Cys-less EnvZ variants expressed from plasmid pRD400 (86). EPB30/pRD400 cells expressing the C277M variant resulted in CFP and YFP fluorescence similar to those harbouring the control vector (EPB30/pEB5) under both osmotic regimes, therefore, it was not considered for further analysis (***Figure 6.3***). The C277A variant facilitated steady-state output similar to plasmid-based wild-type EnvZ under both regimes, while C277S resulted in slightly lower steady-state signal output (***Figure 6.4***). Based on these results, we elected to continue with the C277A under conditions that produced results similar to MDG147/pEB5 cells (***Figure 6.2-A, Figure 6.2-B*** and ***Figure 6.4***).

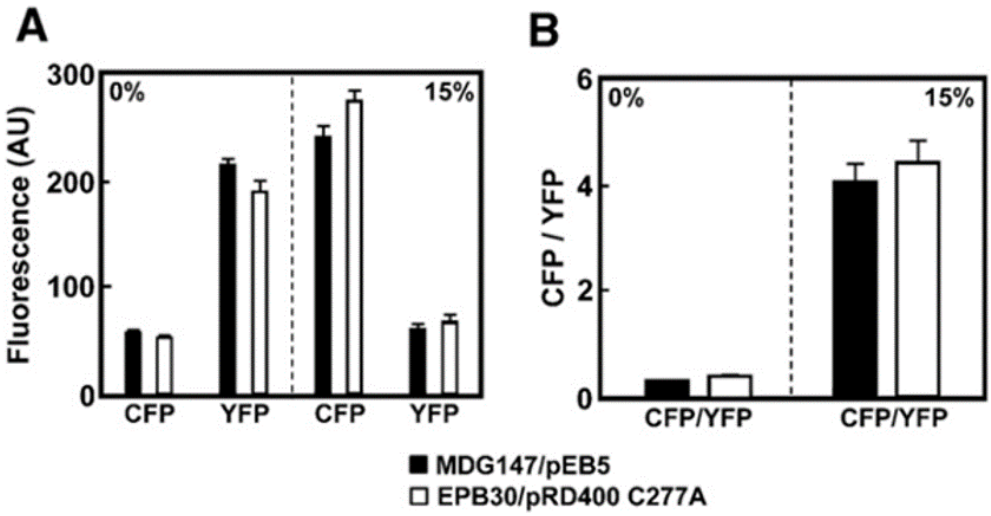

Figure 6.2. Signal output of the Cys-less variant of EnvZ.
(A) CFP and YFP fluorescence from MDG147/pEB5 (filled) and EPB30/pRD400 C277A (Cys-less; empty) cells grown under the low- (0% sucrose) and high-osmolarity (15% sucrose) regimes. **(B)** The CFP/YFP ratio from MDG147/pEB5 (filled) and EPB30/pRD400 C277A (Cys-less; empty) cells grown under the low- and high-osmolarity regimes estimates EnvZ signal output. Error bars represent standard deviation of the mean with a sample size of $n \geq 3$.

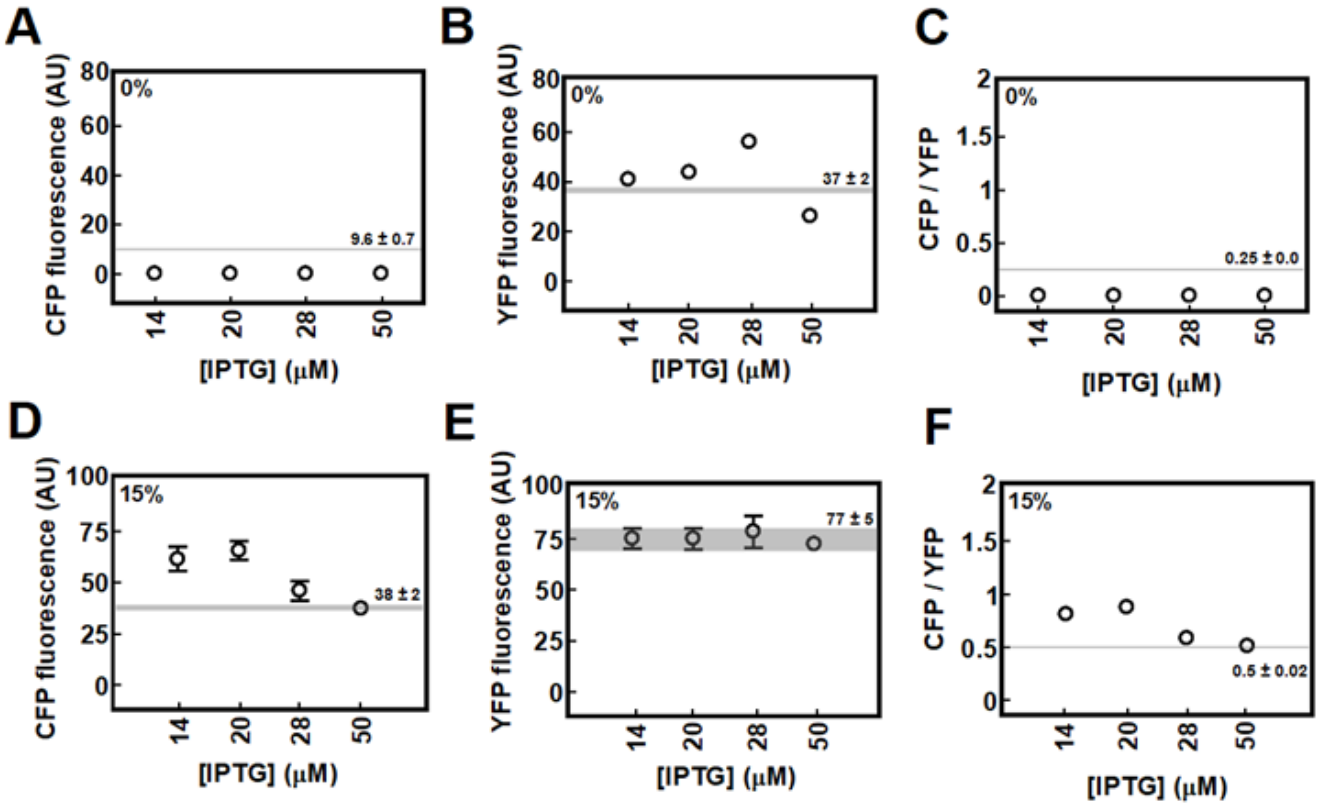

Figure 6.3. Comparison of signal output from EPB30/pEB5 (ΔenvZ) cells and those expressing the C277M variant of EnvZ.
CFP fluorescence **(A),** YFP fluorescence **(B)** and CFP/YFP ratio **(C)** from EPB30/pRD400 cells grown under the low-osmolarity regime (0% sucrose) expressing the C277M variant of EnvZ at different concentrations of IPTG. CFP fluorescence **(D),** YFP fluorescence **(E)** and CFP/YFP ratio **(F)** from EPB30/pRD400 cells grown under the high-osmolarity regime (15% sucrose) expressing the C277M variant of EnvZ at different concentrations of IPTG. In all panels, the shaded area represents the mean with a range of one standard deviation of the mean from EPB30/pEB5 (ΔenvZ) cells. Values represented by the shaded area are also provided to aid in comparison. Error bars represent standard deviation of the mean with a sample size of $n \geq 3$.

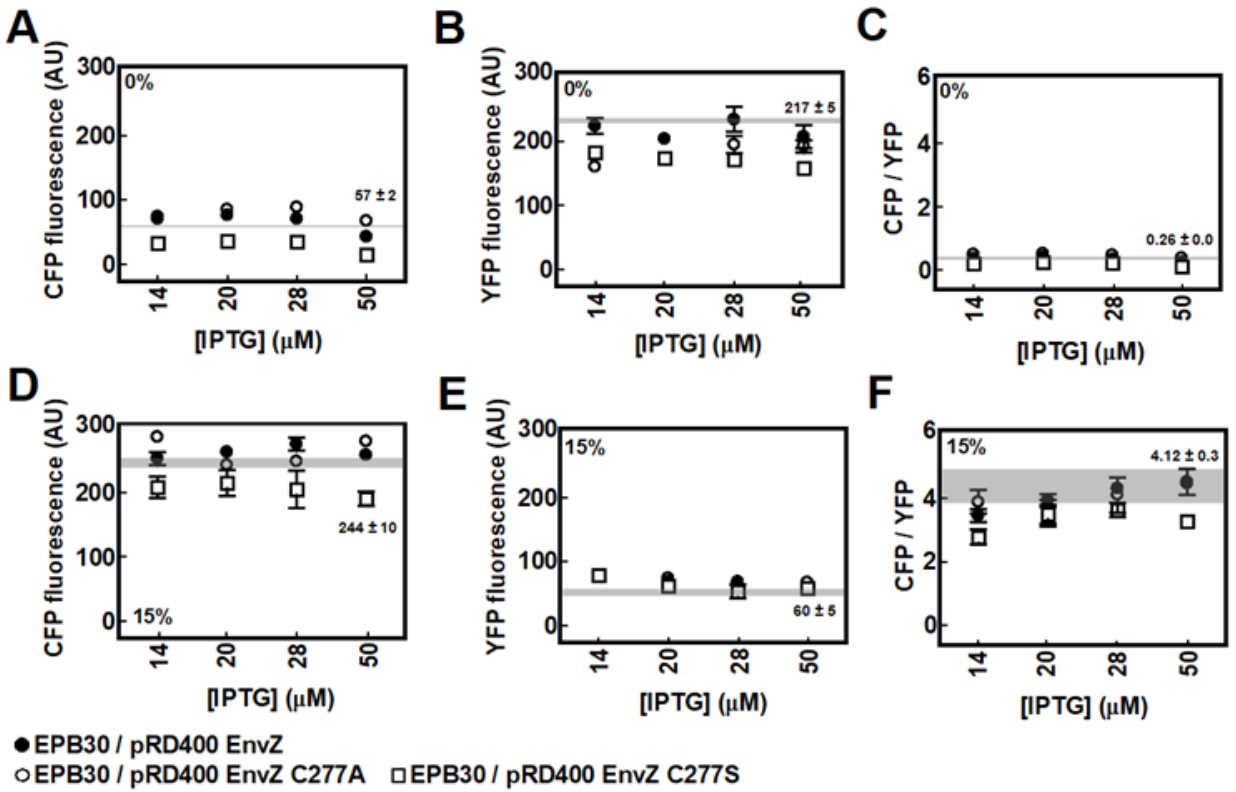

Figure 6.4. Comparison of signal output from the wild-type (filled circles), the C277A (empty circles) and the C277S variants (empty squares) of EnvZ.

CFP fluorescence **(A)**, YFP fluorescence **(B)** and CFP/YFP ratio **(C)** from EPB30/pRD400 cells grown under the low-osmolarity regime (0% sucrose) expressing the wild-type, C277A or C277S variant of EnvZ at different concentrations of IPTG. CFP fluorescence **(D)**, YFP fluorescence **(E)** and CFP/YFP ratio **(F)** from EPB30/pRD400 cells grown under the high-osmolarity regime (15% sucrose) expressing the wild-type, C277A or C277S variant of EnvZ at different concentrations of IPTG. In all panels, the shaded area represents the mean with a range of one standard deviation of the mean from MDG147/pEB5 cells. The values represented by the shaded area are also provided to aid in comparison. Error bars represent standard deviation of the mean with a sample size of $n \geq 3$.

6.3.3 Mapping TM1 Surfaces Responsible for Maintenance of EnvZ

As described above, positions 11 through 41 were selected to ensure that all residues potentially comprising TM1 were converted to a Cys residue. A library of single-Cys-containing EnvZ proteins was created by employing standard site-directed mutagenesis using pRD400 containing the C277A variant as a template (***Figure 6.2***). Although several attempts were made, a Cys residue could not be placed at position 32. We observed that the entire library, with a few exceptions, was expressed within EPB30/pRD400 cells grown under the low- or high-osmolarity regime (***Figure 6.7***). Under both the low- and high-osmolarity regimes the L23C variant was found at significantly lower steady-state levels. In addition, the monomeric form of the P41C variant was only quantifiable when EPB30/pRD400 cells were grown under the high-osmolarity regime (***Figure 6.7***).

For EPB30/pRD400 cells each expressing a single-Cys-containing receptor, we measured CFP fluorescence, YFP fluorescence and also calculated the CFP/YFP ratio, which serves as an estimate of steady-state EnvZ signal output. EPB30/pRD400 cells expressing the C277A variant were used as the baseline for comparison (***Figure 6.2-A, Figure 6.2-B*** and ***Figure 6.4***). Under the low-osmolarity regime, a shift in signalling output toward the "on" state results in increased CFP fluorescence (***Figure 6.6-A***), decreased YFP fluorescence (***Figure 6.6-B***) and an overall increase in the CFP/YFP ratio (***Figure 6.5-A*** and ***Figure 6.5-B***), while a shift toward the "off" state appears as decreased CFP (***Figure 6.6-A***), increased YFP (***Figure 6.6-B***) and a decrease in CFP/YFP ratio (***Figure 6.5-A*** and ***Figure 6.5-B***).

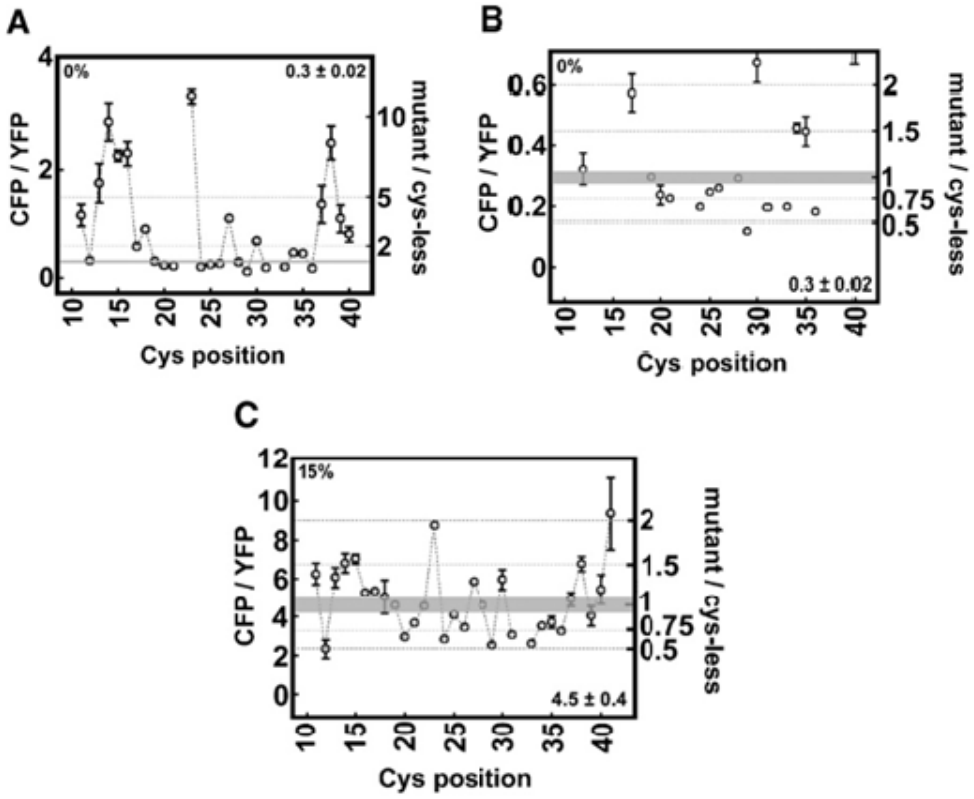

Figure 6.5. Signal output from the library of single-Cys-containing EnvZ variants.
(A) CFP/YFP ratios from EPB30/pRD400 cells expressing one of the single-Cys-containing EnvZ variants grown under the low-osmolarity (0% sucrose) regime. These ratios are also compared to EPB30/pRD400 cells expressing the Cys-less (C277A) variant and are used to demarcate the Cys-containing variants in ***Figure 6.13-B.*** **(B)** Magnified version of panel A in order to emphasise the region up to a 2-fold increase in CFP/YFP over cells expressing the Cys-less variant. **(C)** CFP/YFP ratios from EPB30/pRD400 cells expressing one of the single-Cys-containing EnvZ variants grown under the high-osmolarity (15% sucrose) regime. These ratios are also compared to EPB30/pRD400 cells expressing the Cys-less (C277A) variant and are used to demarcate the Cys-containing variants in ***Figure 6.13-B.*** It is important to note that cells expressing the P41C variant were analysed only when grown under the high-osmolarity regime. The shaded areas represent the mean and a range of one standard deviation of mean. These values are provided to aid in comparison. Lines extending from the Cys-less panel are used to help with the comparison against the Cys-containing variants. Error bars represent standard deviation of the mean with a sample size of $n \geq 3$.

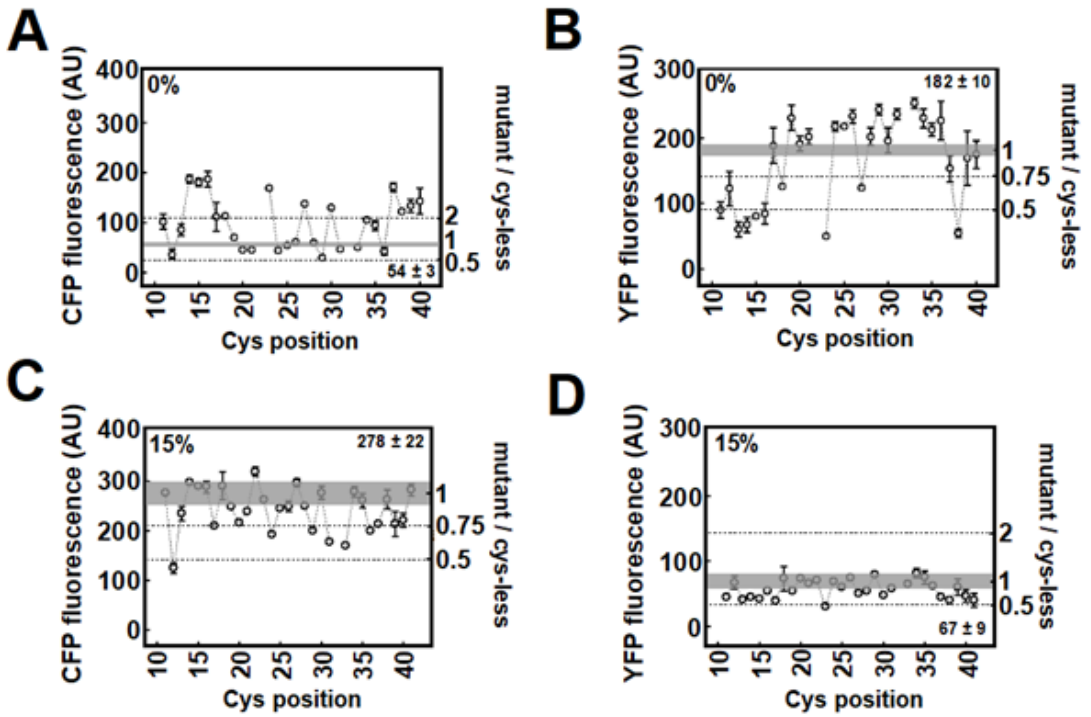

Figure 6.6. Signal output from the library of single-Cys-containing EnvZ variants.

CFP fluorescence **(A)** and YFP fluorescence **(B)** from EPB30/pRD400 cells expressing one of the single-Cys-containing EnvZ variants grown under the low-osmolarity (0% sucrose) regime. These ratios are also compared to EPB30/pRD400 cells expressing the C277A variant (Cys-less) with induction at 50 μM IPTG. CFP fluorescence **(C)** and YFP fluorescence **(D)** from EPB30/pRD400 cells expressing one of the single-Cys-containing EnvZ variants grown under the high-osmolarity (15% sucrose) regime. These ratios are also compared to EPB30/pRD400 cells expressing the C277A variant (Cys-less) with induction at 50 μM IPTG. It is important to note that the P41C variant could only be expressed within cells grown under the high-osmolarity regime. In all panels, the shaded area represents the mean with a range of one standard deviation of the mean from EPB30/pRD400 cells expressing the C277A variant (Cys-less) with induction at 50 μM IPTG. The values represented by the shaded area are also provided to aid in comparison. Lines extending from the Cys-less panel are used to help with the comparison against the Cys-containing variants. Error bars represent standard deviation of the mean with a sample size of $n \geq 3$.

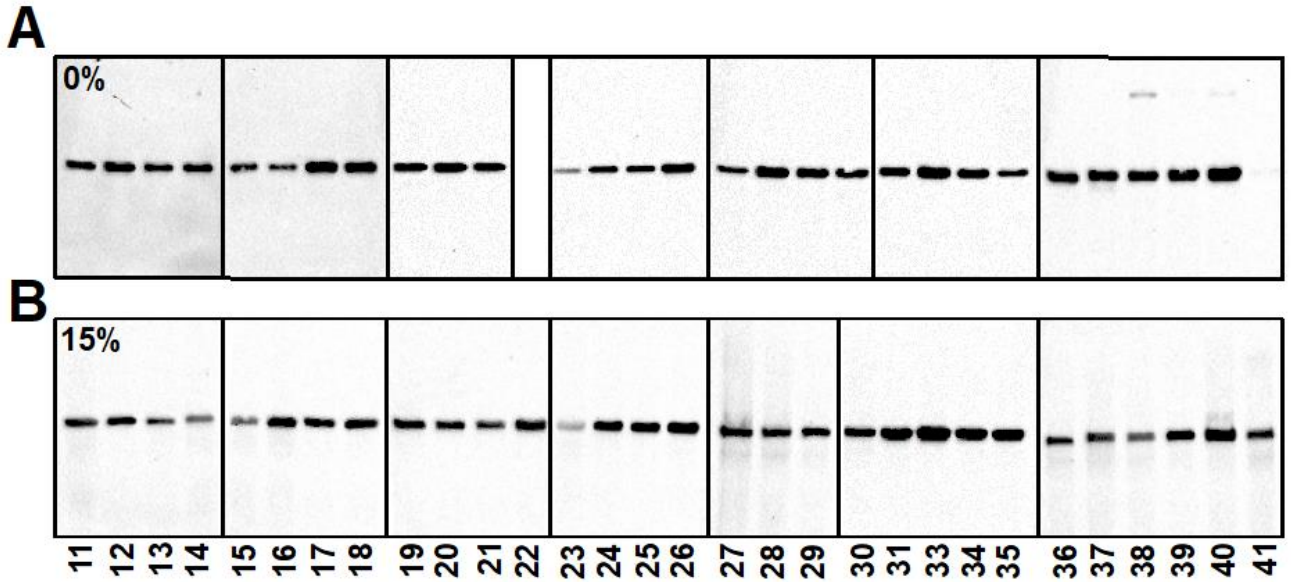

Figure 6.7. Steady-state expression of the single-Cys-containing variants of EnvZ. EPB30/pRD400 cells grown under the different osmolarity regimes.

(A) low- (0% sucrose) or **(B)** high-osmolarity (15% sucrose) regime expressing one of the single-Cys-containing EnvZ variants. **(A)** Cells expressing the L22C variant did not grow under the low-osmolarity regime. Lower steady-state levels of the L23C variant were also observed. In addition, the P41C variant was nearly absent when expressed in cells grown under the low-osmolarity regime. **(B)** When EPB30/pRD400 cells were grown under the high-osmolarity regime, lower than normal steady-state levels of L23C were observed.

Several trends were observed during analysis of the entire single-Cys-containing library. When EPB30/pRD400 cells were grown under the low-osmolarity regime, EnvZ was less tolerant of Cys substitutions at the N- and C-terminal regions of the library. In most cases, this results in a shift toward the "on" state of EnvZ, demonstrated by an increase in CFP fluorescence and a decrease in YFP fluorescence. These boundary regions appear to flank a core of alternating increases and decreases in EnvZ signal output, suggesting that multiple tightly packed EnvZ helices exist within the hydrophobic core of the inner membrane. It should also be noted that when EPB30/pRD400 cells where grown under the low-osmolarity regime, a Cys at residue position 22 prevented cellular growth, however, this was not observed when cells were grown under the high-osmolarity regime (***Figure 6.5, Figure 6.6*** and ***Figure 6.7***). Interestingly, these results occurred adjacent to the position that possessed the most-biased steady-state signal output (Cys-23). When EPB30/pRD400 cells were grown under the high-osmolarity regime, we observed a similar pattern of changes in the CFP fluorescence (***Figure 6.6-C***), YFP fluorescence (***Figure 6.6-D***) and in CYP/YFP ratio (***Figure 6.5-C***), however, these changes were smaller in magnitude, perhaps due to the fact that the EnvZ/OmpR circuit was already activated and thus disturbances due to altered surface interactions would be of a smaller magnitude.

6.3.4 Identifying Surfaces Involved in TM1-TM1' Dimerisation

Based on the effect of the individual Cys substitutions on EnvZ signal output, a helical pattern is detected within the hydrophobic core of the membrane. Therefore, we were interested in determining whether the helical surface participating in TM1-TM1' interaction surface could be identified. To accomplish this, the library of single-Cys-containing variants was expressed in EPB30/pRD400 cells and upon reaching an OD_{600nm} of approximately 0.3, cells were subjected to 250 M molecular iodine for 10 minutes and subsequently analysed by non-reducing SDS-PAGE. These conditions have been previously shown to promote disulphide formation in various membrane-spanning

receptors *in vivo* (183). Upon comparison of the wild-type and the C277A variant, under either osmotic regime, the presence of a higher molecular weight band confirmed the necessity of Cys-277 removal (***Figure 6.8***).

Based on these results, EPB30/pRD400 cells expressing the single-Cys-containing EnvZ variants were grown under the low- (0% sucrose) and high-osmolarity (15% sucrose) regimes and subjected to molecular iodine, non-reducing SDS-PAGE and immunoblotting against the C-terminal V5 epitope (***Figure 6.9***). Data were tabulated for every position with the exception of residue position 32, which could not be made as described above. We observed three regions, each with a different extent of disulphide bond formation. The N-terminal region (region I in ***Figure 6.12***), comprising residues 11 to 18, exhibited almost no cross-linking, except for a minimal amount at positions 11 and 15. The second region (II), consisting of positions 19 to 37, demonstrated alternating low and high levels of disulphide formation consistent with the hydrophobic core of TM1. The final region (III) consists of the C-terminal periplasmic positions in our library, residues 38 through 41, where the apparent helical pattern is interrupted and an overall greater extent of sulfhydryl-reactivity is observed. Altering the reaction conditions as shown in ***Figure 6.10*** and ***Figure 6.11*** further supported the differentiation of the TM1 into Regions I through III.

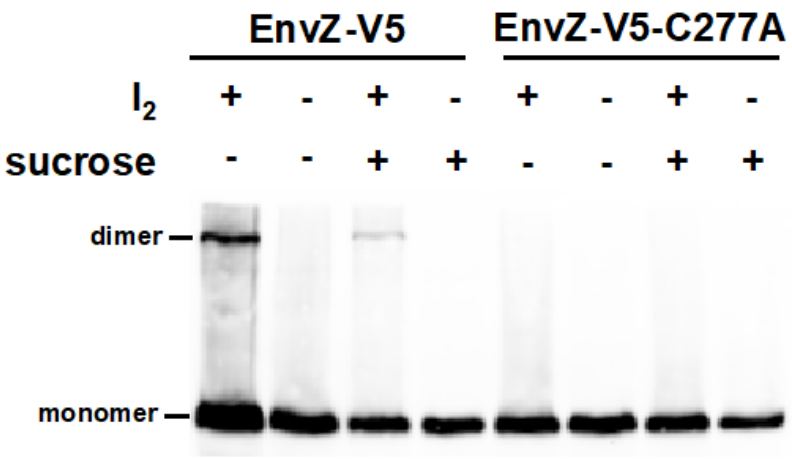

Figure 6.8. Sulfhydryl-reactivity of the wild-type and Cys-less (C227A) variants of EnvZ.
Comparison of EPB30/pRD400 cells expressing the wild-type and C277A variants of EnvZ upon subjecting them to molecular iodine. Cells were grown under the low- (without sucrose) or high-osmolarity (with 15% sucrose) regimes until an OD_{600nm} of approximately 0.2-0.3. Cultures were then subjected to 250 μM molecular iodine. When EPB30/pRD400 cells were expressing the wild-type version of EnvZ, both under the low- and high-osmolarity regimes, a dimeric species was observed. Conversely, when the C277A variant was expressed, no dimeric species were observed. These results confirm the necessity of removing the native Cys residue at position 277.

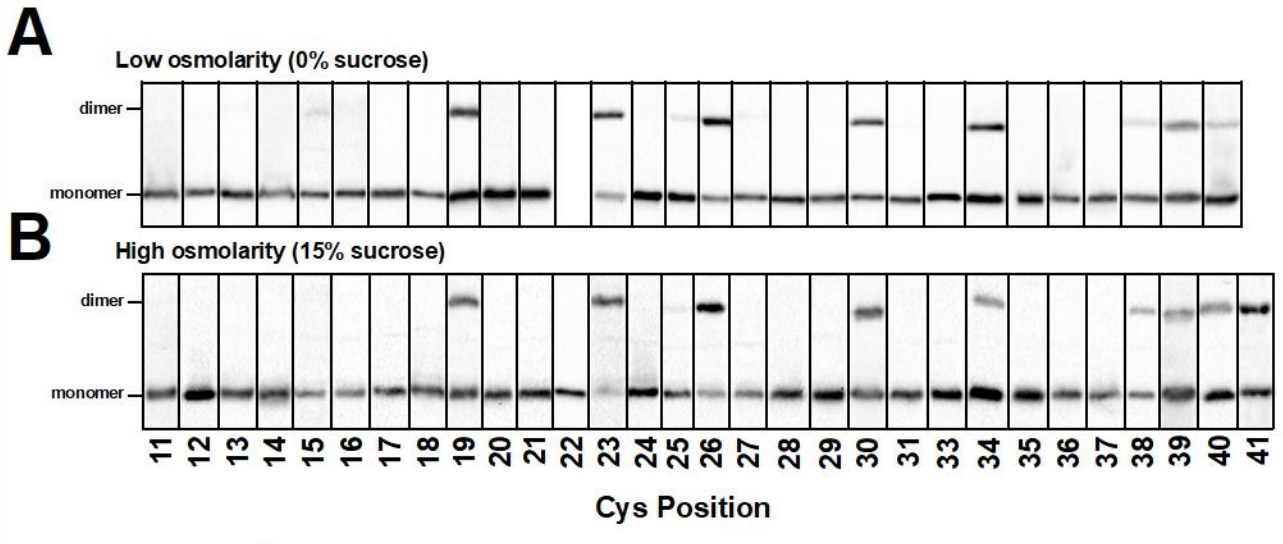

Figure 6.9. Immunoblotting analysis of the sulfhydryl-reactivity experimentation.
EPB30/pRD400 cells grown under the low-osmolarity **(A)** or high-osmolarity **(B)** regimes were subjected to conditions described in ***Figure 6.8.*** It was observed that particular single-Cys-containing variants resulted in the presence of dimeric EnvZ moieties. A minimum of four immunoblots were used to determine the data points presented in ***Figure 6.12***.

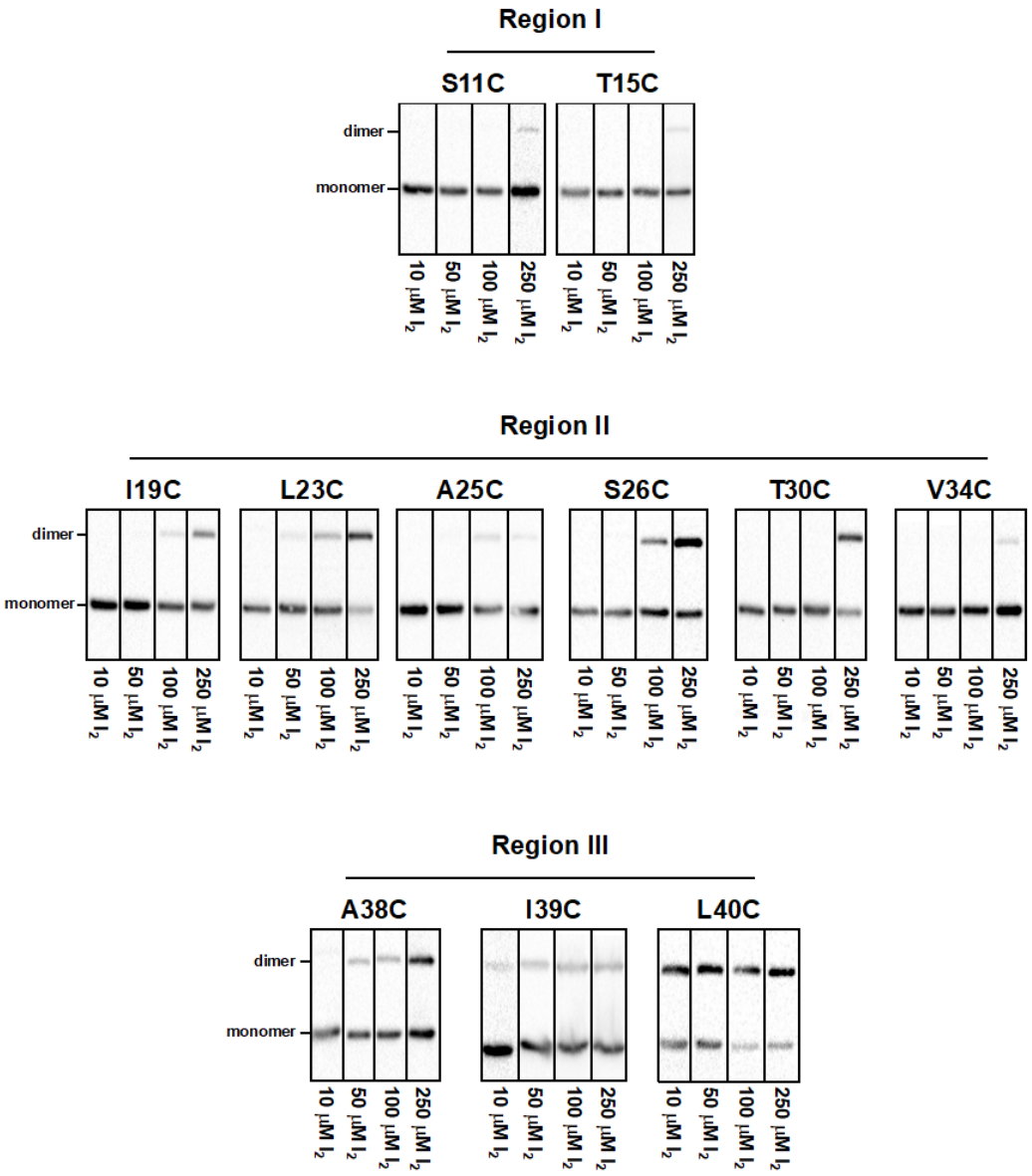

Figure 6.10. Concentration-dependent sulphydryl-reactivity analysis of the single-Cys-containing EnvZ variants.

EPB30/pRD400 cells expressing one of the single-Cys-containing variants that were shown to form a disulphide under the low-osmolarity growth regime (0% sucrose) in ***Figure 6.12*** were assessed in a modified sulfhydryl-reactivity protocol. Under these conditions, the total reaction time was held constant at 10 minutes and the concentration of iodine was altered over a 25-fold range (10 μM, 25 μM, 50 μM and 250 μM final). As described in the text, these results reinforce our delineation of TM1 into Regions I-III.

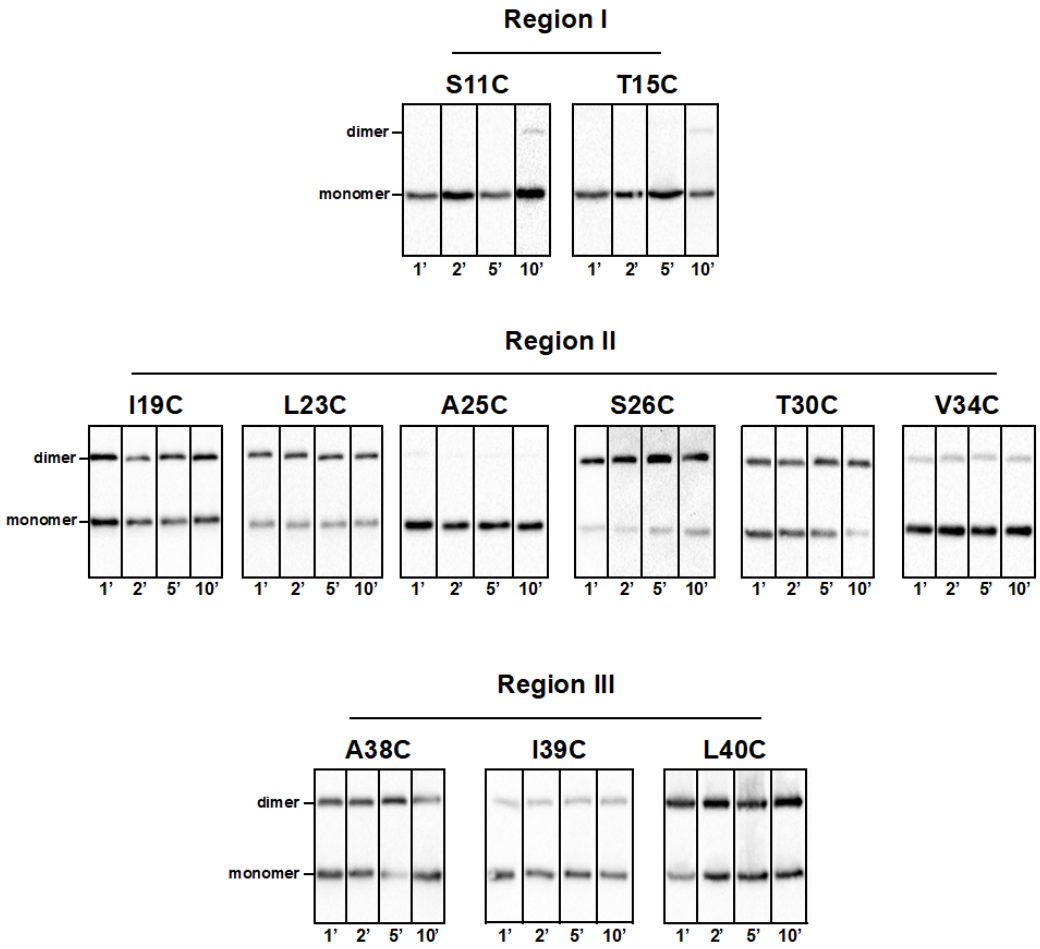

Figure 6.11. Time-dependent sulphydryl-reactivity analysis of the single-Cys-containing EnvZ variants.

EPB30/pRD400 cells expressing one of the single-Cys-containing variants that were shown to form a disulphide under the low-osmolarity growth regime (0% sucrose) in ***Figure 6.12*** were assessed in a modified sulfhydryl-reactivity protocol. Under these conditions, the concentration of iodine was held constant at 250 μM final and the reaction time was altered over a 10-fold range (1, 2, 5 and 10 minutes). As described in the text, these results reinforce our delineation of TM1 into Regions I-III.

6.4 Discussion

6.4.1 Establishing the Surface of TM1 That Promotes Dimerisation

The results of sulfhydryl-reactivity experiments were plotted on a helical net (186) to visualise the TM1-TM1' interaction surface. Using the well-defined distance and angular constraints of a disulphide bond (187,188), we assessed the relative distance between Cys residues along the TM1-TM1' interface. These constraints can be estimated from the distance between β-carbons in disulphide bonds, which range from 3.4 to 4.6 Å in protein crystal structures (189). Therefore, when we employ a fixed concentration of molecular iodine (250 M) and reaction time (10 minutes), the extent of crosslinking correlates with the distance between the Cys residues (***Figure 6.9***). Based on this correlation, residue positions 23/23' and 26/26' would be in closest proximity. By extension, the significant reduction in crosslinking as the Cys residues become more distal from these positions within the membrane core suggests that the TM1 and TM1' helices cross at an angle that results in increased distance between residues near the membrane boundaries. Therefore, we propose that the major TM1-TM1' interaction surface consists of residues Ile-19, Leu-23, Ser-26, Thr-30 and Val-34 (***Figure 6.13-A***). In addition, minor reactivity was observed with residues Ser-11 and Thr-15, suggesting that they are quite distant but most likely reside on the same surface as the TM1-TM1' interface. Adjacent residues at the periplasmic end of TM1, ranging from position 38 to 40 also exhibited extensive cross-linking, however the helical pattern was interrupted suggesting that a less uniform structure exists within these residues (***Figure 6.12*** and ***Figure 6.13-A***). Also important to note is that no significant differences in the TM1-TM1' interface were observed when cells were grown under the low- (0% sucrose) or high-osmolarity (15% sucrose) regime (***Figure 6.12***).

We believe that the residues examined can be formally divided into three distinct regions (***Figure 6.13-A***) based on results obtained when changing the concentration of iodine (***Figure 6.10***) or the reaction time (***Figure 6.11***). The EnvZ variants within Region I (S11C and T15C) follow a distinct pattern of forming

disulphide bonds only in the presence of the highest concentration of iodine (250 M) and the longest duration (10 minutes). These data suggest the Cys residues are either very distant, such that they irregularly form a disulphide bond, or are internal to the inner leaflet of the cytoplasmic membrane. The variants in Region II (I19C, L23C, S26C, T30C, V34C and A25C to a minor extent) all follow a similar pattern that is different than the variants in the first region. Here, a minor extent of crosslinking at the distal ends of the region, namely I19C and V34C, is observed, while a maximal amount is seen near the core that is comprised of L23C and S26C. This is further demonstrated by comparing the extent of crosslinking at the higher concentrations of iodine (100 M and 250 M). In addition, unlike residues in Region I, the reaction is complete after 1 minute regardless of the overall extent of crosslinking (***Figure 6.11***). The variants found in Region III (A38C, I39C and L40C) follow a third distinct pattern. EnvZ A38C exhibited a much greater extent of crosslinking than V34C, and thus does not conform to the crossing helix pattern. In addition, EnvZ I39C and L40C show crosslinking at all concentrations of iodine (***Figure 6.10***) and thus suggest that either the helix becomes broken/unwound, or that these residues reside in the periplasm, or both. It is also worth noting that when cells were grown under the low osmolarity regime and in the absence of iodine (***Figure 6.7***), crosslinking occurred at positions 38 through 40, suggesting that they may reside within the oxidising environment of the periplasm.

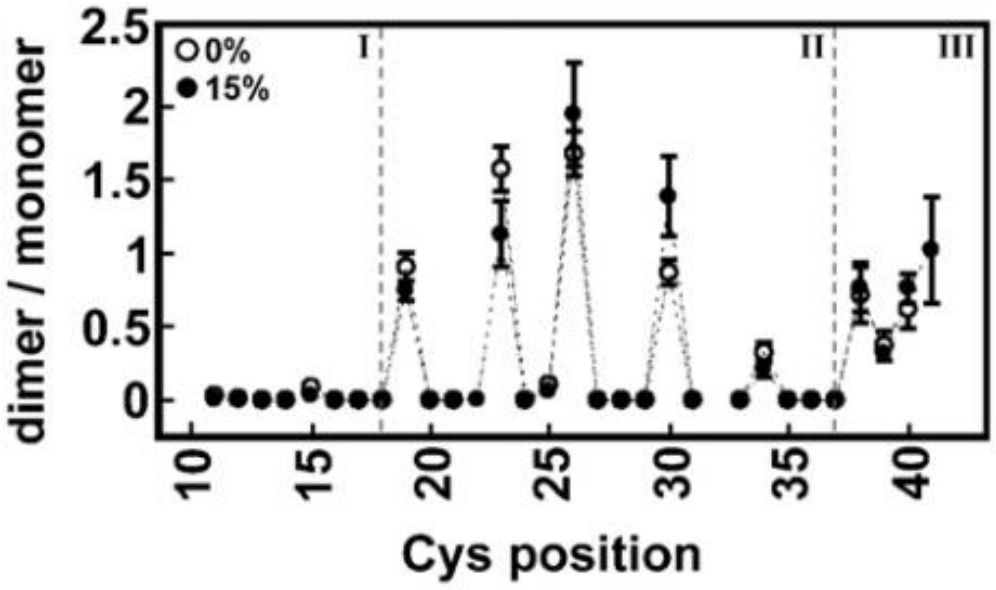

Figure 6.12. Extent of sulfhydryl-reactivity for each single-Cys-containing variant. EPB30/pRD400 cells growing under different osmolarity regimes.

The low- (empty circles, 0% sucrose) or high-osmolarity (filled circles, 15% sucrose) regimes were analysed to determine the ratio of dimeric:monomeric EnvZ at each position as shown in ***Figure 6.9.*** As described within the text, three distinct regions (I, II and III) were observed. Error bars represent standard deviation of the mean with a sample size of $n \geq 3$.

6.4.2 Mapping Surfaces of TM1 Responsible for Maintenance of Baseline EnvZ Signal Output

In order to visualise which surfaces of TM1 are responsible for maintenance of steady-state EnvZ signal output, we mapped the signal output of the family of single-Cys-containing receptors onto a helical net (***Figure 6.13-B***). This analysis resulted in the identification of three subdomains intolerant of Cys substitutions (signal output greater than 150% of the cys-less variant): the cytoplasmic end of TM1 (Surface I), three residues in the core of the membrane (Surface II) and the periplasmic end of TM1 (Surface III). We did not consider surfaces II and III as contiguous because surface III may be due to breaching the periplasmic boundary, while surface II remained buried but truly intolerant of Cys substitution. This becomes more clear when cells are grown under the high-osmolarity (15% sucrose) regime (***Figure 6.13-B***). It is also important to emphasise that the two residues in the membrane core (positions 17 and 24) are subject to both sulfhydryl-reactivity and intolerance of Cys substitution with regard to steady-state signal output. Overall, similar patterns were observed when EPB30/pRD400 cells were grown under the high-osmolarity regime (15% sucrose), although the degree of increased signal output was smaller, perhaps because the EnvZ/OmpR circuit was already activated (***Figure 6.13-B***).

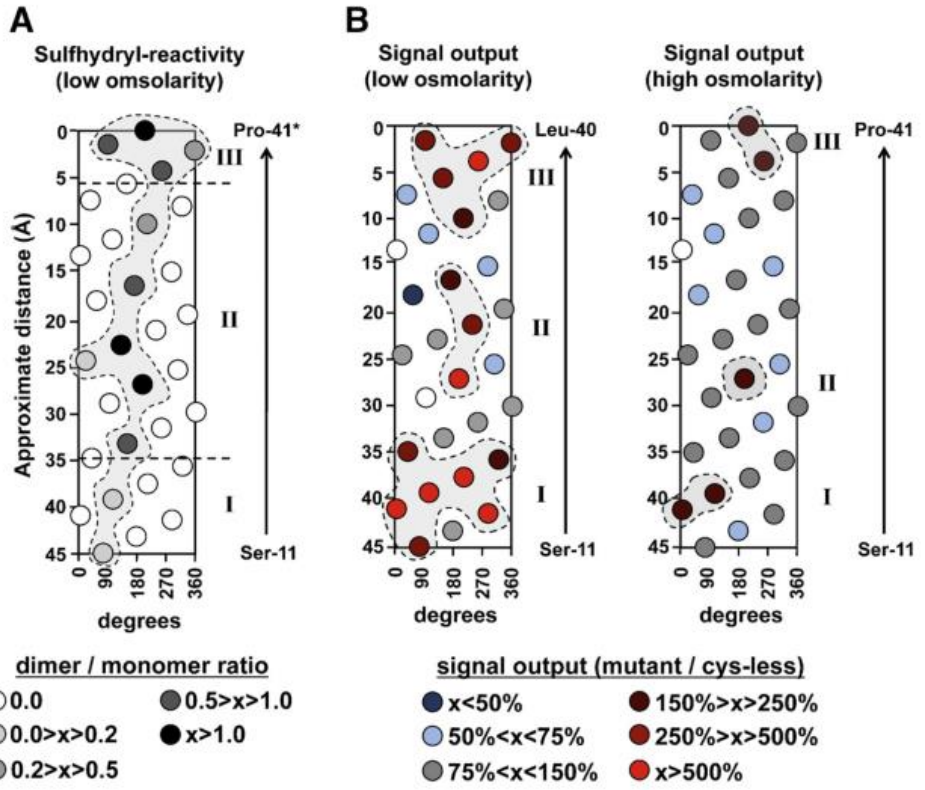

Figure 6.13. Helical net diagrams illustrating the TM1-TM1' interface and surfaces important for maintenance of baseline EnvZ signal output.

(A) The TM1-TM1 interface remains similar when EPB30/pRD400 cells are grown under the low- (0% sucrose) or high-osmolarity (15% sucrose) regime. The extent of TM1-TM1' crosslinking, measured as the ratio of dimeric:monomeric EnvZ moieties at each position is represented by the intensity of darkness. Residue positions 23 and 26, which reside in close proximity, result in the greatest extent of cross-linking. As the position of the Cys residue is moved toward the cytoplasmic end of the helix, a decrease in reactivity is observed. The divergence from a helical pattern at the periplasmic end of TM1 may indicate that the periplasmic boundary of the membrane has been breached and/or that the helicity is not observed within this region. It should be noted that the P41C, indicated with an asterisk, variant could only be analysed when grown under the high-osmolarity regime. **(B)** Cys substitutions that result in decreased signal output compared to the cys-less variant are presented in blue colours, while those resulting in increased signal output are indicated in red. Regions responsible for maintenance of baseline signal output fall into three contiguous surfaces (red dots residing under a transparent grey area): one at the cytoplasmic end (surface I), a small one within the membrane core (surface II) and one at the periplasmic end of the helix (surface III). These surfaces are less pronounced when cells are grown under the high-osmolarity regime, possibly because the EnvZ/OmpR circuit is already stimulated by external osmolarity. The white circles represent the Cys-32 mutant that could not be created and the Cys-22 variant that failed to grow under the low-osmolarity regime.

Two EnvZ mutants that reside within the region we analysed (V33E and P41L) were previously shown to result significantly greater increased steady-state signal output (190,191). Our data with EnvZ P41C is in agreement with the previously published results with P41L, which demonstrates that loss of the Pro residue results in greatly increased steady-state EnvZ signal output. In fact, the P41C variant of EnvZ results in the greatest change in signal output when grown under the high-osmolarity regime (***Figure 6.5***). However, with EnvZ V33C, we observed different results than those previously published with the V33E variant. This difference suggests that the loss of Val-33 is not the major driving force for changing steady-state signal output and that the increased activation is most likely due to the insertion of a Glu residue. This is not unexpected as we previously demonstrated (109) that residues with longer side chains within their R-group possess the ability to snorkel and interact with, or be repulsed from in this case, the negatively charged phospholipid head groups in the cytoplasmic membrane. This may explain why our V33C variant did not exhibit similar properties to the previously published EnvZ V33E.

6.4.3 Evaluation Within the Context of Current Models for Transmembrane Communication

These data demonstrate that the TM1-TM1' interface does not significantly change when EPB30/pRD400 cells are grown under regimes possessing different osmolarities (***Figure 6.12***). This suggests that TM1-TM1' might be relatively static in a manner consistent with results previously observed with the aspartate and ribose/galactose chemoreceptors (104) and also recently with DcuS, the C_4-dicarboxylate sensor of *E. coli* (192). However, other types of signalling mechanisms that involve more dynamic roles for TM1 and/or TM1' have been observed. For example, a rotation between TM1 and TM1' within McpB of *Bacillus subtilis* was seen upon addition of arginine (178), its cognate stimulus, whereas our results suggest that no rotation occurs along the TM1-TM1' interface in response to osmolarity. In addition, small piston-type displacements of TM1 have been observed in the periplasmic domain of NarX and the TorT-TorS complex (179,180) and these might not be detectable within the current iteration of our assay.

From another perspective, our results are in agreement with recent analyses involving PhoQ that proposed the existence of water-filled hemichannel spanning through the cytoplasmic end of the TM domain (193). Our data suggesting that TM1 and TM1' cross at an angle resulting in an increasing distance between the residues as they become further distal from the membrane core is consistent with the presence of water hemichannel possessing a cytoplasmic-facing opening. The proposed necessity of a polar residue is also consistent with our previous results involving "aromatic tuning" and the repositioning of non-polar hydrophobic residues around the cytoplasmic end of TM2 resulting in modified signal output (42,86,109). Recently, further experimentation proposed a scissor-type model, which would also be consistent with our helical crossing angles. We are planning to undertake further experimentation to thoroughly assess these models (135). In light of the plethora of proposed signalling mechanisms, recent publications (133,134) suggest that different subclasses of bacterial receptors may employ

alternate mechanisms of signal transmission and that every proposed mechanism should not be imposed upon all bacterial membrane-spanning receptors.

Chapter 7: *In vivo* cross-linking and transmembrane helix dynamics support a bidirectional non-piston model of signalling within *E. coli* EnvZ

7.1 Disclaimer

This chapter is adapted from (Yusuf *et al.*, unpublished), which summarises the work focusing on the signalling mechanism of the second transmembrane domain (TM2) of EnvZ. Roger R. Draheim conceptualised the project and designed the framework of the experiments. Annika Heininger, the at the Institute of Biochemisty, Goethe University Frankfurt, created the single-Cys-containing EnvZ library, optimised the cell collection and protein analysis technique, and finally collected signal output data via fluorescence spectrophotometry. I continued the project by collecting and analysing immunoblotting data of the single-Cys library (plus further optimising techniques used when necessary), and Robert J. Lawrence assisted in collecting additional data required upon submission. Thanwarat Chavalwan and Phillipa Cheesman conducted additional experiments required after submission.

7.2 Introduction

Most porins involved in antibiotic transport by Gram-negative bacteria belong to the classical OmpF and OmpC families (166). Transcription of these porins is governed by the intracellular concentration of phospho-OmpR (OmpR-P), which is controlled by EnvZ in response to changes in periplasmic interactions with MzrA and environmental osmolarity (8,34,126–128,138) ***(Figure 7.1-A)***. At low intracellular levels of OmpR-P, transcription of *ompF* is upregulated, whereas at higher levels of OmpR-P, transcription of *ompF* is repressed and transcription of *ompC* is activated. This results in a predominance of OmpF at low osmolarity and OmpC at higher osmolarities or in the presence of MzrA (130,131,194) ***(Figure 7.1-B)***. Dramatic modification of porin balance, which has been observed within clinical isolates from patients undergoing antibiotic treatment, strongly supports further characterization of the underlying mechanisms of porin regulation by EnvZ (169,171–175,195). In

addition, it was recently shown that mutations in EnvZ within a porin-deficient (*ompC*$^{-}$ *ompF*$^{+}$) *E. coli* strain resulted in increased carbapenem resistance (196). Thus, in addition to maintenance of porin balance, EnvZ also plays another not well-understood role in mediating antibacterial resistance that warrants further elucidation.

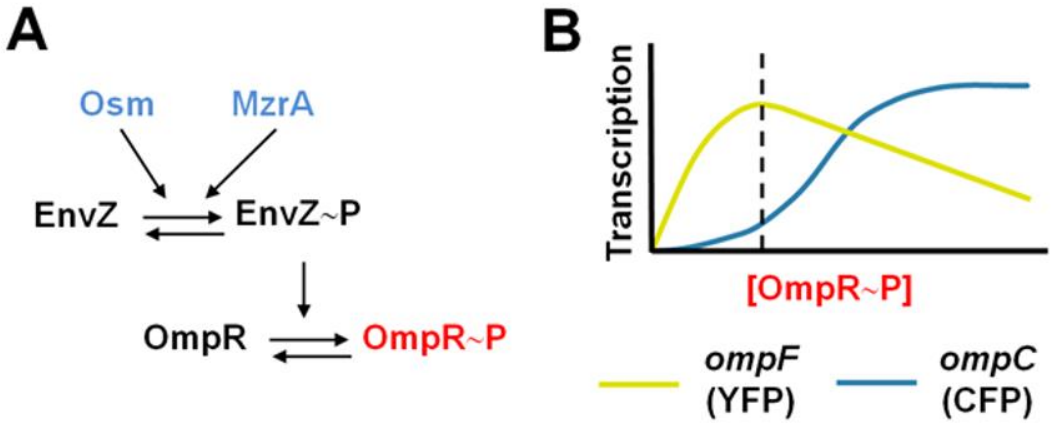

Figure 7.1. Monitoring modulation of EnvZ signal output upon stimulus perception.
(A) EnvZ signal output controls porin expression. It is a bifucntional sensor histidine kinase with both kinase and phosphatase activities. The ratio of these activities is modulated by the presence of extracellular osmolarity and the absence/presence of MzrA (blue). **(B)** The intracellular level of phosphorylated OmpR (OmpR-P) is controlled by EnvZ signal output and OmpR-P levels govern transcription of *ompF* and *ompC*. Strains MDG147 and EPB30 (ΔenvZ) contain transcriptional fusions of *yfp* to *ompF* (yellow) and *cfp* to *ompC* (cyan), which facilitates easy monitoring of intracellular OmpR-P levels by measuring the CFP/YFP ratio. The dashed line indicates an estimation of the baseline OmpR-P levels from EPB30/pRD400 cells grown under the low-osmolarity regime (0% sucrose).

A substantial body of evidence suggests that EnvZ participates in bidirectional allosteric processing. A cytoplasmic fragment of EnvZ ($EnvZ_c$), consisting of residues Arg-180 through Gly-450, has been shown to mediate physiologically appropriate responses to increasing NaCl and sucrose concentrations *in vitro* and to increasing sucrose *in vivo* (32). These results led the suggestion that the peripalsmic and transmembrane domains of EnvZ play a negligible role in osmosensing with the exception of anchoring EnvZ within the membrane and thereby reducing a three-dimensional search by OmpR to a two-dimensional search (32). In addition, it was initially suggested membrane anchoring might reduce the conformational dynamics

of EnvZ to physiologically relevant levels, as $EnvZ_c$ was found to have greater specific activity than full-length membrane-bound EnvZ (32,197). Further studies demonstrated that peripheral interactions between the cytoplasmic domains and the lipid membrane were essential in increasing the kinase activity of the cytoplasmic domain of EnvZ, including the observation of a roughly 25-fold in $EnvZ_c$ signal output while maintaining regulation, *i.e.* a 2-fold increase in autophosphorylation, in response to sucrose *in vitro* (198). In summary, these results confirm that molecular dynamics within the cytoplasmic domain of EnvZ govern response to osmolarity and that lipid-receptor interactions play a modulating the signal output of EnvZ.

Alternatively, MzrA, modulator of EnvZ and OmpR protein A, was identified as a suppressor of a *bamB degP* double mutation. Upon further analysis, it was shown that MzrA is an upstream regulator of EnvZ signal output that is independent of signal output modulation due to osmolarity, pH and procaine (138). MzrA was subsequently shown to localize to the inner membrane and interact with EnvZ within the peripalsmic space (8) to serve as a connector between the CpxA/CpxR and EnvZ/OmpR signaling circuits (138). It is also known as a connector of which only a few examples have been found (199–201).

When taken together, these results demonstrate that the TMD of EnvZ is responsible for allosterically coupling sensory input from the attached periplasmic and cytoplasmic domains. By extension, bidirectional communication through the TMD is required to properly modulate porin expression. Thus, we were interested in how cytoplasmic osmosensing could modulate the conformational dynamics of the TMD and subsequently that of the periplasmic domain. Understanding how EnvZ transduces signal across the biological membrane would be a significant step toward direct manipulation of porin balance in bacterial cells exhibiting MDR.

To address these lines of enquiry, we have created a single-Cys-containing library of EnvZ mutants across the second TM helix (TM2) that physically connects the periplasmic and the cytoplasmic domains of EnvZ. *In vivo* analysis of this library revealed three regions within the TM domain, of which the periplasmic region undergoes a non-piston-type conformational change. CG-MD simulations of the

aromatically tuned and wild-type EnvZ TM2 variants supported these results. We conclude by discussing these results in the context of governance of porin balance and that mechanisms of transmembrane communication can be classified based on the periplasmic domains that the bacterial receptor possesses.

7.3 Results

7.3.1 Creating a Single-Cys-containing Library within TM2 of EnvZ

We previously created a Cys-less version of EnvZ from *E. coli* that had its sole Cys residue changed to an Ala residue (C277A). The Cys-less variant is expressed from pRD400, which results in the addition of a seven-residue linker (GGSSAAG) and a C-terminal V5 epitope (GKPIPNPLLGLDST). We previously found that the Cys-less version of EnvZ had similar steady-state signal output and response to environmental osmolarity as the wild-type version of EnvZ making it suitable for comparisons of *in vivo* sulfhydryl-reactivity and signal output analysis. We initially determined that no major rearrangements occur along the TM1-TM1' interface upon stimulus perception (41). As minimal change was observed along this helical interface in response to osmolarity, we continued by examining the TM2-TM2' interface. We began by determining which residues comprise TM2 by subjecting the full EnvZ sequence to DGpred (202) and TMHMM v2.0 (158), which suggested that Leu-160 to Ile-181 and Leu-160 to Ile-179 comprise TM2 respectively. Based on these analyses, we employed site-directed mutagenesis using the Cys-less variant as a template to create a library of single-Cys-containing EnvZ proteins that spanned from positions 156 to 184.

We observed that nearly the entire library was expressed within EPB30/pRD400 cells grown under the low- or high-osmolarity regime. Variants possessing a Cys at position 156 showed low levels of signal output when grown under the low-osmolarity (0% sucrose) regime. However, when grown under the high-osmolarity regime, no variants showed reduced expression level ***(Figure 7.2)***. These results indicate that the library was suitable for further *in vivo* experimentation.

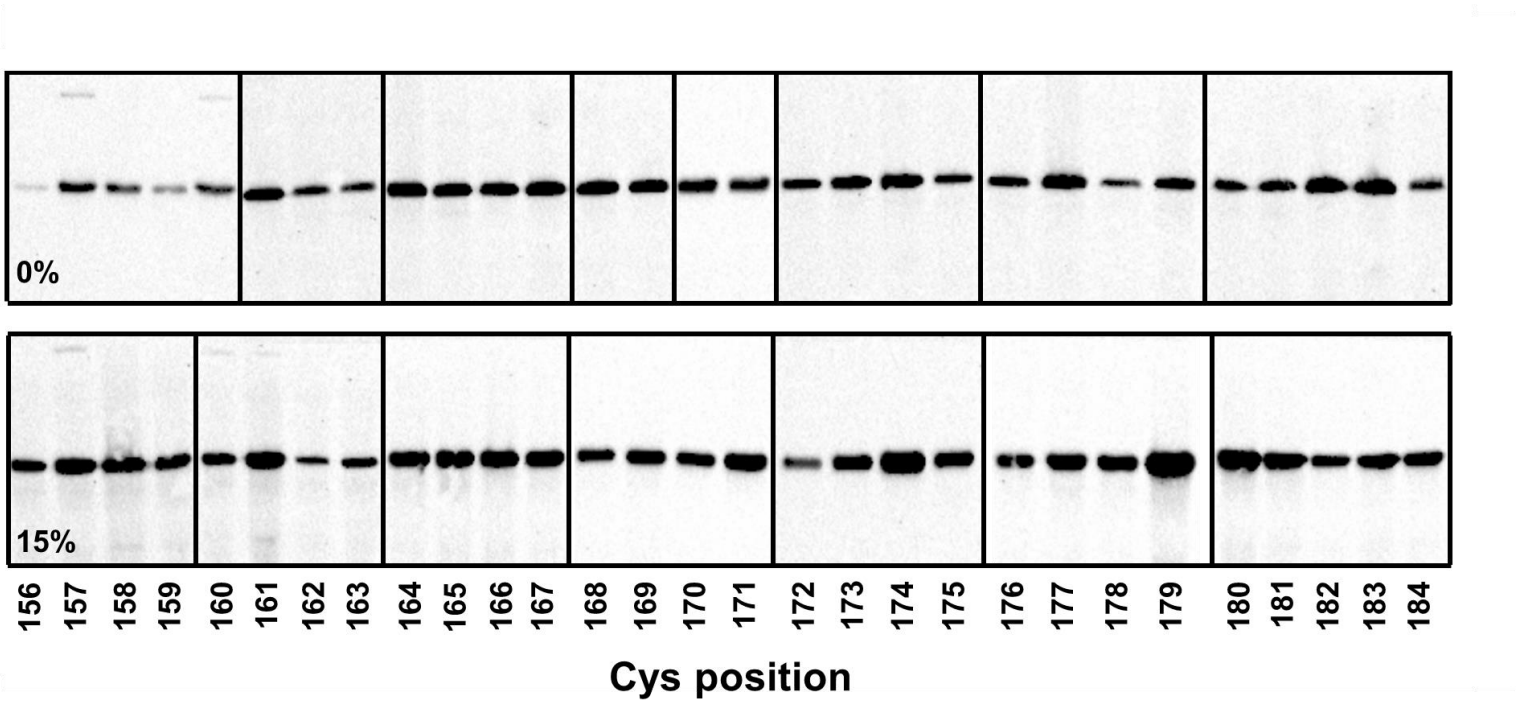

Figure 7.2. Steady-state expression of EnvZ variants containing a single Cys residue within TM2.
EPB30/pRD400 cells expressing one of the single-Cys-containing variants were grown under the low- (0% sucrose) or high-osmolarity (15% sucrose) regimes. Under the low-osmolarity regime, reduced steady-state levels of the D156C variant were observed. In addition, disulfide formation was observed for the F157C and L160C variants in the absence of any additional oxidizing agent. When EPB30/pRD400 cells were grown under the high-osmolarity regime, the F157C, L160C and F161C variants exhibited disulfide formation in the absence of any oxidizing agent.

7.3.2 Mapping TM2 Surfaces Important for Maintenance of EnvZ Signal Output

We began by expressing each of the single-Cys-containing variants in EPB30/pRD400 cells, which allowed us to measure CFP fluorescence, YFP fluorescence, and to calculate the CFP/YFP ratio that estimates steady-state EnvZ signal output ***(Figure 7.1-B)***. Cells expressing the Cys-less C277A were used as a baseline comparison ***(Figure 7.3)***. When EPB30/pRD400 cells are grown under the low-osmolarity regime, a shift in signalling output toward the "on" or kinase-dominant state results in increased CFP fluorescence, reduced YFP fluorescence and an increase in the overall CFP/YFP ratio, while a shift toward the "off" or phosphatase-dominant state appears as decreased CFP, increased YFP and a decrease in CFP/YFP ratio **(*Figure 7.4* and *Figure 7.5*).**

Several trends were observed during analysis of the library of Cys-containing EnvZ receptors. When EPB30/pRD400 cells were grown under the low-osmolarity regime, EnvZ was less tolerant of Cys substitutions at the N- and C-terminal regions of the library. At the N-terminus, signal output from receptors containing a Cys at positions 156, 162 and 163 were very elevated, exhibiting greater than a 5-fold increase in CFP/YFP, while receptors possessing a Cys in the C-terminus at positions 179, 181, 182 and 184 were elevated, possessing over a 2-fold increase in CFP/YFP. These boundary regions appear to flank a core of alternating increases and decreases in EnvZ signal output, as observed between residue positions 165 and 180, suggesting that multiple tightly packed EnvZ helices exist within the hydrophobic core of the inner membrane **(*Figure 7.5-A* and *Figure 7.5-B*).** When grown under the high-osmolarity regime, a pattern appeared where Cys substitutions resulted in significant decreases in signal output ***(Figure 7.5-C)***. Of the 29 mutants analysed, 13 supported less than 75% of the normal wild-type signal output.

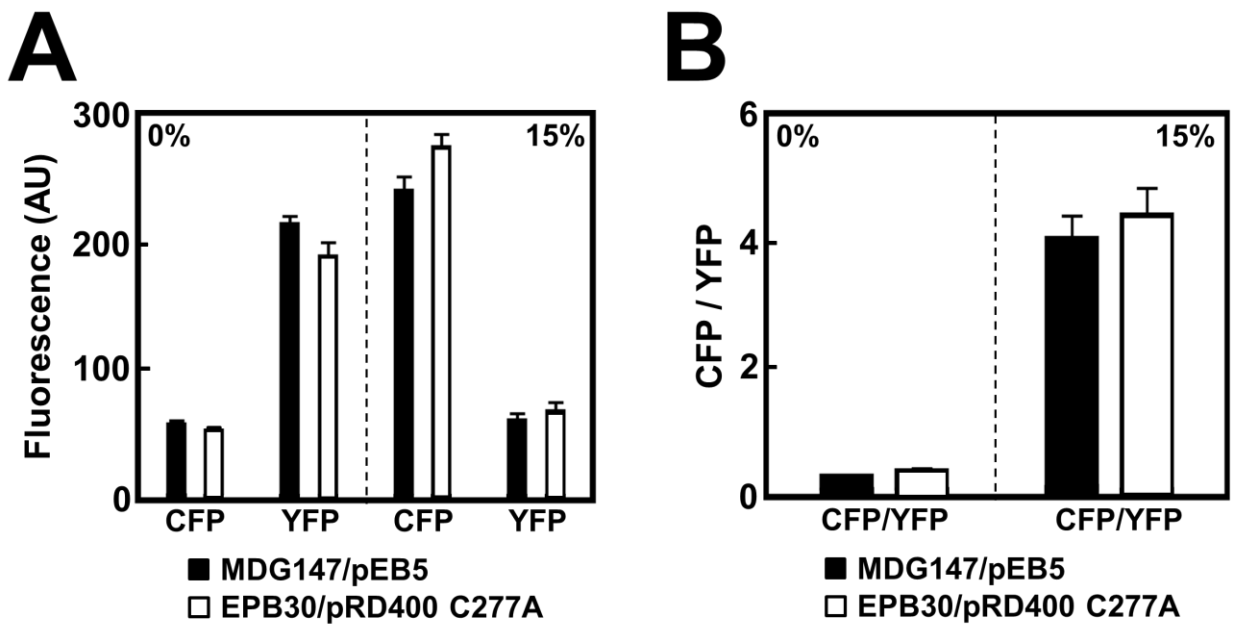

Figure 7.3. Steady-state signal output from the Cys-variant of EnvZ.

(A) CFP and YFP fluorescence from MDG147/pEB5 (filled) and EPB30/pRD400 C277A (Cys-less; empty) cells grown under the low- (0% sucrose) and high-osmolarity (15% sucrose) regimes. **(B)** The CFP/YFP ratio from MDG147/pEB5 (filled) and EPB30/pRD400 C277A (Cys-less; empty) cells grown under the low- and high-osmolarity regimes estimates EmvZ signal output. Error bars represent standard error of the mean with a sample size of $n \geq 3$. Reprinted from BBA Biomembranes, volume 1858, Annika Heininger, Rahmi Yusuf, Robert J. Lawrence and Roger R. Draheim, Identification of transmembrane helix 1 (TM1) surfaces important for EnvZ dimerisation and signal output, pages 1868-1875, Copyright 2016, with permission from Elsevier.

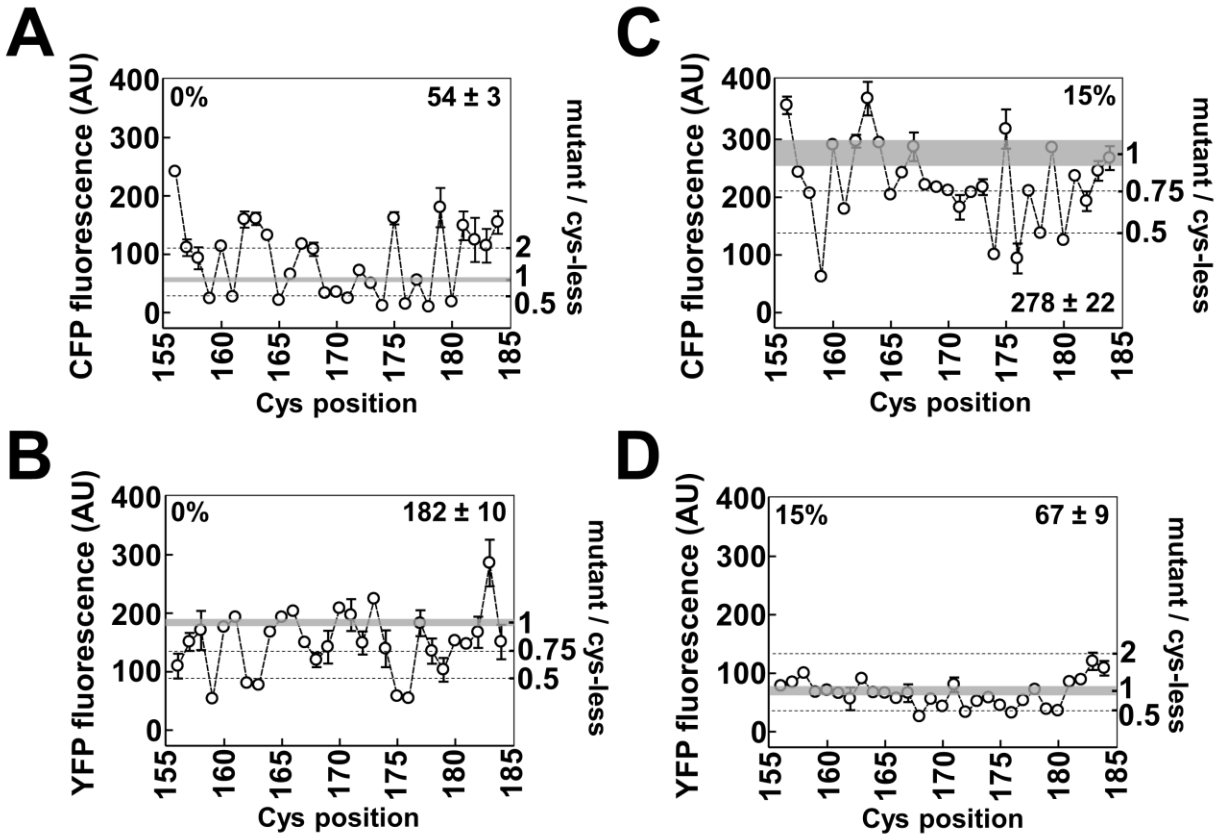

Figure 7.4. Signal output from the single-Cys-containing EnvZ variants.

CFP **(A)** and YFP **(B)** fluorescence from EPB30/pRD400 cells expressing one of the receptors from the library grown under the low-osmolarity (0% sucrose) regime. CFP **(C)** and YFP **(D)** fluorescence from EPB30/pRD400 cells expressing one of the single-Cys-mutants from the library grown under the high-osmolarity (15% sucrose) regime. On the right axes, the ratio of signal output compared to EPB30/pRD400 cells expressing the Cys-less mutant is also presented to aid in comparison. In all panels, the shaded area represents the mean with a range of one standard deviation of the mean from EPB30/pRD400 cells expressing the Cys-less variant of EnvZ ***(Figure 7.3)***. Error bars represent standard error of the mean with an $n \geq 3$.

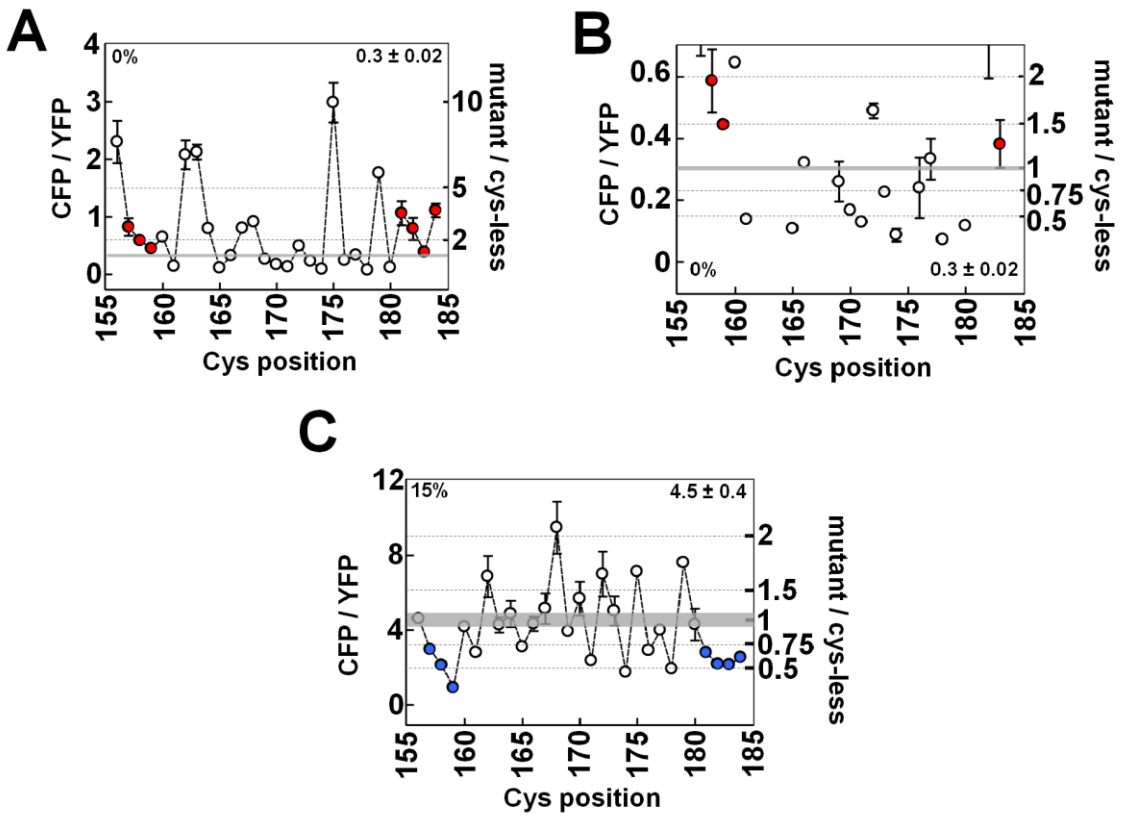

Figure 7.5. Signal output from the library of single-Cys EnvZ variants.

(A) CFP/YFP from EPB30/pRD400 cells expressing one of single-Cys variants grown under the low-osmolarity (0% sucrose) regime. On the right axis, these CFP/YFP ratios are compared to the Cys-less (C277A) variant. **(B)** Magnified version of panel A in order to emphasise the region up to a 2-fold increase in CFP/YFP. **(C)** CFP/YFP from EPB30/pRD400 cells expressing one of the single-Cys variants grown under the high-osmolarity (15% sucrose) regime. On the right axis, these CFP/YFP ratios are compared to the Cys-less (C277A) variant. The flipped mutants are highlighted with a red dot in panel A (increased signal output) and a blue dot in panel C (decreased signal output). The shaded areas represent the mean signal output from the Cys-less variant of EnvZ with a range of one standard error of mean. These values are provided to aid in comparison. Error bars represent standard deviation of the mean with a sample size of $n \geq 3$.

Most striking is the inverse effect on EnvZ signal output of the Cys substitutions that flank the hydrophobic core of TM2. For these residues, when grown under the low-osmolarity regime, the presence of a Cys resulted in an increase in signal output of more than 25%, *i.e.* shifted toward the on or kinase-dominant state (red dots in ***Figure 7.5-A***) and a reduction in signal output of more than 25%, *i.e.* shifted toward the off or phosphate-dominant state, when grown under the high-osmolarity regime (blue dots in ***Figure 7.5-C***). These flipped positions reside at the N- and C-terminal ends of the region we examined and outside of the proposed hydrophobic TMD core ***(Figure 7.5)***. Within the hydrophobic core, Cys substitutions show similar changes when cells are grown under the low- and high-osmolality regimes. These results suggest that the flanking regions are not simply rigid structural conduits for signal transduction but may have higher-order roles in signal transduction, such as MzrA interaction or functioning as a control cable at the N- and C-terminal regions respectively (8,122–124,138,203).

7.3.3 Identifying Surfaces Involved in TM2-TM2' Interactions

Sulfhydryl-reactivity experimentation is well-characterised and has been employed on many soluble and membrane-spanning proteins and higher-order complexes (204). The *in vivo* nature of this assay facilitated mapping of the TM2-TM2' interface under different osmotic conditions, which is an important first step toward understanding how EnvZ processes allosteric inputs from periplasmic MzrA binding and cytoplasmic osmosensing into a single uniform modulation of bacterial porin balance ***(Figure 7.1)***. In a similar manner to mapping TM1-TM1' interactions (41), Cys-containing EnvZ variants were expressed in EPB30/pRD400 cells and upon entering the early exponential phase ($OD_{600nm} \approx 0.25$) they were subjected to 250 μM molecular iodine for 10 minutes analysed by non-reducing SDS-PAGE and immunoblotting ***(Figure 7.6)***.

We observed three distinct regions within TM2. The N-terminal region (region I in ***Figure 7.7***), comprised of residues 156 to 163, exhibited significant

cross-linking under the low-osmolarity regime (0% sucrose) and almost no crosslinking under the high-osmolarity (15% sucrose) regime. The second region (II) consisting of positions 164 to 179, demonstrated altering low and high levels of disulphide-formation consistent the crossing of TM2 and TM2' within the hydrophobic core of the TMD. The final region (III), from residues 180 to 184, shows no crosslinking ***(Figure 7.7)***. It should be noted that this significant difference at the periplasmic end of the TMD between cells grown under the low- and high-osmolarity regime was not observed during similar analyses of TM1 (41). ***Figure 7.8*** visually summarises the patterns of signal output and cross-linking for all single-Cys variants in comparison to the Cys-less mutant, indicating positions sensitive to substitutions and the extent of signal modulation as the result of these substitutions.

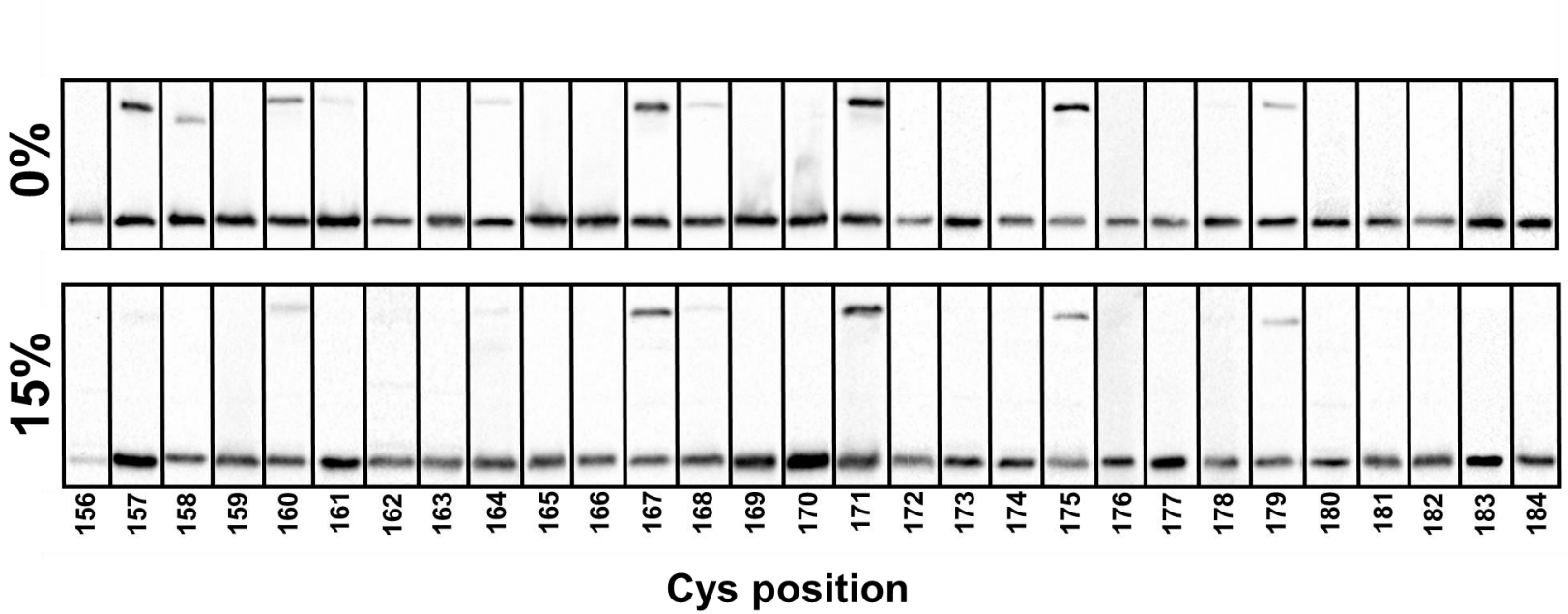

Figure 7.6. Immunoblotting analysis of the sulfhydryl-reactivity experimentation.
EPB30/pRD400 cells expressing one of the single-Cys-containing EnvZ receptors were grown under the low- (0%) or high- (15%) regimes until an OD_{600nm} of approximately 0.25 was reached. Cultures were then subjected to 250 μM molecular iodine. Particular Cys-containing EnvZ receptors resulted in the presence of dimeric EnvZ moieties that migrated at a slower rate than the monomeric species. A minimum of three immunoblots were used for each of the data points present in *Error! Reference source not found.*.

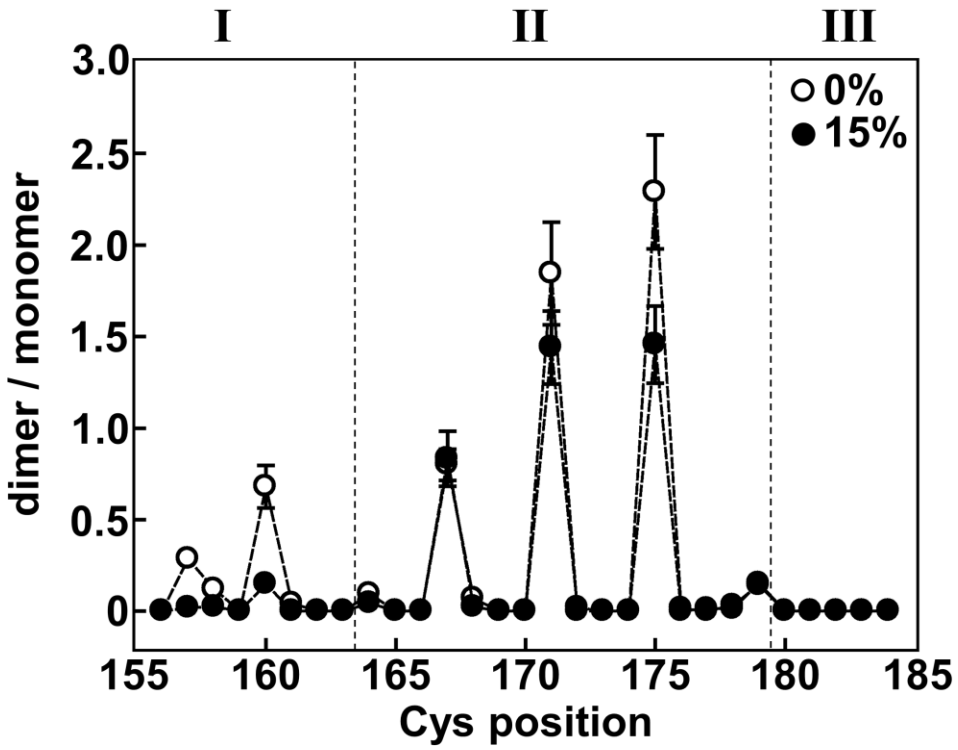

Figure 7.7. Extent of sulfhydryl-reactivity for each single-Cys-containing EnvZ variant.
EPB30/pRD400 cells were grown under the low- (empty circles, 0% sucrose) or high-osmolarity (filled circles, 15% sucrose) regimes and subjected to 250 μM molecular iodine for 10 minutes when their OD_{600nm} reached approximately 0.25. As shown in ***Figure 7.9***, this allowed us to determine the dimer/monomer ratio represented on the Y-axis. Three distinct regions, denoted I, II and III were observed and are described in the text. Error bars represent the standard error of the mean with a sample size of $n \geq 3$.

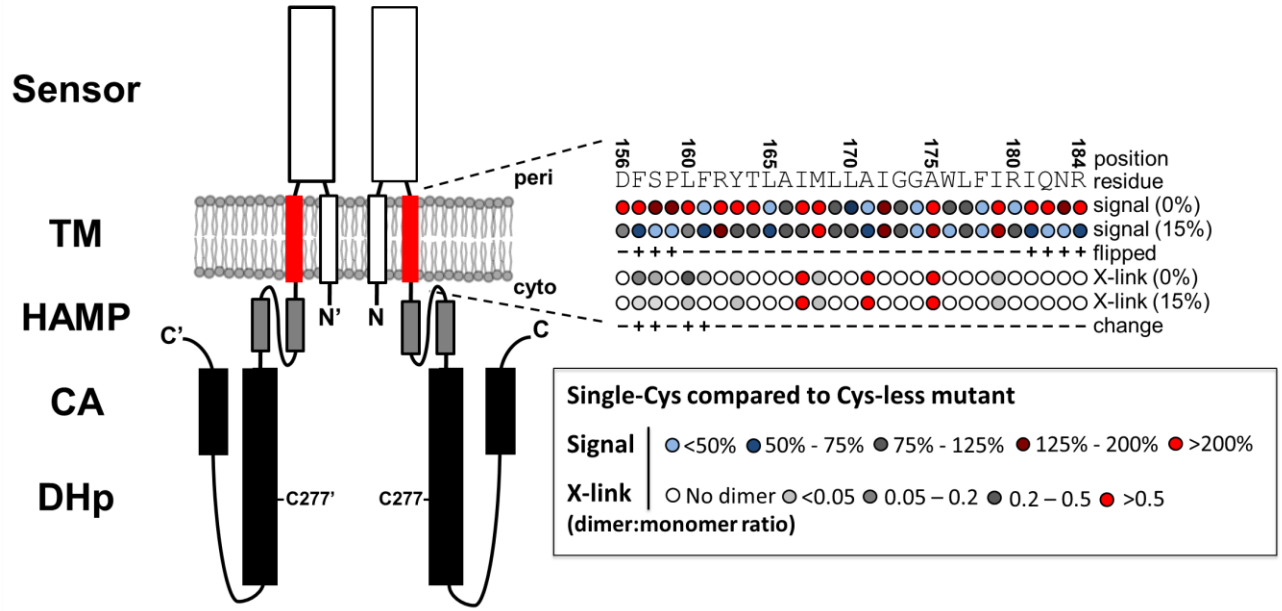

Figure 7.8. EnvZ domains and residues modified during site-directed mutagenesis of the second transmembrane domain.
EnvZ functions as a homodimer with a cytoplasmic N-terminus, the first transmembrane helix (TM1, white), a large periplasmic domain (sensor, white), the second transmembrane helix (TM2, red), a membrane-adjacent HAMP domain (grey) and the cytoplasmic domains responsible for dimerization and histidylphosphortransfer (DHp, black) and catalytic ATPase activity (CA, black). The position of the original Cys-277 residue that was mutated to Ala to produce the Cys-less EnvZ is provided. The residues subjected to Cys substitution and their position in the primary sequence is provided. Signal output from each single-Cys-containing variant is compared to the Cys-less (C277A) variant: less than 50% of Cys-less (light blue), between 50% and 75% of Cys-less (dark blue), between 75% and 125% of Cys-less (grey), between 125% and 200% (dark red) and greater than 200% (light red). Residue positions exhibiting flipped signal output are indicated with a plus. The extent of sulphydryl-reactivity is also presented in five categories based on dimer-to-monomer ratio: no dimer present (white), less than 0.05 (light grey), between 0.05 and 0.2 (medium grey), between 0.2 and 0.5 (dark grey) and greater than 0.5 (red). Positions that exhibit a significant change in cross-linking between the low- and high-osmolarity regimes are indicated with a plus.

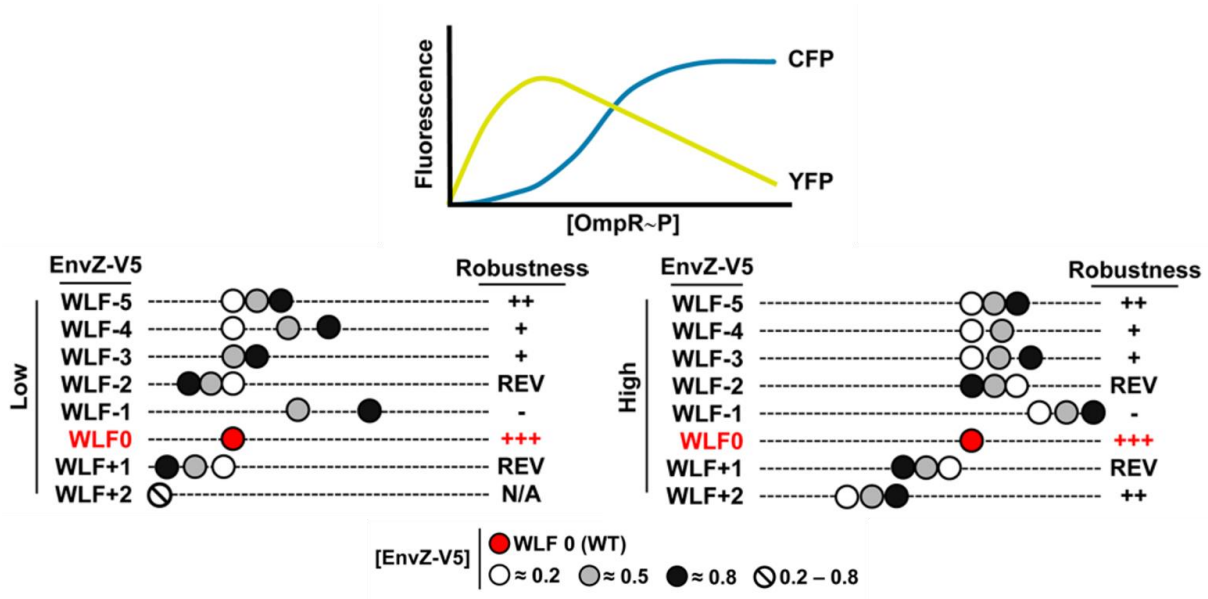

Figure 7.9. Comparison of signal output from osmosensing circuits containing the various aromatically tuned EnvZ receptors.

Steady-state signal output from circuits containing the WLF series of aromatically tuned variants expressed in EPB30/pRD400 cells grown under the low (left middle-panel) or high (right middle-panel) osmolarity regime is shown. The intracellular levels of phospho-OmpR are estimated through use of the antisymmetrical reporter system presented in ***Figure 7.1-B***. Signal output at low (open circles), medium (gray circles), and high levels (filled circles) of EnvZ-V5 expression (0.2, 0.5, and 0.8, respectively) is presented for comparison. The extent of sensitivity to changes in the amount of EnvZ present is also summarized as robustness. In this column, N/A represents not applicable, as in there is no reasonable amount of signal output, whereas REV indicates reversed, where a decrease in activity is observed as the level of EnvZ-V5 increases. Reprinted from ACS Synthetic Biology, volume 4, Morten Nøholm, Gunnar von Heijne and Roger R. Draheim, Forcing the Issue: Aromatic Tuning Facilitates Stimulus-Independent Modulation of a Two-Component Signaling Circuit, pages 474-481, Copyright 2015, with permission from the American Chemical Society.

7.4 Discussion

7.4.1 Non-piston Transmembrane Communication by EnvZ

EnvZ has been shown to allosterically process cytoplasmic changes in osmolarity and upon interaction with MzrA within the periplasmic. Here, our *in vivo* analysis demonstrated that only the periplasmic end of EnvZ TM2 undergoes a conformational transition upon cytoplasmic stimulus perception and suggests that the asymmetric piston-type displacement employed by Tar is not used by EnvZ. To our knowledge, this is the first example of a periplasmic end of TM2 being affected by a cytoplasmic stimulus observed within EnvZ. Various experimentation has also been performed with the aromatically tuned variants of TM2 from both Tar and EnvZ. Previously, a linear correlation was observed between the position of the aromatic residue in Tar TM2, the position of the helices *in vitro* and *in silico* and the signal output from each Tar receptor (42,86,96,109). Here, *in silico* analysis of EnvZ TM2 demonstrates that such a linear correlation is absent and that EnvZ functions by a non-piston mechanism in which both tilting and azimuthal rotation play a substantial role in modulation of signal output ***Figure 7.10.***

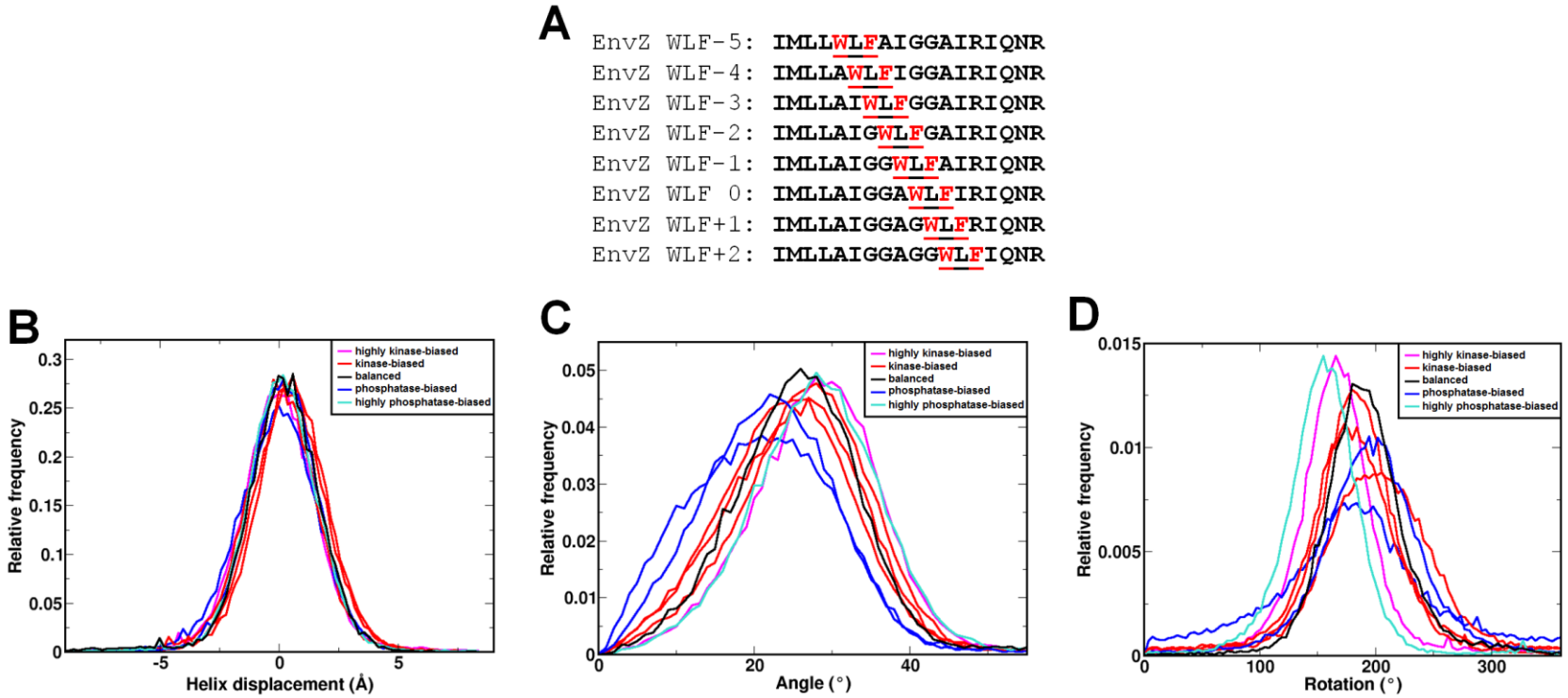

Figure 7.10. Aromatic tuning and signal output from EnvZ.

(A) When aromatic tuning was performed in EnvZ, a Trp-Leu-Phe triplet (red) was repositioned within the C-terminal region of TM2. **(B)** Helix displacements, **(C)** tilt distributions and **(D)** azimuthal rotational distributions of the aromatically tuned EnvZ TM2 helices. Histograms are shown for all time points of all membranes of each ensemble. Aromatically tuned mutants have been classified based on their signal output as shown in ***Figure 7.11*** into five categories: highly kinase biased (WLF-1; pink), moderately kinase biased (WLF-5, WLF-4, WLF-3; red), balanced (wild-type; black), moderately phosphatase biased (WLF-2, WLF+1, dark blue) and highly phosphatase biased (WLF+2, bright blue).

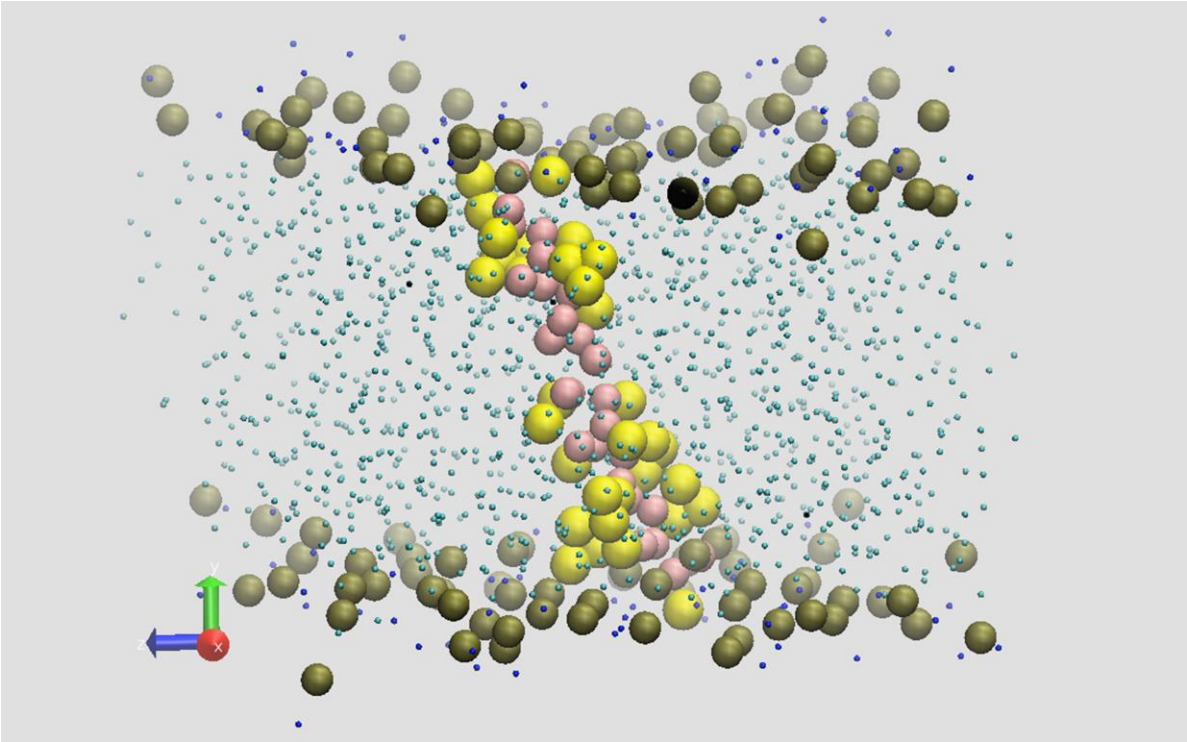

Figure 7.11. A randomly selected (number 63) simulation of the wild-type EnvZ TM2 was selected for demonstration.
The blue and cyan dots represent water molecules, while the bronze spheres represent the phosphate in DPPC. The backbone carbon atoms of the peptide are shown pink, while the yellow spheres represent side chains.

7.4.2 Correlations between Domain Composition and Mechanism of Signal Transduction

Comparisons of recently published *apo* and *holo* high-resolution (~1.9 Å) crystal structures of the *E. coli* nitrate sensor NarQ that contain the periplasmic, TM and HAMP domains reveal extensive structural rearrangements involving a piston-like motion of TM1 relative to TM2 of approximately 2.5 Å. These displacements result in a lever-like rotation of individual HAMP domains upon binding of cognate ligand (205). Based on these results, the authors posit that receptors containing a membrane-adjacent HAMP domain function by a piston-type displacement of TM helices while those that lack such domains transduce signal by rotation of TM helices. We previously postulated a related yet different categorization of signaling mechanisms also based on the domain structure of bacterial receptors (206). We proposed that receptors containing a periplasmic four-helix bundle transduce signal across the membrane by piston-type displacements and that the attached membrane-adjacent HAMP domains might possess one of a multitude of signaling mechanisms including a gearbox-type rotation (114), a dynamic bundle (124) or potentially other mechanisms (206). Differentiating between these classification systems will provide a theoretical framework for understanding domain-based intra-protein allosteric communication by bacterial receptors. A recent authoritative structural-based review of transmembrane communication by bacterial receptors addresses these different suggestions (207).

The results presented here also examines whether SHKs that possess membrane-adjacent HAMP domains function solely by piston-type displacements or whether other signaling mechanisms might be employed. The results here with EnvZ should be compared with previous findings from the aspartate chemoreceptor (Tar) and the recent NarQ structures (12,205,208,209) as these three are ideal candidates for comparison because they all possess a membrane-adjacent HAMP domain, however, while Tar and NarQ possess a periplasmic four-helix bundle, EnvZ possesses a periplasmic PDC/CACHE domain (210,211). The authors of the recent NarQ structures posit that the presence or absence of the

membrane-adjacent HAMP domain may be the difference between receptors employing piston-type mechanisms of transmembrane communication as compared to other mechanisms (205). However, differences employed during transmembrane communication by the Tar and EnvZ TMDs observed here and previously strongly suggest that Tar and EnvZ possess different mechanism of TM communication even though both possess a membrane-adjacent HAMP domain. Our previous work analyzed AS1 helices from *E. coli* NarX, *E. coli* Tar, *E. coli* EnvZ and Af1503, the HAMP domain resulting in the initial high-resolution structure (114), and found that the Tar and NarX AS1 helices possess similar properties, which the AS1 helices from both EnvZ and Af1503 fail to possess. Recent comparisons of the *apo* and ligand-bound structures of the combined periplasmic-TM-HAMP domain from *E. coli* NarQ demonstrate that binding of ligand results in symmetrical displacements of TM1 relative to TM2 of approximately 2.5 Å (205). These results are similar to Tar, which functions by asymmetrical TM2 displacement also possesses a periplasmic four-helix-bundle (12,208,209,212).

Act III:
"It's (not) alive!": Frankenstein Science in Two-Component Signalling

Chapter 8: Background

As mentioned throughout Chapter 1, specifically within 1.4, the two-component system would be an ideal novel antibiotic target due to its abundance in bacteria and rarity in higher organism or even lack thereof in mammals. Here, our approach to the matter and construction of a synthetic system for the purpose of high-throughput screening is explained.

8.1 An Overview of Synthetic Biosensors

Synthetic biosensors have been one of the most popular applications of Synthetic Microbiology, allowing research in this field to branch out to other field of research requiring rapid and sensitive detection of specific molecules. *E. coli* systems are especially popular as templates to create these synthetic sensors, as they contain conserved residues of classical receptors, which ensures symmetry during the creation of chimeras, as well as there being a wealth of information of *E. coli* systems which are still unavailable for many other microbes.

In the creation of chimeric sensors, the main challenge seems to be finding the best fusion point, which would maintain sensory function. The creation of a library of chimeric chemoreceptor has been attempted, showing the versatility of the *E. coli* Tar receptor to be coupled with most sensory domains at different fusion points, even in the absence of sequence or structural homology (213). Furthermore, EnvZ-based chimeric receptors expressed using pRD400 plasmid has been applied to conduct high-throughput screening (HTS) platform ***(Figure 8.1)***; construction of chimeras exploits homology in the transmembrane and HAMP region (214). This project attempts to do both, by creating a library of functional interspecies EnvZ-based chimera to be used in a fully optimised novel HTS.

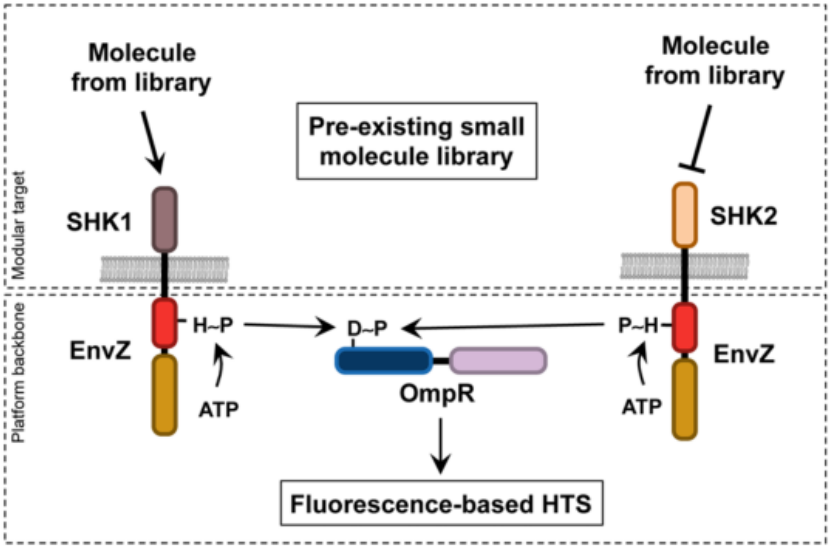

Figure 8.1. Schematic of a novel high-throughput screening platform utilising an EnvZ-based chimeric receptor.
Chimeras were expressed within EPB30 cells using the pRD400 backbone. Sensory regions for the chimeras were taken from *E. coli* aspartate (Tar) and nitrate/nitrite (NarX) chemoreceptors. *Image taken from* (214).

8.2 Integrating the Chimeric Gene, *phoQenvZ-V5*, in the Backbone of pRD400

Like most cloning vectors, these *envZ* expressing plasmids originated from pBR322 (ATCC® 31344™), which contains the *bla* (Ap^R) and *tet* (Tc^R) genes, pMB1 *ori* and *rop* ***(Figure 8.2)***. Addition of the *lacI* operon, *ompB* operon, and ColE1 ori together with M13 IG (intergenetic region) to replace the *tet* gene and pMB1 ori resulted in pFR29 (131). Deletion of the *ompR* gene and M13 IG resulted in pEnvZ. Furthermore, the addition of a V5 tag to the *envZ* gene resulted in pRD400 ***(Figure 4.1)***; pRY100 was made by replacing *envZ-v5* with *phoQenvZ-V5* ***(Figure 8.3)***. Furthermore, as with pRD400, pRY100 is expressed within the EPB30 cell line, which contains *cfp* and *yfp* to *ompC* and *ompF* translational gene fusions ***(Figure 4.1)***.

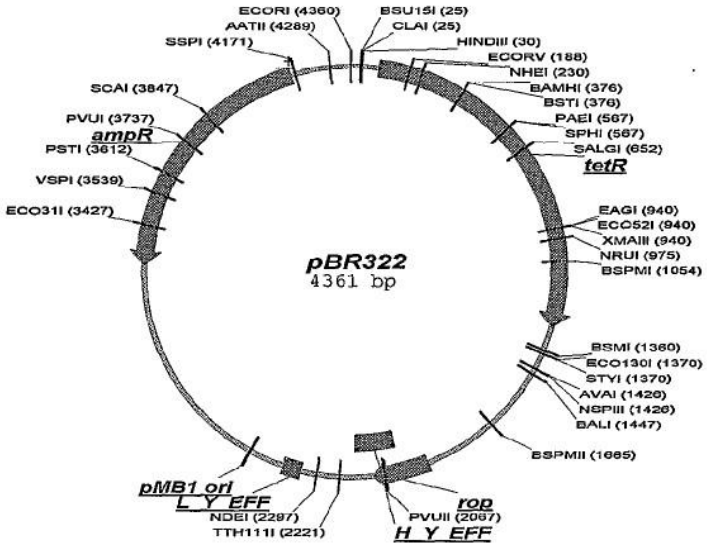

Figure 8.2. Schematic map of pBR322 (ATCC® 31344™).
Prominent features of this plasmid include the *bla* (Ap^R) and *tet* (Tc^R) genes as markers, and pMB1 ori and *rop* to maintain plasmid low copy number.

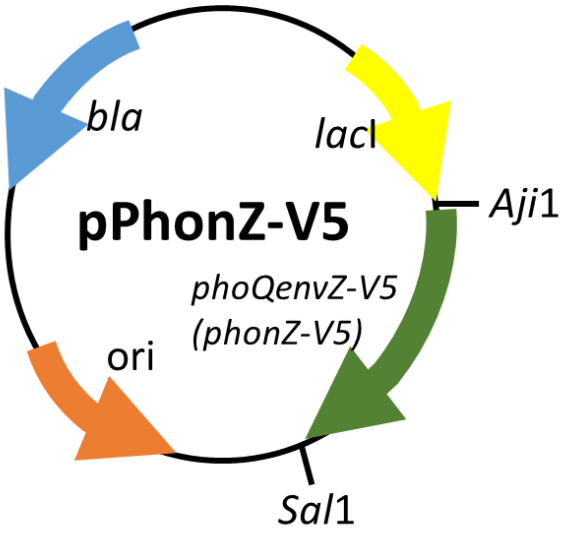

Figure 8.3. Schematic map of pPhonZ-V5.
This plasmid retains the *bla* gene from pBR322, as well as the ColE1ori and *lacI* operon from pFR29. *Aji*I and *Sal*I were used to replace *envZ-V5* in pRD400 to *phoQenvZ-V5* via restriction digest.

8.3 The Hybrid Sensor: PhoQ-EnvZ (PhonZ)

For our prototype chimera, we had chosen the magnesium sensor, PhoQ of *Salmonella enterica* serovar Typhimurium due to its similar topology with EnvZ, *i.e.* having a periplasmic sensing domain with two transmembrane domains, and its involvement in virulence regulation. In its native two-component system, PhoP/PhoQ, PhoQ autophosphorylates under low concentration of magnesium, as this HK associates it with an 'intracellular' environment, *e.g.* phagosome, and then phosphorylates its cognate response regulator, PhoP (215). PhoQ/PhoP multitasks via transcriptional cross-talks with a variety of two-component systems; most of these relationships are not yet fully understood. ***Figure 8.4*** illustrates the cooperation between PhoQ and EnvZ in controlling the expression of one of the Salmonella pathogenicity islands to ensure survival within host cells. Along with EnvZ/OmpR, PhoP/Q coordinates the SsrA/B system, which regulates virulence genes in the Salmonella Pathogenicity Island-2 (SPI-2) (216). In addition, PhoQ/PhoP regulates the iron sensing TCS, PmrB/PmrA, which controls LPS modifications resulting in polymyxin resistance (215,217), a relationship also found in other pathogens, such as *Pseudomonas aeruginosa* (218).

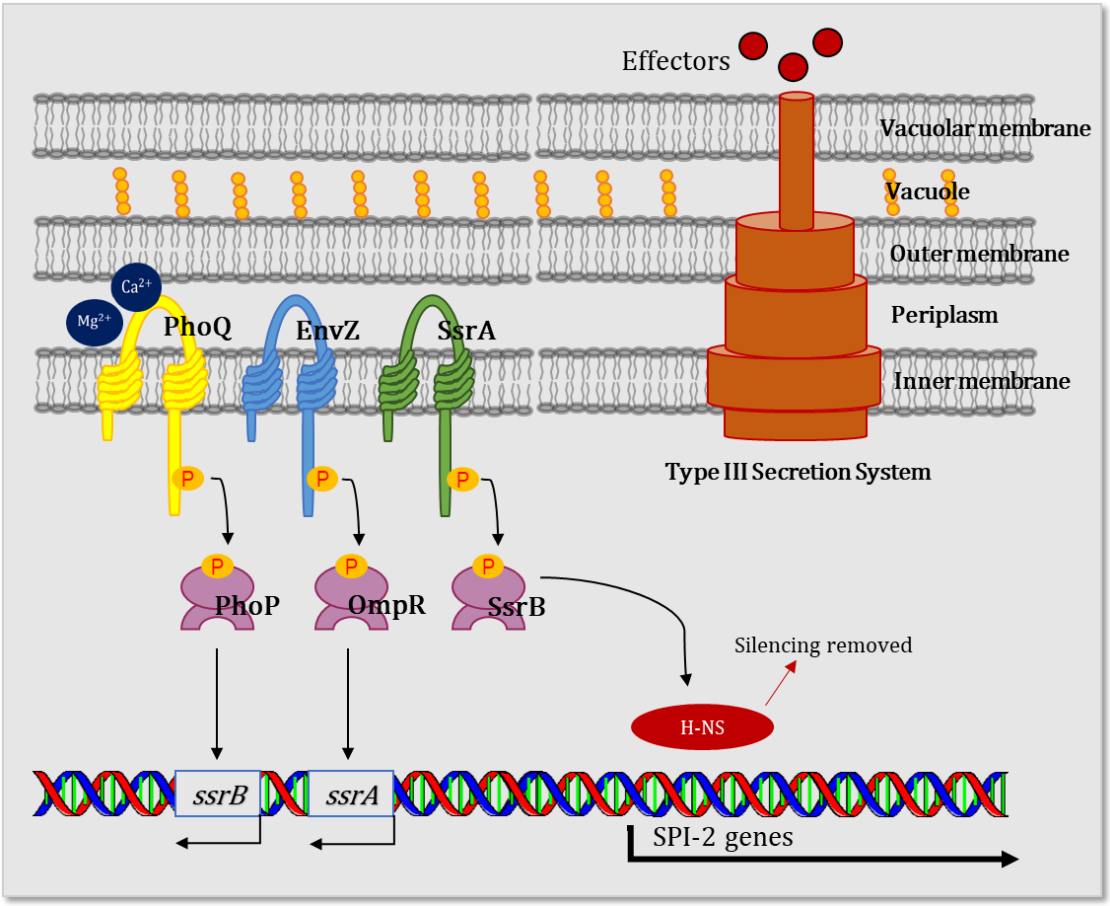

Figure 8.4. Cross-talk between PhoQ/PhoP and EnvZ/OmpR to control virulence via Salmonella Pathogenicity Island 2 (SPI-2) genes.

PhoQ interacts with Ca^{2+} and Mg^{2+}, while EnvZ responds to changes in osmolarity. Their cognate RRs, PhoP and OmpR, controls transcription of *ssrA* and *ssrB*, respectively. SsrA phosphorylates at low pH, and its cognate RR, SsrB removes silencing of SPI-2 genes by the histone-like nucleoid-structuring protein (H-NS), which results in the assembly of Type III Secretion Systems (T3SS), an injector-like protein that secrets effector molecules responsible for systemic infections (219). *Image adapted from MBInfo, Mechanobiology Institute, National University of Singapore, 2018.*

Chapter 9: Materials & Methods

This chapter explains the techniques used to construct and create the chimeric receptor, starting from chimera gene design to analysis of receptor expression via immunoblotting and analysis of signal output via fluorescence spectrophotometry, including aromatic tuning used to modulate signal pattern.

9.1 Bacterial Strains and Plasmids

E. coli strain MG1655 (F- λ- *ilvG rfb50 rph1*) was used to control for light scattering and cellular autofluorescence, whilst strain EPB30 (MDG147 *envZ::kan*) (153) derived from MDG147 [MG1655 Φ(*ompF*$^{+}$-*yfp*$^{+}$) Φ(*ompC*$^{+}$-*cfp*$^{+}$)] (132) was used for analysis of steady-state signal output from osmosensing circuits. Plasmid pRY100 was constructed by replacing *envZ* in pRD400 (86) with *PhoQ-EnvZ* or *phonZ*, while retaining the original IPTG-based induction of *envZ*, a seven-residue linker (GGSSAAG) and a C-terminal V5 epitope tag (GKPIPNPLLGLDST). Plasmid pEB5 served as an empty control vector that does not express EnvZ. MG1655 transformed with pEB5, EPB30 transformed with pRD400 and EPB30 transformed with pRY100 was used for receptor expression and signal output analysis.

9.2 Designing the Chimeric Receptor, PhonZ

Domain prediction for the *Salmonella* Typhimurium PhoQ receptor was obtained from Uniprot (P0DM80 – PHOQ_SALTY), coupled with transmembrane domain predictions from TMHMM Server v. 2.0 (158). The PhoQ protein sequence was analysed with the Prabi-Gerland's Coiled-coil Prediction Server to look for sequence homology with EnvZ at the linker region following the second transmembrane, which would then become the fusion point of the two receptors. This server would also show aromatic residues on the PhoQ second transmembrane domain that could be used for aromatic tuning. Plasmids containing the *phonZ* gene and primers (***Figure 9.1***) used for aromatic tuning of pRY100 were supplied by Eurofins Scientific™.

WW-3 : WWWIAASLRPIEA
WW-2 : WIWWAASLRPIEA
WW-1 : WIAWWASLRPIEA
WW : WIAAWWSLRPIEA
WW+1: WIAAIWWLRPIEA
WW+2 : WIAAIAWWRPIEA
WW+3 : WIAAIAAWWPIEA

Figure 9.1. Amino acid sequences encoded by primers used for aromatic tuning (SDM-PCR) of pPhonZ.

9.3 Analysis of Chimeric Receptor Expression *In Vivo*

Bacterial cultures were grown as described previously (86) with slight modifications. Fresh colonies were used to inoculate 2-ml overnight culture of minimal medium A (160) supplemented with 0.2% glucose. Ampicillin, sucrose and IPTG were added where appropriate. Cells were grown overnight at 37°C and 200 rpm, and diluted 1:1000 into 7-ml of fresh medium. When the final bacterial cultures reached an OD_{600nm} ~ 0.3, cell pellets were collected and resuspended in standard 6X reducing SDS-PAGE buffer. Cells were lysed with heat-thaw cycles and analysed on 10% SDS/polyacrylamide gels. Standard buffers and conditions were used for electrophoresis, immunoblotting and detection with enhanced chemiluminescence (161). Anti-V5 (Invitrogen) was used as the primary antibody, while peroxidase-conjugated anti-mouse IgG (Sigma) was employed as the secondary antibody. Digitised images were acquired with a ChemiDoc MP workstation (Bio-Rad), analysed with ImageJ v1.49 (162) and quantified with QtiPlot v0.9.8.10.

9.4 Analysis of Signal Output *In Vivo*

Bacterial cells were grown as described above, with modifications in the sucrose (between 0-15%) and MgSO4 (between 0-10 mM) concentrations as necessary. When the cells reach an OD_{600nm} ~ 0.3, chloramphenicol was added to a final concentration of 170 µg/ml to inhibit protein synthesis. Cell pellets were collected from 5 ml of culture and resuspended in 100-µl of fresh media. Fluorescence measurement was promptly performed in 96-well plates with a Varian

Cary Eclipse (Palo Alto, CA). CFP fluorescence was measured using an excitation wavelength of 434 nm and an emission wavelength of 477 nm, while YFP fluorescence was measured using an excitation wavelength of 505 nm and an emission wavelength of 527 nm. These values were corrected for differences in cell density by dividing the fluorescent intensities by OD_{600nm} and for light scattering/cellular autofluorescence by subtracting the CFP and YFP fluorescence intensities determined for MG1655/pEB5 cells.

Chapter 10: Constructing the Functional Ion-sensing Chimeric Receptor PhoQ-EnvZ (PhonZ)

10.1 Disclaimer

Experiments involving pPhonQEnvZ-V5 (pPhonZ-V5) were mainly conducted by myself, assisted by Lucy V. Eke. Thanwarat Chavalwan performed additional experiments to confirm those initial results. Further experiments involving the SEVA plasmid system was conducted by myself and Phillipa Cheesman. Roger R. Draheim conceptualised the project and designed the framework of the experiments.

10.2 Results

10.2.1 Utilising EnvZ Signalling in Chimeric TCS

Similar to EnvZ, the PhoQ sensor histidine kinase (HK) of *S.* Typhimurium structurally follows the canonical HK template: membrane-anchored by two transmembrane domains with a periplasmic sensory domain, in addition to having the conserved sequence homology on the HAMP domain also found in other two-component systems. Supported by previous successful attempts at chemoreceptor-EnvZ chimera design (214), the fusion point chosen to create PhoQ-EnvZ (PhonZ) is located near the end of the C-terminal of the HAMP domain of PhoQ and a parallel location at the end of the HAMP domain of EnvZ (***Figure 10.1***), allowing the newly created receptor to fully retain the sensory part of PhoQ supported by a well-defined EnvZ/OmpR pathway.

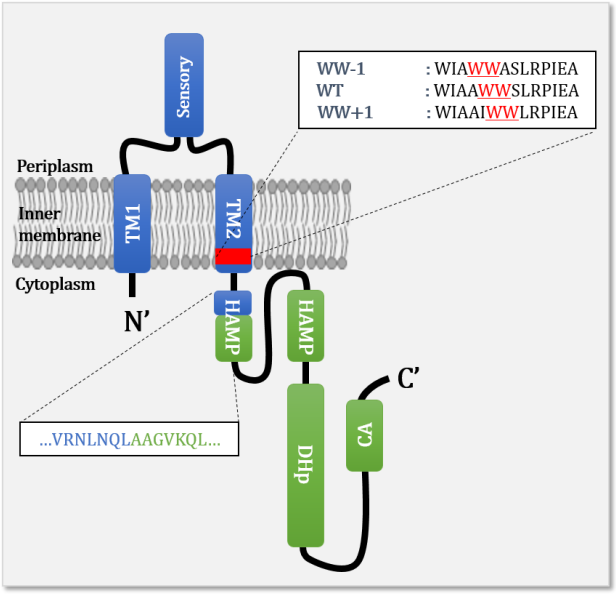

Figure 10.1. Domain organization of the chimeric receptor PhoQ-EnvZ (PhonZ). The blue region of the receptor originated from PhoQ, while the green region originated from EnvZ-V5 (residues belonging to each HK counterpart are highlighted with these corresponding colours). The red area shows the residues modified by aromatic tuning.

Control of receptor expression is crucial in achieving a steady state signal output, measurable here by CFP/YFP ratios. EPB30/pRD400 requires induction of its *envZ-V5* gene by 20 µM IPTG in minimal media A to produce a signal output that is similar to that of MDG147/pEB5 (86). Alterations in EnvZ-V5 expression would result in fluctuating levels of CFP (or OmpC) without any significant changes in levels of YFP (or OmpF), therefore compromising the steady state signal (86).

EPB30/pRD400 was grown under standard conditions for immunoblotting analysis (minimal media A supplemented with 50 µM IPTG) (86), while EPB30/pRY100 was grown in a similar media with varying concentrations of IPTG: 0, 0.1, 0.2, 0.5, 1, 2 and 5 µM. To account for variability of receptor expression in the presence of stimulus, varying concentration of sucrose (w/v) were also implemented (between 0 - 15%). As EnvZ retains the ability to detect increase in extracellular osmolarity via its cytoplasmic domains, PhonZ would also have this sensory function albeit with significant decrease in

sensitivity. Samples obtained from both strains were run side by side on one gel allowing for comparability between EnvZ-V5 and PhonZ-V5 bands during quantification (***Figure 10.2***).

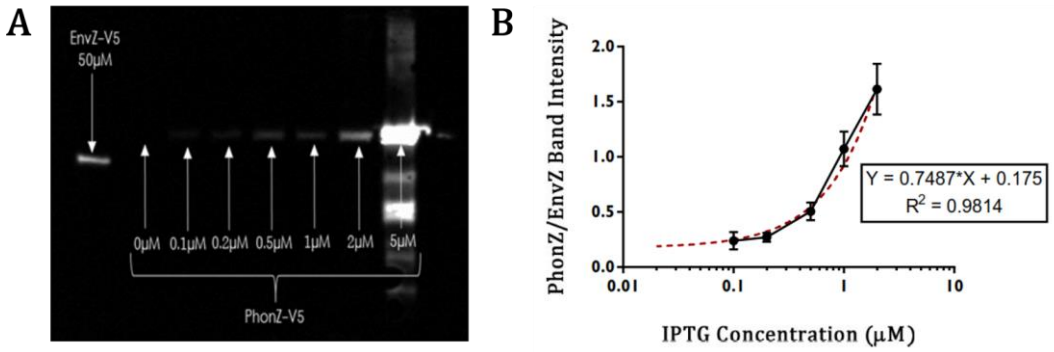

Figure 10.2. Immunoblotting analysis of untuned PhonZ receptor expression.
Immunoblotting image of EnvZ-V5 and PhonZ-V5 **(A)** was quantified and plotted to show the connection between receptor expression and IPTG concentration, in units of PhonZ/EnvZ ratio **(B)**. Each data point on the X-axis consists of the average value of PhonZ/EnvZ band intensity for cells grown under varying sucrose concentration, with 4 replicates for each concentration.

Immunoblotting results showed that IPTG concentration of 1 μM could produce the most similar expression of PhonZ-V5 with EnvZ-V5, thus this IPTG concentration would be used for subsequent analysis of PhonZ-V5 signal output.

10.2.2 Aromatic Tuning of PhonZ-V5

An expected issue when creating a synthetic two-component system is loss of function. Modifications in aromatic amino acid residues in the transmembrane domain of a membrane-anchored histidine kinase has been shown to affect signal output, thus inspiring the conception of a stimulus-independent signal output modulation called 'aromatic tuning' (42). Here this technique is utilised to restore the function of a synthetic biosensor, practically by shifting the position of aromatic residues in the transmembrane via SDM-PCR.

Six different modifications were attempted for PhonZ-V5 (***Figure 10.1***); however, only mutants EPB30/pPhonZ-V5-WW-1 and EPB30/pPhonZ-V5-

WW+1 were successfully made. It was possible that certain mutations in the receptor might affect survivability of the cell, though the reason for this is still unclear.

10.2.3 Signal Output Analysis of EPB30/pPhonZ-V5 Variants

Fluorescence spectrophotometry was used to quantify the CFP and YFP levels produced by the PhonZ-V5 system. These values were then corrected by optical density (OD) to compensate for cell to cell density, and corrected by CFP and YFP values of MG1655/pEB5 for light scattering. ***Figure 10.3*** summarises the results of fluorescence analysis of all three PhonZ-V5 variants.

There was no increase in CFP in all concentrations of magnesium for PhonZ, despite a slight decrease of YFP as magnesium increases ***(Figure 10.3-A)***. The PhonZ-WW-1 receptor displayed the opposite profile. YFP remained low and stationary for this receptor across the whole range or magnesium concentrations, whereas its CFP were nearly three-fold higher of YFP and with a slight increase at concentrations above 0.1 mM ***(Figure 10.3-B)***. PhonZ-WW+1 had the lowest expression of YFP compared to the other two PhonZ variants, and similar to PhonZ-WW-1, this amount remained relatively stationary; interestingly, an exponential increase of CFP occurred between magnesium concentration 0.1 to 2 mM, implying possible dose-responsive substrate-receptor interaction ***(Figure 10.3-C)***.

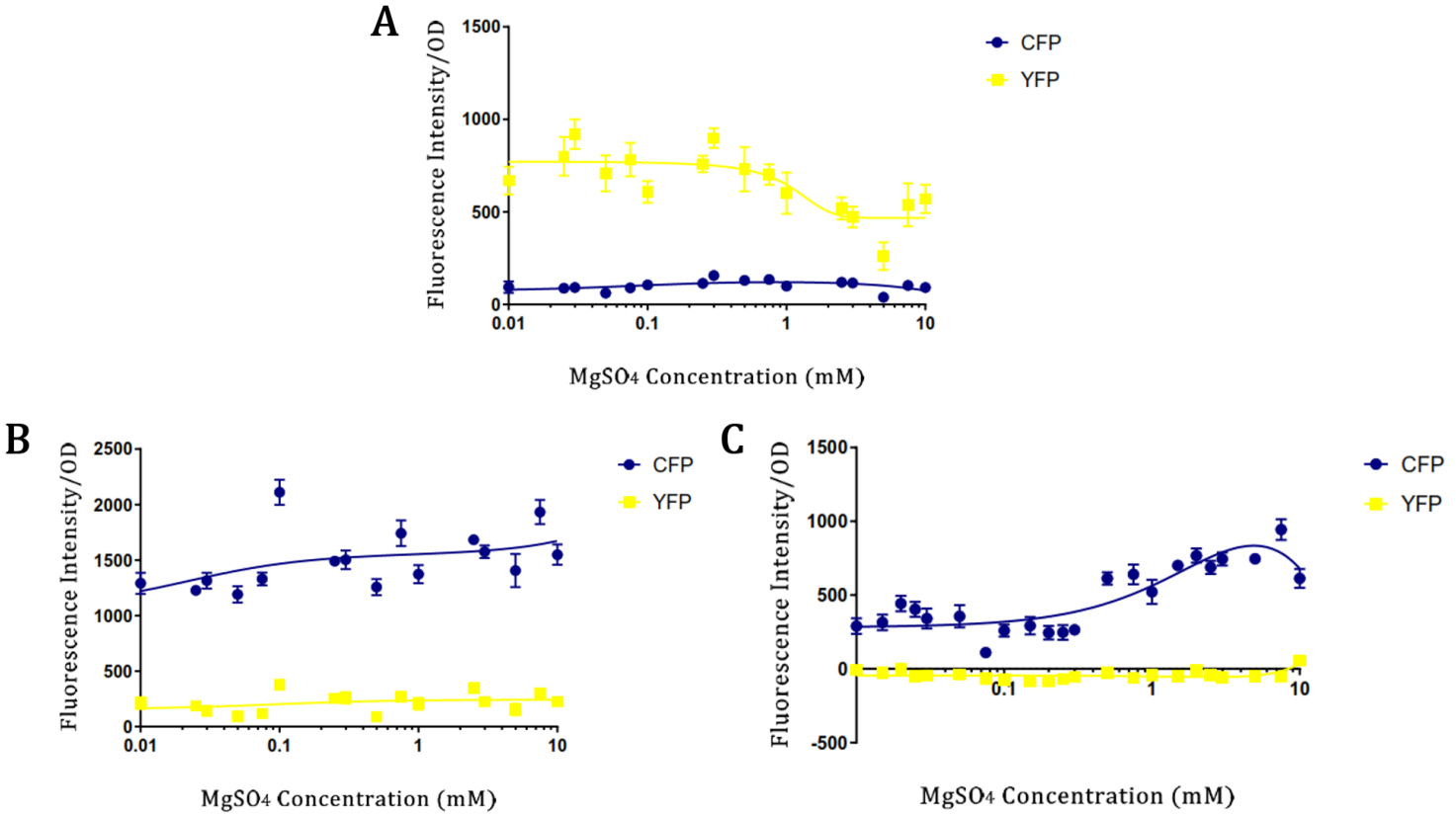

Figure 10.3. Results of signal output analysis of three PhonZ variants.

CFP and YFP levels (a.u.) of untuned PhonZ **(A)** PhonZ-WW-1 **(B)** and PhonZ-WW+1 **(C)** were measured via fluorescence spectrophotometry, and corrected for optical density (OD) and light scatter (CFP and YFP of EPB30/MG1655). Measurements were taken at OD_{600nm} 0.2-0.4. Each data point is an average of 8 duplicates. Aromatic tuning modulated the level of CFP, while YFP remains low or zero; the contrary was observed for the untuned PhonZ variant. Graphs were generated using GraphPad Prism 7.0, and trendlines were calculated using the dose-response (stimulation) function with Hill slope = 1.0.

10.2.4 Phenotypic Anomalies of EPB30/pPhonZ-V5-WW+1

While it was no surprise that mutations on the aromatically tuned variants might impact growth rate, extreme phenotypic anomalies were noticeable on the mutant containing PhonZ-WW+1. Growth of this cell line was significantly impaired due to the cells forming non-dividing filaments ***(Figure 10.4-A)***. When the cells eventually multiplied, overexpression of fluorescence proteins could be physically observed as the growth media turned dark yellow to bright green, varying depending on magnesium concentration ***(Figure 10.4-B)***.

In *E. coli* cells, an interaction between the PhoP/PhoQ with septation inhibitor protein, QueE, is present. When sublethal cationic antibacterial peptides is detected by PhoQ, this receptor then activates PhoP; this response regulator positively regulates QueE, which binds to divisome and prevents septation, thus creating filamentous cells (220). As chromosomal *phoP/Q* were not deleted or knocked-off from our EPB30 cell line, cross-talk bias from this system paired with effects of the aromatic tuning itself might have affected the signalling of our synthetic system.

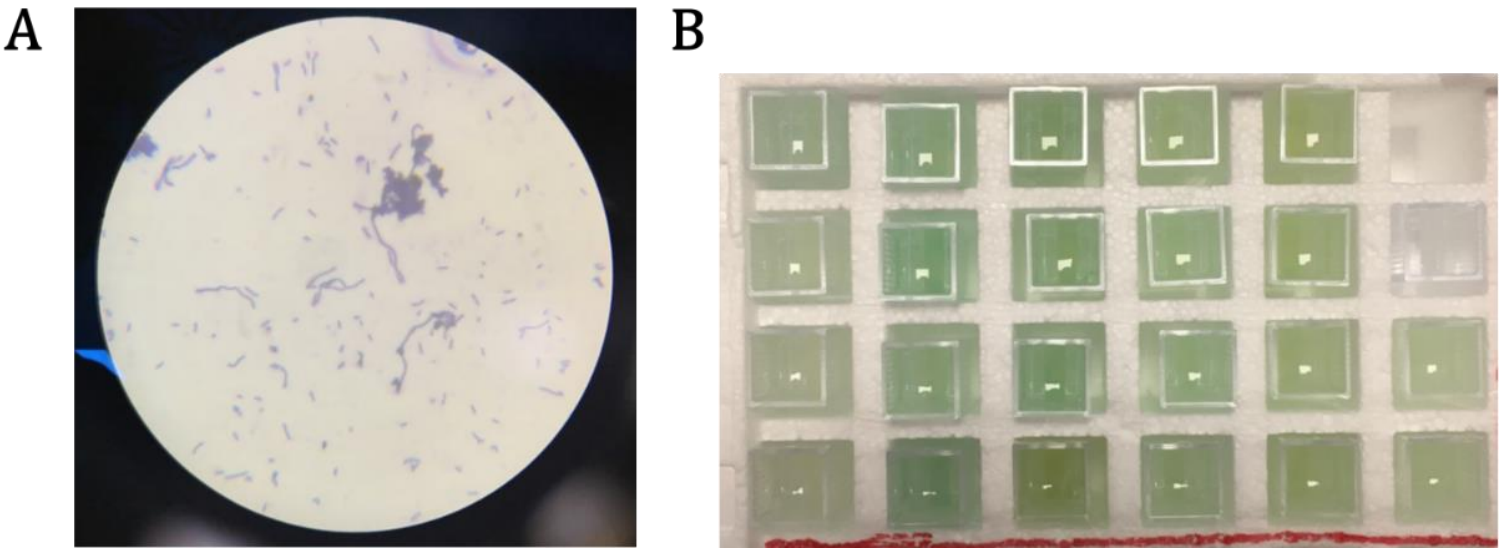

Figure 10.4. Phenotypic anomalies observed during PhonZ-WW+1 growth.
Electron microscopic image of EPB30/pPhonZ-V5-WW+1 cells (stained with Crystal Violet and magnified 1000X) showing long filamentous cells amongst normal dividing cells **(A)**, and green liquid colonies growing in 1X MMA supplemented with 1 µM IPTG with varying concentrations of $MgSO_4$, placed in 2mL cuvettes **(B)**.

10.2.5 Confirmation of Initial Results

Due to the unusual phenotypic profile produced by the PhonZ-WW+1 receptor, each pPhonZ variant was sequenced and re-confirmed; no unwanted mutations were found. These plasmids were again transformed into new EPB30 cells, and the previous signal output analysis repeated. Results obtained with these recreated cells are presented in ***Figure 10.5.***

CFP and YFP of all three PhonZ-V5 variants in the new EPB30 cells greatly decreased compared to those produced by the previous cell lines ***(Figure 10.3)***. Both CFP and YFP of PhonZ were lower than values obtained from MG1655/pEB5, hence corrected values for these measurements were entirely below zero ***(Figure 10.5-A)***. Signal output produced by the PhonZ-WW-1 and PhonZ-WW+1 were nearly identical; YFP values were lower than MG1655/pEB5 and CFP were higher, both with little to no increase throughout the whole concentration regime ***(Figure 10.5-B*** and ***Figure 10.5 C)***. Neither variant showed dose-responsive substrate-receptor interaction.

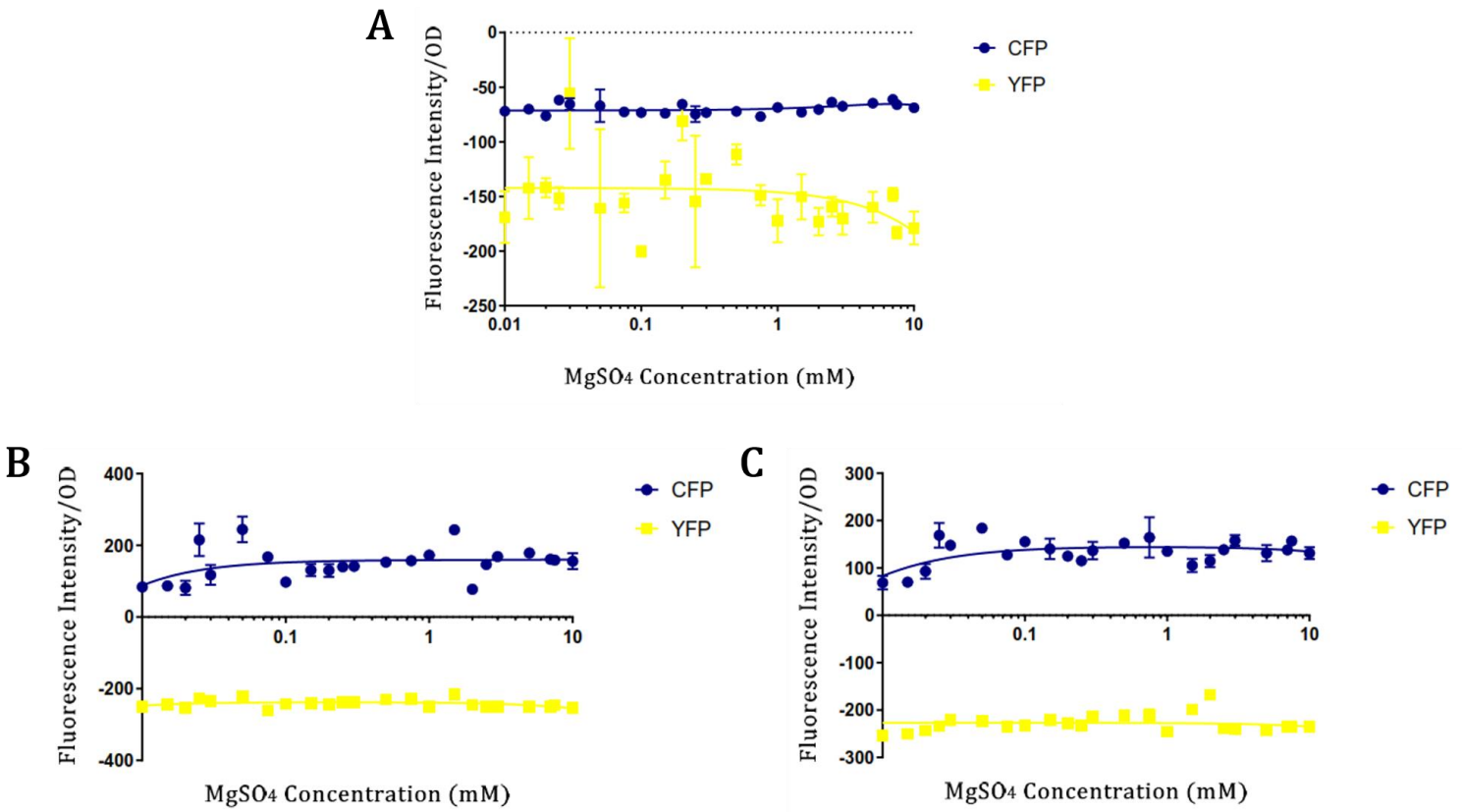

Figure 10.5. Results of signal output analysis of three PhonZ variants (re-transformed into new EPB30).

CFP and YFP levels (a.u.) of untuned PhonZ **(A)** PhonZ-WW-1 **(B)** and PhonZ-WW+1 **(C)** were measured via fluorescence spectrophotometry, and corrected for optical density (OD) and light scatter (CFP and YFP of EPB30/MG1655). Measurements were taken at OD_{600nm} 0.2-0.4. Each data point is an average of 4 duplicates. Aromatic tuning modulated the level of CFP, while YFP remains low (negative values due to light scatter correction). Graphs were generated using GraphPad Prism 7.0, and trendlines were calculated using the dose-response (stimulation) function with Hill slope = 1.0.

10.3 Discussion

10.3.1 Aromatic Tuning Modulates Signal Output of PhonZ-V5

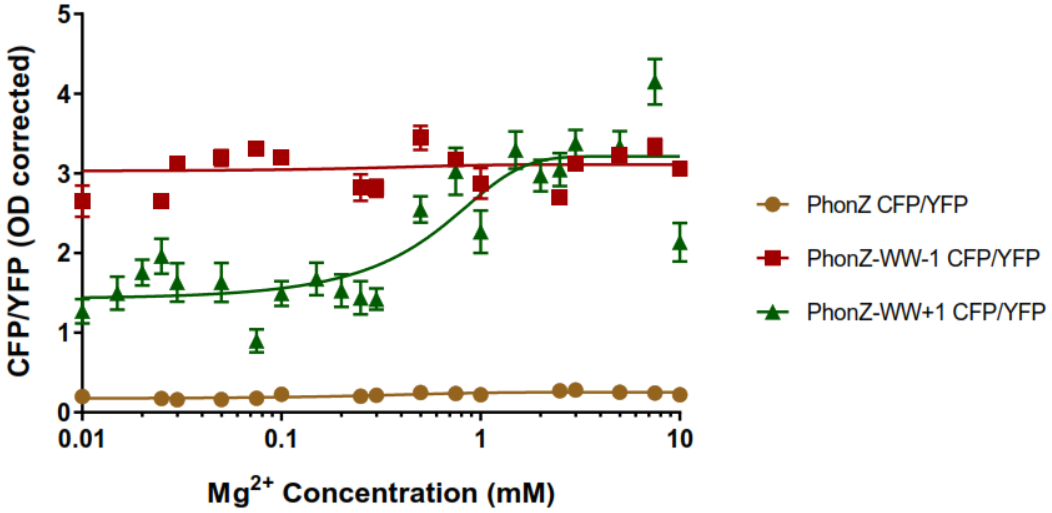

Figure 10.6. Signal output (CFP/YFP) of three PhonZ-V5 variants expressed in EPB30/pPhonZ-V5, EPB30/pPhonZ-V5-WW-1 and EPB30/pPhonZ-V5-WW+1 cells. Data presented in ***Figure 10.3*** recalculated as CFP/YFP ratios. Unmodified PhonZ (brown) was locked on the 'OFF' state, while the PhonZ-WW-1 (red) was locked on the 'ON' state. PhonZ-WW+1 (green) showed a dose-response pattern. Graphs were generated using GraphPad Prism 7.0, and trendlines were calculated using the dose-response (stimulation) function with Hill slope = 1.0.

In order to observe the dynamic range of the receptor, it is important to see the relationship between CFP and YFP, as the ratio of ompC and ompF porins change following fluctuations in extracellular osmolarity, or in this case, extracellular magnesium concentration. Ideally, a working receptor should have a relatively wide dynamic range with a clear distinction between its OFF and ON state ***(Figure 4.1-B)***. This would allow us to quantify changes in receptor activity when the cell is subjected to blockers or inhibitors during screening of novel antimicrobials.

Figure 10.6 summarises the CFP/YFP patterns of the three PhonZ variants under the presence of stimulus. The wild-type PhonZ failed to interact with the stimulus and was locked on the 'OFF' state as CFP/YFP level remains close to zero and relatively stationary throughout the whole range of magnesium concentrations applied. Moving the WW pair along the second transmembrane

domain caused drastic changes to this pattern. The CFP/YFP level of PhonZ-WW-1 showed that this variant seemed to be locked on the 'ON' state; expressing high amounts of CFP over YFP even at lower magnesium concentrations with very little dynamic range throughout the whole concentration regime. Promising results were thought to have been obtained with the PhonZ-WW+1 as the CFP/YFP expression pattern showed an exponentially increasing pattern, mimicking that of a dose-response curve. Magnesium concentrations above 0.1 mM appeared to have switched ON the receptor. Sequencing results later on confirmed that no unwanted mutations were present in the plasmid, implying that chromosomal mutations, not the aromatic tuning, had caused this effect.

10.3.2 Aromatic Tuning Failed to Establish Steady State Signal

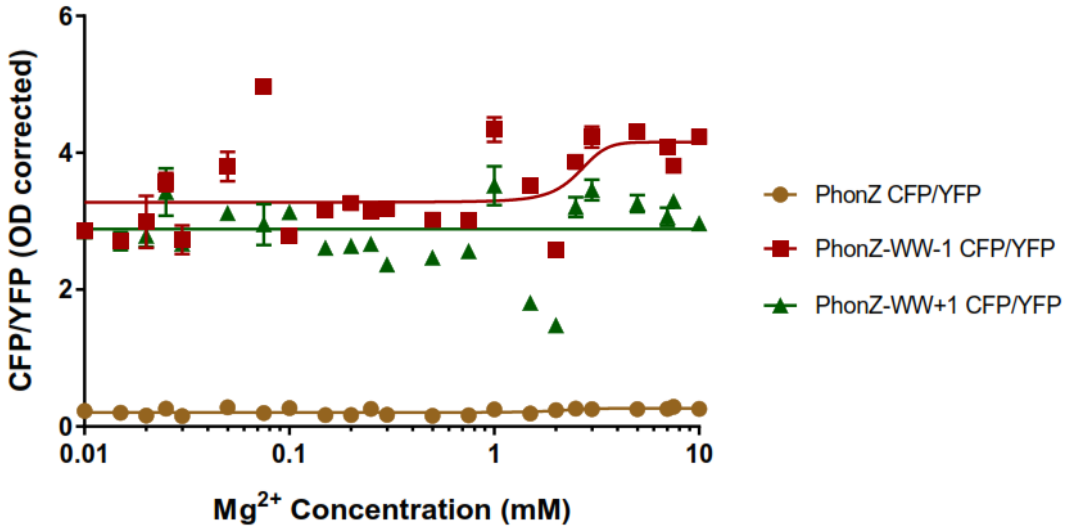

Figure 10.7. Signal output (CFP/YFP) of three PhonZ-V5 variants expressed in EPB30/pPhonZ-V5, EPB30/pPhonZ-V5-WW-1 and EPB30/pPhonZ-V5-WW+1 cells (re-transformed into new EPB30).
Data presented in ***Figure 10.5*** recalculated as CFP/YFP ratios. Unmodified PhonZ (brown) was locked on the 'OFF' state, while both PhonZ-WW-1 (red) and PhonZ-WW+1 (green) was locked on the 'ON' state. Graphs were generated using GraphPad Prism 7.0, and trendlines were calculated using the dose-response (stimulation) function with Hill slope = 1.0.

To confirm results obtained in ***Figure 10.6***, an independent experiment was conducted using new competent EPB30 cell lines. ***Figure 10.7*** summarises the

CFP/YFP patterns of the three PhonZ variants in the new EPB30 cell lines, under the presence of stimulus. Unmodified PhonZ remained locked on the 'OFF' state, as before. Conversely, both PhonZ-WW-1 and PhonZ-WW+1 seemed to be locked on the 'ON' state, with only a slight increase in signal for the WW-1 variant. Conclusively, aromatic tuning failed to restore receptor function of PhonZ and steady state signal output could not be achieved.

10.3.3 The SEVA Plasmid Platform as a Possible Solution

One of the bottlenecks of creating a synthetic system in bacteria is forcing a cell to express a new-to-nature or completely artificial protein that is somehow still as functional as its wild-type counterpart. Construction of conventional plasmids in Molecular Biology and Synthetic Microbiology utilised a modified version of bacterial-derived plasmids, containing mainly the expression cassette (EC), which is a transcriptional unit consisting of the gene(s) of interest and regulatory sequences required for expression in mammalian cells, and the bacterial backbone (BB), which consists of antibiotic resistance gene and origin of replication required for its survival in bacterial cells (221). As these functional components are integrated within naturally occurring segments, conventional plasmids often contain unwanted internal sites and restriction sequences, making the plasmid unnecessarily large, which lowers the efficiency of plasmid production (221,222).

The Spanish-made Standard European Vector Architecture (SEVA) was made to tackle this limitation (222,223), by minimising and simplifying plasmid design to only contain three interchangeable modules: the cargo, which contains the promoter and gene of interest, and housekeeping components, namely the origin of replication and the marker ***(Figure 10.8-A)***.

In line with the minimalistic design, SEVA's nomenclature is based on the user's selection of the three modules ***(Figure 10.8-B)***. Our plasmid design for PhonZ expression is coded 434 (Sp^R, LacI, pBBR1). The LacI promoter was chosen to enable a tighter regulation of PhonZ expression (224), which might

solve the problem of porin overexpression we had previously. The pBBR1 replication origin was chosen for compatibility with *E. coli* cell lines, and to allow compatibility with other *E. coli* replication (RK2) origins for future projects. The resulting plasmid used in our SEVA experiments is mapped out in ***Figure 10.9***.

Figure 10.10 shows the result of expression analysis of PhonZ generated by this new SEVA plasmid. The three different variants of RBS strengths produced noticeably very different expression levels, which were visible even on the blot images ***(Figure 10.10-A)***. As done previously ***(Figure 10.2)***, expression of PhonZ variants grown in different concentrations of IPTG were quantified and compared to EnvZ, which was also expressed under different RBS strengths. ***Figure 10.10-B*** shows that the weakest ribosome binding site produced the tightest control of receptor expression, whereas the medium and strong RBS showed leakage of signal with 4-fold more PhonZ expression. Moving forward, the p434-PhonZ-V5 variant with weak RBS would be the most likely generate a tunable signal output necessary to produce a dose-response pattern.

Overall the new plasmid design showed promising results as control on RBS interaction clearly resulted in significant difference in receptor expression. It is likely that this modulation would also affect signal output, which characteristics still need to be investigated.

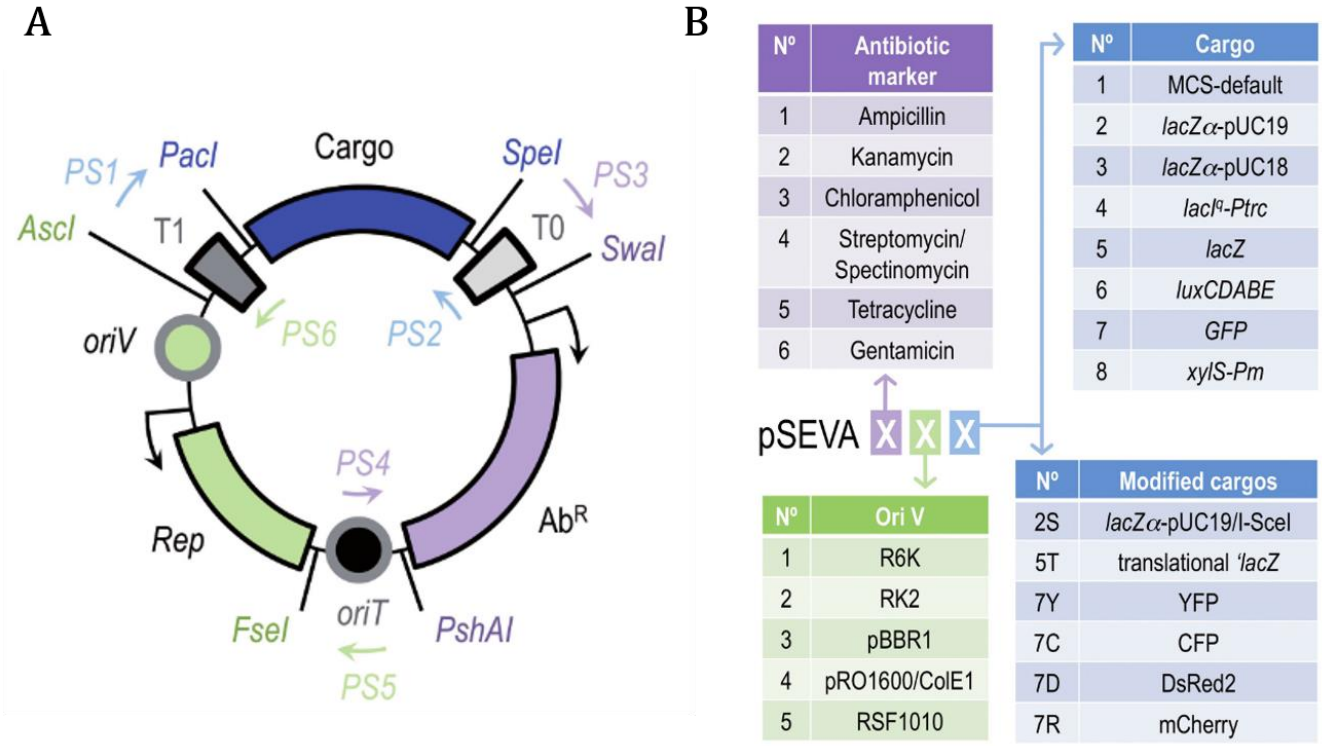

Figure 10.8. The overall organisation of the SEVA plasmid.

(A) SEVA plasmids are constructed from three variable modules: the cargo (blue), the origin of replication (green) and the selective marker (purple). **(B)** Options provided for the modules becomes the nomenclature of the plasmid generated; our plasmid, p434 uses spectinomycin-resistant with a pBR1 ori and LacI promotor. *Image taken from* (222).

Figure 10.9. Circular map of plasmid p434-PhonZ-V5-StrongRBS.
p434 refers to the SEVA database code for Sm/Sp resistance, pBBR1 ori and LacI promoter, which is linked to the PhonZ-V5 gene flanked by our choice of restriction sites for *Bam*HI and *Hind*III. In addition, three different ribosome binding site (RBS) strengths were created: weak, medium and strong.

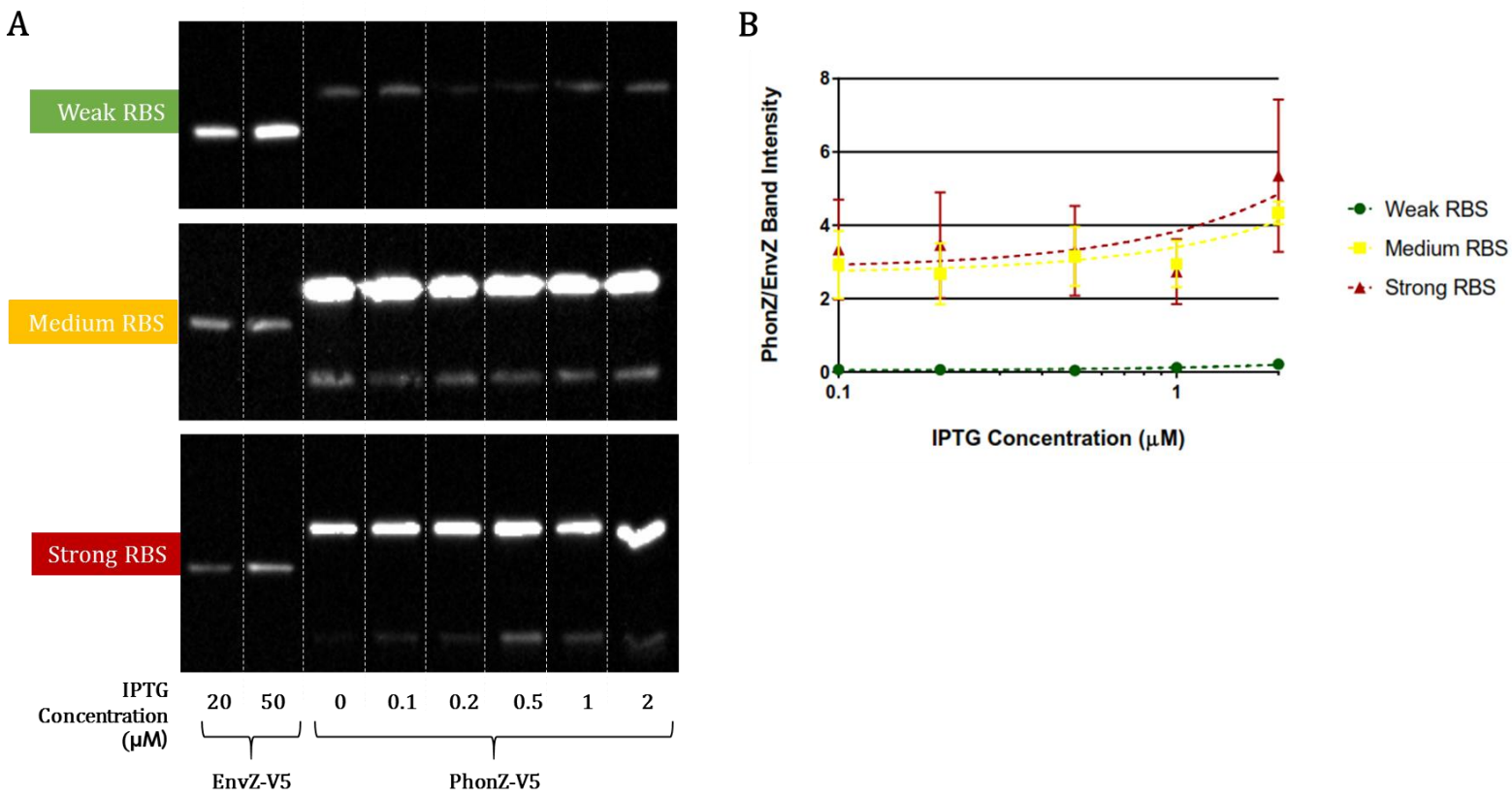

Figure 10.10. Analysis of PhoQ-EnvZ (PhonZ) receptor expression *in vivo*.

Three p434-EnvZ-V5 and p434-PhonZ-V5 variants with different ribosome-binding site (RBS) strengths, weak (green), medium (orange) and strong (red), were analysed for receptor expression using immnoblotting. **(A)** The three panels of blot images exhibit different levels of receptor expressions. Strains expressing EnvZ were grown at 20 and 50 μM IPTG concentrations, while strains expressing PhonZ were grown at IPTG concentrations between 0 – 2 μM. **(B)** Quantification of the PhonZ bands were done with respect to its corresponding EnvZ control. The graph shows ratio of PhonZ/EnvZ band intensity for the different RBS variants. The strain containing the weakest RBS strength displayed the best control of receptor expression.

Act IV:
Epilogue

Chapter 11: Conclusions and Future Plans

11.1 *E. coli* EnvZ Transmembrane Signalling

EnvZ is categorised as a Class I receptor due to its phosphotransfer signalling mechanism. Within this class, EnvZ represents the largest group of homodimeric transmembrane (TM)-bound receptors, characterised by two α-helical TM domains, a periplasmic-sensing domain, and cytoplasmic dimerization and histidine phosphotransfer (DHp) and catalytic ATP-binding (CA) domains. Despite not being involved in signal perception, for membrane-anchored histidine kinases the transmembrane domain(s) becomes a defining feature of the receptor. Interestingly, this domain is often overlooked compared to the more dynamic domains of the HK located in the cytoplasm. Therefore, the findings in this study becomes a valuable source of information to this less understood domain, especially for a prominent member of the transmembrane HKs group, such as EnvZ.

In general, three models represent the most likely interaction between helices in transmembrane signalling. The helical rotation model was found in periplasmic sensors, LuxQ, AgrC and DesK, whilst the piston model was most notably recognised in the Tar chemoreceptor and the diagonal scissoring model was found in PhoQ, both models demonstrated by cysteine cross-linking and molecular simulations (207). Here, also using cysteine cross-linking and molecular dynamics, we addressed how EnvZ transmembrane signalling fits into one of these models.

Due to the complexity of the results, we have published results of our studies of EnvZ TM domains in two separate publications. Studies of the first transmembrane domain (TM1 and TM1') revealed that the most dynamic part of the helices were residues located on the membrane interface closest to the periplasm. EnvZ has been shown to interact with another transmembrane protein, MzrA, using its periplasmic sensory domain (8,138), which might have been the

cause of this dynamic movement. The remaining part of TM1, however, seemed to be mainly involved in membrane anchoring and were relatively static in the presence of stimulus.

Studies of the second transmembrane domain (TM2 and TM2') revealed a more interesting story. This domain seemed to be more dynamic than the first, implying more involvement in signalling or at least, signal transfer, rightfully so as it connects two important domains in EnvZ signalling: the periplasmic sensory domain and the dimerization domain (DHp). We employed Coarse-Grained Molecular Dynamics platforms to model the interaction of these homodimeric helices and predicted that a non-piston movement had occurred when stimulus was presented in the environment and signalling was activated.

Further studies on interaction between two TM domains, *i.e.* the four helical bundle of both TM1s and TM2s, would be necessary to support these findings and provide a much better understanding on transmembrane dynamics. These studies are currently being conducted in our research group, again using cysteine cross-linking and molecular dynamics. Several models of interaction between four helical bundles are depicted in ***Figure 11.1***.

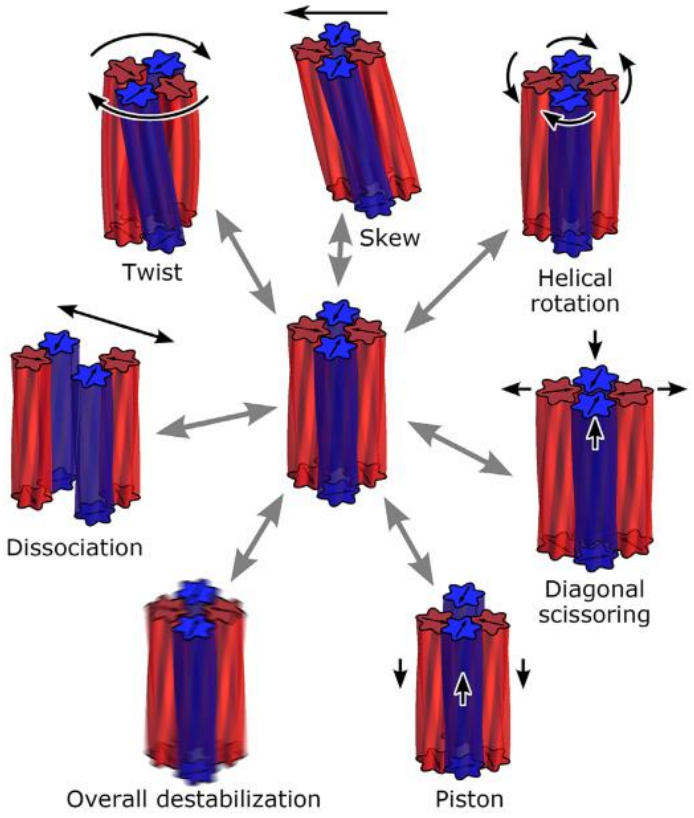

Figure 11.1. Seven models that has been proposed for four helical transmembrane bundles. The most likely interactions, and ones that has been shown through direct experimental data were the piston (Tar), diagonal scissoring (PhoQ) and helical rotation models (LuxQ, AgrC and DesK). *Image taken from* (207).

11.2 Characterisation of EnvZ-based Biosensors

This study has demonstrated that the pRD400 backbone, which has been a valuable tool in many of our studies involving EnvZ, requires reassessment and redesign to be able to accommodate the expression of synthetic systems. This plasmid was designed based on the classical *E. coli*-originted cloning vector pBR322, and furthermore, pFR29, therefore still retaining some native features of the plasmid, *i.e.* origin of replications, antibiotic marker and restriction sites. In synthetic microbiology, this method of conventional plasmid design, containing redundant features from previous generations, could sometimes hinder efficient expression of synthetic proteins.

Aromatic tuning of the PhonZ receptor expressed using this backbone has been attempted; however, results have shown that this method failed to restore the sensory function of the PhoQ half, thus a steady state baseline signal could not be established. Signal output analysis revealed that while aromatic tuning turned the PhonZ receptor from 'OFF' to 'ON' (for both PhonZ-WW-1 and PhonZ-WW+1), neither variant has the wide dynamic range that is crucial for a baseline signal to start high-throughput screening. Therefore, a more modular and minimalist design containing only features required to express a desired phenotype is necessary.

The standardised plasmid-design platform, SEVA (Standard European Vector Architecture), provides this service. Solving the difficulty in Systems and Synthetic Biology of deploying new-to-nature systems with complex phenotypes in a standard *E. coli* cell, the SEVA system removes redundant DNA sequences in classical plasmids to eliminate any possible undesired effects (222). We have redesigned our plasmid using this platform, which resulted in the creation of plasmid pSEVA434-PhonZ-V5-(Weak/Medium/Strong)RBS. Protein expression analysis showed promising results as receptor expression are better controlled than with the conventional plasmid, pRY100, as three different RBS variants produced different ranges of expression. Furthermore, signal output analysis will be conducted to recognise if the three different RBS, plus aromatic tuning could force the system to produce a steady state signal with a dose-response profile.

Upon the success of creating a few functional EnvZ-based synthetic system—starting with PhoQ-EnvZ, QseC-EnvZ (experiments currently conducted by Phillipa Cheesman), AgrC-EnvZ, MtrB-EnvZ and WalK-EnvZ—more pathogenically related chimeras could be created to expand the collection into a library, which would be screened against a drug library provided by LifeArc, formerly MRC Technology. Branching outside the university, the Draheim group is currently building a UK-China collaboration to investigate a multidrug resistant swine pathogen, spearheaded by Oxford Drug Design and Huazhong Agricultural University, in addition to a joint-project with a New Zealand-based research group to construct and screen a *Pseudomonas* plant pathogen library.

In the distant future, the biosensor range could be expanded to include non-pathogenically related histidine kinases. Synthetic biosensors have been utilised to solve issues in varying fields of science, mainly environmental, *e.g.* the Edinburgh pH-based arsenic biosensor presented in iGEM 2006, and medical, *e.g.* the probiotic *E. coli* Nissle used to indicate liver metastasis (225) and the cancer cell-targeting *E. coli* expressing synthetic adhesins (226). Several attempts has also been done to create chimeras that might have economical value (227–230). As soon as the initial bottleneck of designing an expression vector and protein scaffold are overcome, a synthetic biosensor could be versatile enough to include any sensor for any function, thus opening many doors into other fields of microbiology.

Appendix

A. Ethics Approval

FORM UPR16

Research Ethics Review Checklist

UNIVERSITY OF PORTSMOUTH

Please include this completed form as an appendix to your thesis (see the Research Degrees Operational Handbook for more information

Postgraduate Research Student (PGRS) Information			**Student ID:**	797155
PGRS Name:	Rahmi Yusuf			
Department:	PHBM	**First Supervisor:**	Roger Draheim	
Start Date: (or progression date for Prof Doc students)		**01-10-2014**		
Study Mode and Route:	Part-time ☐ Full-time ☒	MPhil ☐ PhD ☒	MD ☐ Professional Doctorate ☐	

Title of Thesis:	Synecdoche, Two-Component Systems: E. coli EnvZ/OmpR as a Model of Transmembrane Communication and Chimeric Biosensor Design
Thesis Word Count: (excluding ancillary data)	35,396

If you are unsure about any of the following, please contact the local representative on your Faculty Ethics Committee for advice. Please note that it is your responsibility to follow the University's Ethics Policy and any relevant University, academic or professional guidelines in the conduct of your study

Although the Ethics Committee may have given your study a favourable opinion, the final responsibility for the ethical conduct of this work lies with the researcher(s).

UKRIO Finished Research Checklist:
(If you would like to know more about the checklist, please see your Faculty or Departmental Ethics Committee rep or see the online version of the full checklist at: http://www.ukrio.org/what-we-do/code-of-practice-for-research/)

a) Have all of your research and findings been reported accurately, honestly and within a reasonable time frame?	YES ☒ NO ☐
b) Have all contributions to knowledge been acknowledged?	YES ☒ NO ☐
c) Have you complied with all agreements relating to intellectual property, publication and authorship?	YES ☒ NO ☐
d) Has your research data been retained in a secure and accessible form and will it remain so for the required duration?	YES ☒ NO ☐
e) Does your research comply with all legal, ethical, and contractual requirements?	YES ☒ NO ☐

Candidate Statement:

I have considered the ethical dimensions of the above named research project, and have successfully obtained the necessary ethical approval(s)

Ethical review number(s) from Faculty Ethics Committee (or from NRES/SCREC):	D2BA-2DFF-418B-CA2C-5FCE-C5E5-E842-7C2A

If you have *not* submitted your work for ethical review, and/or you have answered 'No' to one or more of questions a) to e), please explain below why this is so:

Signed *(PGRS)*:		**Date:** 17-07-2018

UPR16 – April 2018

University of Portsmouth

Certificate of Ethics Review

Project Title:	Mechanisms of transmembrane communication employed by two-component signalling systems
User ID:	797155
Name:	Rahmi Yusuf
Application Date:	27/07/2016 17:43:28

You must download your certificate, print a copy and keep it as a record of this review.

It is your responsibility to adhere to the University Ethics Policy and any Department/School or professional guidelines in the conduct of your study including relevant guidelines regarding health and safety of researchers and University Health and Safety Policy.

It is also your responsibility to follow University guidance on Data Protection Policy:

- General guidance for all data protection issues
- University Data Protection Policy

You are reminded that as a University of Portsmouth Researcher you are bound by the UKRIO Code of Practice for Research; any breach of this code could lead to action being taken following the University's Procedure for the Investigation of Allegations of Misconduct in Research.

Any changes in the answers to the questions reflecting the design, management or conduct of the research over the course of the project must be notified to the Faculty Ethics Committee. **Any changes that affect the answers given in the questionnaire, not reported to the Faculty Ethics Committee, will invalidate this certificate.**

This ethical review should not be used to infer any comment on the academic merits or methodology of the project. If you have not already done so, you are advised to develop a clear protocol/proposal and ensure that it is independently reviewed by peers or others of appropriate standing. A favourable ethical opinion should not be perceived as permission to proceed with the research; there might be other matters of governance which require further consideration including the agreement of any organisation hosting the research.

GovernanceChecklist
A1-BriefDescriptionOfProject: This project focuses upon the biophysical mechanisms of signal transmission by a class of proteins known as "sensor kinases" across the bacterial membrane.
A2-Faculty: Science
A3-VoluntarilyReferToFEC: No
A5-AlreadyExternallyReviewed: No
B1-HumanParticipants: No
HumanParticipantsDefinition

Certificate Code: D2BA-2DFF-418B-CA2C-5FCE-C5E5-E842-7C2A Page 1

B2-HumanParticipantsConfirmation: Yes
C6-SafetyRisksBeyondAssessment: No
SafetyRisksBeyondAssessmentWarning
D2-PhysicalEcologicalDamage: No
PhysicalEcologicalDamageWarning
D4-HistoricalOrCulturalDamage: No
HistoricalOrCulturalDamageWarning
E1-ContentiousOrIllegal: No
ContentiousOrIllegalWarning
E2-SociallySensitiveIssues: No
SociallySensitiveWarning
F1-InvolvesAnimals: No
InvolvesAnimalsWarning
F2-HarmfulToThirdParties: No
HarmfulToThirdPartiesWarning
G1-ConfirmReadEthicsPolicy: Confirmed
G2-ConfirmReadUKRIOCodeOfPractice: Confirmed
G3-ConfirmReadConcordatToSupportResearchIntegrity: Confirmed
G4-ConfirmedCorrectInformation: Confirmed

B. Curriculum Vitae

Rahmi Yusuf

PERSONAL INFO

+44 7842 825598

rahmiyusuf86@gmail.com

26-11-1986

Indonesian

LANGUAGES

Indonesian (native)
English – IELTS 8.0
German – B1

HOBBIES

Travelling
Critiquing films
Reading Fiction
Performing arts
(musicals, plays, ballet)
Rock concerts

EDUCATION

2014 – present **University of Portsmouth (UoP)**, UK
Ph.D., Pharmacy & Biomedical Sciences (PI: Roger R. Draheim)
Thesis: Two-component signalling systems as novel antibiotic targets

2010 – 2012 **Hochschule Furtwangen University (HFU)**, Germany
M.Sc., Biomedical Engineering
Thesis: High-throughput screening of unknown compounds using a zebrafish model

2004 – 2008 **Institut Teknologi Bandung (ITB)**, Indonesia
B.Sc., Microbiology
Thesis: Preliminary study on alcohol production from tapioca powder by *Rhizopus* sp.

WORK EXPERIENCE

2013 **Research intern**
Centre for Bioenergy & Bioproducts, Surya University, Indonesia

2011 – 2012 **Masterarbeit (master-level thesis)**
Institute of Toxicology & Genetics (ITG), Karlsruhe Institute of Technology (KIT), Germany

2011 **HiWi (Student intern)**
Institute of Technical Medicine, HFU, Germany

AWARDS & SCHOLARSHIP

4. **Doctoral scholarship (£200K)**, 2014 – 2018, Indonesia Endowment Fund for Education (LPDP)
3. **Travel grant (£850),** 2018, Faculty of Science, University of Portsmouth, Department of Microbiology, Ohio State University
Topic: Computational Genomics
PI: Prof. Igor B. Jouline
2. **Travel grant (£1K)**, 2017, Faculty of Science, University of Portsmouth, Centre for Biosustainability, Technical University of Denmark (DTU)
Topic: CRISPR-MAGE (CRMAGE)
PI: Dr Morten Nørholm
1. **Travel grant (£1K)**, 2016, Faculty of Science, University of Portsmouth, MRC Cancer Unit, University of Cambridge
Topic: Coarse-Grained Molecular Dynamics (CGMD)
PI: Dr Benjamin Hall

1

Rahmi Yusuf

RESEARCH EXPERIENCE

- Bacterial signalling in antibiotic resistance
- Developing chimeric receptors for high-throughput screening (HTS)
- Experience with pipetting robot (Zephyr® Liquid Handling Workstation) and HTS

RESEARCH INTERESTS

Bacteriology
Synthetic microbiology
Molecular microbiology
Medical & industrial microbiology

SKILL SET

- Microbiology (bacteria, fungi)
- Molecular biology (DNA / Protein analysis)
- Spectroscopy (UV, Fluorescence)
- Microscopy (fluorescence, time-lapse)
- Data analysis (QtiPlot, GraphPad Prism)
- Modelling (Matlab & Simulink)

ARTICLES

5. **Yusuf R.**, Nguyễn T. L., Heininger A., Chavalwan T., Cheesman P., Lawrence R. J., Hall B. A., Draheim R. R., (in revision at mBio), *In vivo* cross-linking and transmembrane helix dynamics support a bidirectional non-piston model of signalling within *E. coli* EnvZ.
4. Mori A. D., Hafidh M., Mele N., **Yusuf R.**, Cerri G., Gavini E., Tozzi G., Barbu E, Conconi M. T., Draheim R. R. and Roldo M., (submitted to Scientific Reports), Evaluation of injectable composite gels containing silver nanowires as bone scaffold material.
3. **Yusuf R.**, Lawrence R. J., Eke L. V., Draheim R. R., (accepted), Tuning Chemoreceptor Signaling by Positioning Residues at the Lipid-Aqueous Interface, *Methods in Molecular Biology*.
2. Heininger A., **Yusuf R.**, Lawrence R. J., Draheim R. R., (2016), Identification of transmembrane helix 1 (TM1) surfaces important for EnvZ dimerisation and signal output, *BBA Biomembranes*, 1858 (8),1868–1875.
1. **Yusuf R.**, Draheim R. R., (2015), Employing aromatic tuning to modulate output from two-component signaling circuits, *Journal of Biological Engineering*, 9, 7.

POSTERS & PRESENTATIONS

4. **Yusuf R.**, [Presentation], Constructing the functional ion-sensing chimeric receptor, PhoQ-EnvZ (PhonZ), *Receptorfest 2018*, July 23rd – 24th, 2018, Cornell University, USA.
3. **Yusuf R.**, Eke L. V., Draheim R. R., [Poster], Two-component signalling systems as novel antibiotic targets, *5th Mol Micro & 4th M4 Meeting*, September 13th – 14th, 2017, University of Birmingham, UK.
2. **Yusuf R.**, Heininger A., Ebenezer I., Draheim R. R., [Poster], Antimicrobial resistance: A fundamental and practical study of *E. coli* EnvZ/OmpR, *Science Together*, July 8th, 2016, University of Portsmouth, UK.
1. **Yusuf R.**, Heininger A., Draheim R. R., [Poster], Establishing a biological platform for the discovery of novel antibiotics, *Institute of Biomolecular and Biomedical Sciences (IBBS) Day*, June 8th, 2016, University of Portsmouth, UK.

CONFERENCES ATTENDED

3. *Pint of Science: Our Body*, 2017, [Organising team], May 15th – 17th, Portsmouth, UK.
2. *Antibiotic Resistance Mechanism Workshop*, 2016, [Attendee], November 24th – 25th, Birmingham, UK.
1. *Biotech Young Entrepreneurs Scheme (YES)*, 2016, [Competing team], October 12th – 14th, Syngenta, Bracknell, UK.

Bibliography

1. Parkinson JS. Genetic Approaches for Signaling Pathways and Proteins. Two-Component Signal Transduct. 1995;
2. Mitrophanov AYA, Groisman EE a. Signal integration in bacterial two-component regulatory systems. Genes Dev [Internet]. 2008;22(19):2601–11. Available from: http://genesdev.cshlp.org/content/22/19/2601.short%5Cnhttp://www.pubmedcentral.nih.gov/articlerender.fcgi?artid=2751022&tool=pmcentrez&rendertype=abstract
3. Mascher T, Helmann JD, Unden G. Stimulus perception in bacterial signal-transducing histidine kinases. Microbiol Mol Biol Rev. 2006;70(4):910–38.
4. Rowland MA, Deeds EJ. Crosstalk and the evolution of specificity in two-component signaling. Proc Natl Acad Sci U S A. 2014;111(15):5550–5.
5. Salazar ME, Laub MT. Temporal and evolutionary dynamics of two-component signaling pathways. Current Opinion in Microbiology. 2015.
6. Podgornaia AI, Laub MT. Determinants of specificity in two-component signal transduction. Curr Opin Microbiol [Internet]. Elsevier Ltd; 2013;16(2):156–62. Available from: http://dx.doi.org/10.1016/j.mib.2013.01.004
7. Alvarez AF, Barba-Ostria C, Silva-Jiménez H, Georgellis D. Organization and mode of action of two component system signaling circuits from the various kingdoms of life. Environ Microbiol. 2016;18(10):3210–26.
8. Gerken H, Misra R. MzrA-EnvZ interactions in the periplasm influence the EnvZ/OmpR two-component regulon. J Bacteriol. 2010;192(23):6271–8.
9. Wadhams GH, Armitage JP. Making sense of it all: Bacterial chemotaxis. Nat Rev Mol Cell Biol. 2004;5(12):1024–37.
10. Taylor BL, Zhulin IB. PAS domains: internal sensors of oxygen, redox potential, and light. Microbiol Mol Biol Rev [Internet]. 1999;63(2):479–506. Available from: http://mmbr.asm.org/content/63/2/479.short%5Cnhttp://www.ncbi.nlm.nih.gov/pubmed/10357859%5Cnhttp://www.pubmedcentral.nih.gov/articlerender.fcgi?artid=PMC98974
11. Möglich A, Ayers RA, Moffat K. Structure and Signaling Mechanism of Per-ARNT-Sim Domains. Structure. 2009;17(10):1282–94.
12. Hazelbauer GL, Falke JJ, Parkinson JS. Bacterial chemoreceptors: high-performance signaling in networked arrays. Trends Biochem Sci. 2008;33(1):9–19.
13. Hazelbauer GL, Lai WC. Bacterial chemoreceptors: providing enhanced features to two-component signaling. Curr Opin Microbiol [Internet]. Elsevier Ltd; 2010;13(2):124–32. Available from: http://dx.doi.org/10.1016/j.mib.2009.12.014

14. Collins KD, Lacal J, Ottemann KM. Internal Sense of Direction: Sensing and Signaling from Cytoplasmic Chemoreceptors. Microbiol Mol Biol Rev [Internet]. 2014;78(4):672–84. Available from: http://mmbr.asm.org/lookup/doi/10.1128/MMBR.00033-14

15. Szurmant H, Ordal GW. Diversity in Chemotaxis Mechanisms among the Bacteria and Archaea. Microbiol Mol Biol Rev [Internet]. 2004;68(2):301–19. Available from: http://mmbr.asm.org/cgi/doi/10.1128/MMBR.68.2.301-319.2004

16. Matilla MA, Krell T. Chemoreceptor-based signal sensing. Curr Opin Biotechnol [Internet]. Elsevier Ltd; 2017;45:8–14. Available from: http://dx.doi.org/10.1016/j.copbio.2016.11.021

17. LeDeaux JR, Yu N, Grossman AD. Different roles for KinA, KinB, and KinC in the initiation of sporulation in Bacillus subtilis. Journal of Bacteriology. 1995. p. 861–3.

18. Tojo S, Hirooka K, Fujita Y. Expression of kinA and kinB of bacillus subtilis, necessary for sporulation initiation, is under positive stringent transcription control. J Bacteriol. 2013;195(8):1656–65.

19. Capra EJ, Laub MT. Evolution of Two-Component Signal Transduction Systems. Annu Rev Microbiol [Internet]. 2012;66(1):325–47. Available from: http://www.annualreviews.org/doi/10.1146/annurev-micro-092611-150039

20. Shulman ST, Friedmann HC, Sims RH. Theodor Escherich: The First Pediatric Infectious Diseases Physician? Clin Infect Dis [Internet]. 2007;45(8):1025–9. Available from: https://academic.oup.com/cid/article-lookup/doi/10.1086/521946

21. Kaper JB, Nataro JP, Mobley HL. Pathogenic Escherichia coli. Nat Rev Microbiol [Internet]. 2004;2(2):123–40. Available from: http://dx.doi.org/10.1038/nrmicro818

22. Dunne KA, Chaudhuri RR, Rossiter AE, Beriotto I, Browning DF, Squire D, et al. Sequencing a piece of history : complete genome sequence of the original Escherichia coli strain. 2017;

23. Liu YF, Yan JJ, Lei HY, Teng CH, Wang MC, Tseng CC, et al. Loss of outer membrane protein C in Escherichia coli contributes to both antibiotic resistance and escaping antibody-dependent bactericidal activity. Infect Immun. 2012;80(5):1815–22.

24. Delcour AH. Outer Membrane Permeability and Antibiotic Resistance. Biochim Biophys Acta [Internet]. 2009;1794(5):808–16. Available from: http://www.ncbi.nlm.nih.gov/pmc/articles/PMC2696358/pdf/nihms114274.pdf

25. Thanassi DG, Cheng LW, Nikaido H. Active efflux of bile salts by Escherichia coli. J Bacteriol. 1997;

26. Villarreal JM, Becerra-Lobato N, Rebollar-Flores JE, Medina-Aparicio L, Carbajal-Gómez E, Zavala-García ML, et al. The Salmonella enterica serovar Typhi ltrR-ompR-ompC-ompF genes are involved in resistance to the bile salt sodium

deoxycholate and in bacterial transformation. Mol Microbiol. 2014;

27. Urdaneta V, Casadesús J. Interactions between Bacteria and Bile Salts in the Gastrointestinal and Hepatobiliary Tracts. Front Med. 2017;

28. Yoshida T, Phadtare S, Inouye M. Functional and Structural Characterization of EnvZ, an Osmosensing Histidine Kinase of E. coli. Methods Enzymol. 2007;423(07):184–202.

29. Khorchid A, Inouye M, Ikura M. Structural characterization of Escherichia coli sensor histidine kinase EnvZ: the periplasmic C-terminal core domain is critical for homodimerization. Biochem J [Internet]. 2005;385(Pt 1):255–64. Available from: http://www.ncbi.nlm.nih.gov/entrez/query.fcgi?cmd=Retrieve&db=PubMed&dopt=Citation&list_uids=15357641

30. Aravind L, Ponting CP. The cytoplasmic helical linker domain of receptor histidine kinase and methyl-accepting proteins is common to many prokaryotic signalling proteins. FEMS Microbiol Lett. 1999;176(1):111–6.

31. Wolanin PM, Thomason PA, Stock JB. Histidine protein kinases: key signal transducers outside the animal kingdom. Genome Biol [Internet]. 2002;3(10):REVIEWS3013. Available from: http://www.pubmedcentral.nih.gov/articlerender.fcgi?artid=244915&tool=pmcentrez&rendertype=abstract

32. Wang LC, Morgan LK, Godakumbura P, Kenney LJ, Anand GS. The inner membrane histidine kinase EnvZ senses osmolality via helix-coil transitions in the cytoplasm. EMBO J [Internet]. Nature Publishing Group; 2012;31(11):2648–59. Available from: http://emboj.embopress.org/cgi/doi/10.1038/emboj.2012.99

33. Foo YH, Gao Y, Zhang H, Kenney LJ. Cytoplasmic sensing by the inner membrane histidine kinase EnvZ. Progress in Biophysics and Molecular Biology. 2015. p. 119–29.

34. Egger LA, Inouye M. Purification and characterization of the periplasmic domain of EnvZ osmosensor in Escherichia coli. Biochem Biophys Res Commun [Internet]. 1997;231(1):68–72. Available from: http://www.ncbi.nlm.nih.gov/pubmed/9070221

35. Tokishita SI, Kojima A, Aiba H, Mizuno T. Transmembrane signal transduction and osmoregulation in Escherichia coli: Functional importance of the periplasmic domain of the membrane-located protein kinase, EnvZ. J Biol Chem. 1991;266(11):6780–5.

36. Kishii R, Falzon L, Yoshida T, Kobayashi H, Inouye M. Structural and functional studies of the HAMP domain of EnvZ, an osmosensing transmembrane histidine kinase in Escherichia coli. J Biol Chem. 2007;282(36):26401–8.

37. Inouye M. Signaling by Transmembrane Proteins Shifts Gears. Cell. 2006. p. 829–31.

38. Park H, Inouye M. Mutational analysis of the linker region of EnvZ, an osmosensor in Escherichia coli. J Bacteriol. 1997;179(13):4382–90.

39. Shin-ichi Tokishita, Atsuko Kojima and TM. Transmembrane Signal Transduction and Osmoregulation in Escherichia coli : Functional Importance of the Transmembrane Regions of Membrane-Located Protein protein kinase which modulates expression of the ompF and signal transduction in Escherichia that thi. J Biochem. 1992;111(6):707–13.

40. Hughson a G, Hazelbauer GL. Detecting the conformational change of transmembrane signaling in a bacterial chemoreceptor by measuring effects on disulfide cross-linking in vivo. Proc Natl Acad Sci U S A. 1996;93(21):11546–51.

41. Heininger A, Yusuf R, Lawrence RJ, Draheim RR. Identification of transmembrane helix 1 (TM1) surfaces important for EnvZ dimerisation and signal output. Biochim Biophys Acta - Biomembr [Internet]. Elsevier B.V.; 2016;1858(8):1868–75. Available from: http://dx.doi.org/10.1016/j.bbamem.2016.05.002

42. Yusuf R, Draheim RR. Employing aromatic tuning to modulate output from two-component signaling circuits. J Biol Eng [Internet]. 2015;9:7. Available from: http://www.pubmedcentral.nih.gov/articlerender.fcgi?artid=4440246&tool=pmcentrez&rendertype=abstract

43. Ottemann KM, Xiao W, Shin YK, Koshland DE. A piston model for transmembrane signaling of the aspartate receptor. Science (80-). 1999;285(5434):1751–4.

44. Stock J, Da Re S. Signal transduction: Response regulators on and off. Curr Biol. 2000;10(11):420–4.

45. Birck C, Mourey L, Gouet P, Fabry B, Schumacher J, Rousseau P, et al. Conformational changes induced by phosphorylation of the FixJ receiver domain. Structure. 1999;7(12):1505–15.

46. Gao R, Stock AM. Biological Insights from Structures of Two-Component Proteins. Annu Rev Microbiol [Internet]. 2009;63(1):133–54. Available from: http://www.annualreviews.org/doi/10.1146/annurev.micro.091208.073214

47. Gao R, Mack TR, Stock AM. Bacterial response regulators: versatile regulatory strategies from common domains. Trends Biochem Sci. 2007;32(5):225–34.

48. Bourret RB. Receiver domain structure and function in response regulator proteins. Curr Opin Microbiol [Internet]. Elsevier Ltd; 2010;13(2):142–9. Available from: http://dx.doi.org/10.1016/j.mib.2010.01.015

49. Galperin MY. Diversity of Structure and Function of Response Regulator Output Domains. 2011;13(2):150–9.

50. Mattison K, Oropeza R, Kenney LJ. The linker region plays an important role in the interdomain communication of the response regulator OmpR. J Biol Chem. 2002;277(36):32714–21.

51. Mizuno T. Compilation of all genes encoding two-component phosphotransfer signal transducers in the genome of Escherichia coli. DNA Res. 1997;4(2):161–8.

52. Aiba H, Nakasai F, Mizushima S, Mizuno T. Phosphorylation of a bacterial activator protein, OmpR, by a protein kinase, EnvZ, results in stimulation of its DNA-binding ability. J Biochem [Internet]. 1989;106(1):5–7. Available from: http://www.ncbi.nlm.nih.gov/pubmed/2674113

53. Barbieri CM, Wu T, Stock AM. Comprehensive analysis of OmpR phosphorylation, dimerization, and DNA binding supports a canonical model for activation. J Mol Biol. 2013;425(10):1612–26.

54. Kenney LJ. Structure/function relationships in OmpR and other winged-helix transcription factors. Curr Opin Microbiol. 2002;5(2):135–41.

55. Tsung K, Brissette RE, Inouye M. Identification of the DNA-binding domain of the OmpR protein required for transcriptional activation of the ompF and ompC genes of Escherichia coli by in vivo DNA footprinting. J Biol Chem. 1989;264(17):10104–9.

56. Pratt LA, Silhavy TJ. OmpR mutants specifically defective for transcriptional activation. J Mol Biol. 1994;243(4):579–94.

57. Kato N, Aiba H, Mizuno T. Suppressor mutations in α-subunit of RNA polymerase for a mutant of the positive regulator, OmpR, in Escherichia coli. FEMS Microbiol Lett. 1996;139(2–3):175–80.

58. Jo YL, Nara F, Ichihara S. Purification and characterization of the OmpR protein, a positive regulator involved in osmoregulatory expression of the ompF and ompC genes in Escherichia coli. J Biol Chem. 1986;261(32):15252–6.

59. Mattison K, Oropeza R, Byers N, Kenney LJ. A phosphorylation site mutant of OmpR reveals different binding conformations at ompF and ompC. J Mol Biol. 2002;315(4):497–511.

60. Qin L, Yoshida T, Inouye M. The critical role of DNA in the equilibrium between OmpR and phosphorylated OmpR mediated by EnvZ in Escherichia coli. Proc Natl Acad Sci U S A. 2001;98(3):908–13.

61. Allen H, Donato J. Call of the wild: antibiotic resistance genes in natural environments. Nat Rev … [Internet]. Nature Publishing Group; 2010;8(4):251–9. Available from: http://www.ncbi.nlm.nih.gov/pubmed/20190823%5Cnhttp://www.nature.com/nrmicro/journal/v8/n4/abs/nrmicro2312.html

62. Williams KJ. The introduction of “chemotherapy” using arsphenamine - The first magic bullet. J R Soc Med. 2009;102(8):343–8.

63. Clardy J, Fischbach MA, Currie CR. The natural history of antibiotics. Curr Biol. 2009;19(11):1–8.

64. Aminov RI. A brief history of the antibiotic era: Lessons learned and challenges for the future. Front Microbiol. 2010;1(DEC):1–7.

65. Kohanski MA, Dwyer DJ, Collins JJ. How antibiotics kill bacteria: From targets to networks. Nat Rev Microbiol. 2010;8(6):423–35.

66. Ocampo PS, Lázár V, Papp B, Arnoldini M, Zur Wiesch PA, Busa-Fekete R, et al. Antagonism between bacteriostatic and bactericidal antibiotics is prevalent. Antimicrob Agents Chemother. 2014;58(8):4573–82.

67. Aminov RI. The role of antibiotics and antibiotic resistance in nature. Environ Microbiol. 2009;11(12):2970–88.

68. Magiorakos AP, Srinivasan A, Carey RB, Carmeli Y, Falagas ME, Giske CG, et al. Multidrug-resistant, extensively drug-resistant and pandrug-resistant bacteria: An international expert proposal for interim standard definitions for acquired resistance. Clin Microbiol Infect [Internet]. European Society of Clinical Infectious Diseases; 2012;18(3):268–81. Available from: http://dx.doi.org/10.1111/j.1469-0691.2011.03570.x

69. Falagas ME, Karageorgopoulos DE. Pandrug Resistance (PDR), Extensive Drug Resistance (XDR), and Multidrug Resistance (MDR) among Gram-Negative Bacilli: Need for International Harmonization in Terminology. Clin Infect Dis [Internet]. 2008;46(7):1121–2. Available from: https://academic.oup.com/cid/article-lookup/doi/10.1086/528867

70. World Health Organization W. WHO | Draft global action plan on antimicrobial resistance. Eur Cent Dis Prev Control [Internet]. 2015;2009. Available from: http://www.who.int/drugresistance/global_action_plan/en/

71. Davies J, Davies D. Origins and Evolution of Antibiotic Resistance. Microbiol Mol Biol Rev [Internet]. 2010;74(3):417–33. Available from: http://mmbr.asm.org/cgi/content/abstract/74/3/417

72. Crum-Cianflone, Duplessis, Crum-Cianflone, Duplessis, Duplessis. Ceftaroline: A New Cephalosporin with Activity Against Methicillin-Resistant Staphylococcus aureus (MRSA) [Internet]. Clinical Medicine Reviews in Therapeutics. 2011. p. 1. Available from: http://www.la-press.com/ceftaroline-a-new-cephalosporin-with-activity-against-methicillin-resi-article-a2466

73. Long SW, Olsen RJ, Mehta SC, Palzkill T, Cernoch PL, Perez KK, et al. PBP2a mutations causing high-level ceftaroline resistance in clinical methicillin-resistant Staphylococcus aureus isolates. Antimicrob Agents Chemother. 2014;58(11):6668–74.

74. Gwynn MN, Portnoy A, Rittenhouse SF, Payne DJ. Challenges of antibacterial discovery revisited. Ann N Y Acad Sci. 2010;1213(1):5–19.

75. Tiwari S, Jamal SB, Hassan SS, Carvalho PVSD, Almeida S, Barh D, et al. Two-Component Signal Transduction Systems of Pathogenic Bacteria As Targets for

Antimicrobial Therapy: An Overview. Front Microbiol [Internet]. 2017;8(October):1–7. Available from: http://journal.frontiersin.org/article/10.3389/fmicb.2017.01878/full

76. Barrett JF, Hoch JA. Two-component signal transduction as a target for microbial anti-infective therapy. Antimicrob Agents Chemother [Internet]. 1998;42(7):1529–36. Available from: http://www.ncbi.nlm.nih.gov/pubmed/9660978%5Cnhttp://www.pubmedcentral.nih.gov/articlerender.fcgi?artid=PMC105640

77. Barrett JF, Goldschmidt RM, Lawrence LE, Foleno B, Chen R, Demers JP, et al. Antibacterial agents that inhibit two-component signal transduction systems. Proc Natl Acad Sci U S A. 1998;95(9):5317–22.

78. Velikova N, Fulle S, Manso AS, Mechkarska M, Finn P, Conlon JM, et al. Putative histidine kinase inhibitors with antibacterial effect against multi-drug resistant clinical isolates identified by in vitro and in silico screens. Sci Rep. 2016;6(May):1–16.

79. Bem AE, Velikova N, Pellicer MT, Baarlen P Van, Marina A, Wells JM. Bacterial histidine kinases as novel antibacterial drug targets. ACS Chem Biol. 2015;10(1):213–24.

80. Stock AM, Robinson VL, Goudreau PN. Two-Component Signal Transduction. Reactions [Internet]. 2000;69:183–215. Available from: http://www.ncbi.nlm.nih.gov/pubmed/10966457

81. Ji G, Beavis R, Novick RP. Bacterial interference caused by autoinducing peptide variants. Science (80-). 1997;276(5321):2027–30.

82. Shin D, Lee EJ, Huang H, Groisman EA. A positive feedback loop promotes transcription surge that jump-starts Salmonella virulence circuit. Science (80-). 2006;314(5805):1607–9.

83. Puthiyaveetil S, Kavanagh TA, Cain P, Sullivan JA, Newell CA, Gray JC, et al. The ancestral symbiont sensor kinase CSK links photosynthesis with gene expression in chloroplasts. Proc Natl Acad Sci [Internet]. 2008;105(29):10061–6. Available from: http://www.pnas.org/cgi/doi/10.1073/pnas.0803928105

84. David M, Daveran ML, Batut J, Dedieu A, Domergue O, Ghai J, et al. Cascade regulation of nif gene expression in Rhizobium meliloti. Cell. 1988;54(5):671–83.

85. Ulrich LE, Zhulin IB. The MiST2 database: A comprehensive genomics resource on microbial signal transduction. Nucleic Acids Res. 2009;38(SUPPL.1).

86. Nørholm MHH, Von Heijne G, Draheim RR. Forcing the issue: Aromatic tuning facilitates stimulus-independent modulation of a two-component signaling circuit. ACS Synth Biol. 2015;4(4):474–81.

87. Wang B, Barahona M, Buck M, Schumacher J. Rewiring cell signalling through chimaeric regulatory protein engineering. Biochem Soc Trans [Internet].

2013;41(5):1195–200. Available from: http://biochemsoctrans.org/lookup/doi/10.1042/BST20130138

88. Stanton BC, Siciliano V, Ghodasara A, Wroblewska L, Clancy K, Trefzer AC, et al. Systematic transfer of prokaryotic sensors and circuits to mammalian cells. ACS Synth Biol. 2014;3(12):880–91.

89. Zhu Y, Inouye M. Analysis of the role of the EnvZ linker region in signal transduction using a chimeric Tar/EnvZ receptor protein, Tez1. J Biol Chem. 2003;278(25):22812–9.

90. Killian JA, Salemink I, De Planque MRR, Lindblom G, Koeppe RE, Greathouse D V. Induction of nonbilayer structures in diacylphosphatidylcholine model membranes by transmembrane α-helical peptides: Importance of hydrophobic mismatch and proposed role of tryptophans. Biochemistry. 1996;35(3):1037–45.

91. De Planque MRR, Boots JWP, Rijkers DTS, Liskamp RMJ, Greathouse D V., Killian JA. The effects of hydrophobic mismatch between phosphatidylcholine bilayers and transmembrane α-helical peptides depend on the nature of interfacially exposed aromatic and charged residues. Biochemistry. 2002;41(26):8396–404.

92. De Planque MRR, Bonev BB, Demmers JAA, Greathouse D V., Koeppe RE, Separovic F, et al. Interfacial anchor properties of tryptophan residues in transmembrane peptides can dominate over hydrophobic matching effects in peptide-lipid interactions. Biochemistry. 2003;42(18):5341–8.

93. De Planque MRR, Greathouse D V., Koeppe RE, Schäfer H, Marsh D, Killian JA. Influence of lipid/peptide hydrophobic mismatch on the thickness of diacylphosphatidylcholine bilayers. A2H NMR and ESR study using designed transmembrane α-helical peptides and gramicidin A. Biochemistry. 1998;37(26):9333–45.

94. Nilsson I, Saaf A, Whitley P, Gafvelin G, Waller C, von Heijne G. Proline-induced disruption of a transmembrane alpha-helix in its natural environment. J Mol Biol [Internet]. 1998;284(4):1165–75. Available from: http://www.ncbi.nlm.nih.gov/entrez/query.fcgi?cmd=Retrieve&db=PubMed&dopt=Citation&list_uids=9837734

95. Braun P, Von Heijne G. The aromatic residues Trp and phe have different effects on the positioning of a transmembrane helix in the microsomal membrane. Biochemistry. 1999;38(30):9778–82.

96. Draheim RR, Bormans AF, Lai RZ, Manson MD. Tuning a bacterial chemoreceptor with protein-membrane interactions. Biochemistry. 2006;45(49):14655–64.

97. Hessa T, Meindl-Beinker NM, Bernsel A, Kim H, Sato Y, Lerch-Bader M, et al. Molecular code for transmembrane-helix recognition by the Sec61 translocon. Nature. 2007;450(7172):1026–30.

98. Welch M, Oosawa K, Aizawa S, Eisenbach M. Phosphorylation-dependent binding

of a signal molecule to the flagellar switch of bacteria. Proc Natl Acad Sci U S A. 1993;90(October):8787–91.

99. Lai RZ, Manson JMB, Bormans AF, Draheim RR, Nguyen NT, Manson MD. Cooperative signaling among bacterial chemoreceptors. Biochemistry. 2005;44(43):14298–307.

100. Draheim RR. The role of protein-membrane interactions in modulation of signaling by bacterial chemoreceptors. PhD Diss. 2007;Texas A&M(May).

101. Ravid S, Matsumura P, Eisenbach M. Restoration of flagellar clockwise rotation in bacterial envelopes by insertion of the chemotaxis protein CheY. Proc Natl Acad Sci U S A. 1986;83(19):7157–61.

102. Hess JF, Oosawa K, Kaplan N, Simon MI. Phosphorylation of three proteins in the signaling pathway of bacterial chemotaxis. Cell. 1988;53(1):79–87.

103. Draheim RR, Bormans AF, Lai RZ, Manson MD. Tryptophan residues flanking the second transmembrane helix (TM2) set the signaling state of the Tar chemoreceptor. Biochemistry. 2005;44(4):1268–77.

104. Falke JJ, Hazelbauer GL. Transmembrane signaling in bacterial chemoreceptors. Trends in Biochemical Sciences. 2001. p. 257–65.

105. Falke JJ, Erbse AH. The Piston Rises Again. Structure. 2009. p. 1149–51.

106. Miller AS, Falke JJ. Side Chains at the Membrane-Water Interface Modulate the Signaling State of a Transmembrane Receptor. Biochemistry. 2004;43(7):1763–70.

107. Isaac B, Gallagher GJ, Balazs YS, Thompson LK. Site-directed rotational resonance solid-state NMR distance measurements probe structure and mechanism in the transmembrane domain of the serine bacterial chemoreceptor. Biochemistry. 2002;41(9):3025–36.

108. Hall BA, Armitage JP, Sansom MSP. Transmembrane helix dynamics of bacterial chemoreceptors supports a piston model of signalling. PLoS Comput Biol. 2011;7(10).

109. Botelho SC, Enquist K, Von Heijne G, Draheim RR. Differential repositioning of the second transmembrane helices from E. coli Tar and EnvZ upon moving the flanking aromatic residues. Biochim Biophys Acta - Biomembr. 2015;1848(2):615–21.

110. Cluzel P, Surette M, Leibler S. An ultrasensitive bacterial motor revealed by monitoring signaling proteins in single cells. Science (80-). 2000;287(5458):1652–5.

111. Ferris HU, Dunin-Horkawicz S, Mondéjar LG, Hulko M, Hantke K, Martin J, et al. The mechanisms of HAMP-mediated signaling in transmembrane receptors. Structure. 2011;19(3):378–85.

112. Ferris HU, Dunin-Horkawicz S, Hornig N, Hulko M, Martin J, Schultz JE, et al.

Mechanism of regulation of receptor histidine kinases. Structure. 2012;20(1):56–66.

113. Ferris HU, Zeth K, Hulko M, Dunin-Horkawicz S, Lupas AN. Axial helix rotation as a mechanism for signal regulation inferred from the crystallographic analysis of the E. coli serine chemoreceptor. J Struct Biol. 2014;186(3):349–56.

114. Hulko M, Berndt F, Gruber M, Linder JU, Truffault V, Schultz A, et al. The HAMP Domain Structure Implies Helix Rotation in Transmembrane Signaling. Cell. 2006;126(5):929–40.

115. Inouye M. Signaling by Transmembrane Proteins Shifts Gears. Cell. 2006;126(5):829–31.

116. Schultz JE, Natarajan J. Regulated unfolding: A basic principle of intraprotein signaling in modular proteins. Trends in Biochemical Sciences. 2013. p. 538–45.

117. Parkinson JS. Signaling Mechanisms of HAMP Domains in Chemoreceptors and Sensor Kinases. Annu Rev Microbiol [Internet]. 2010;64(1):101–22. Available from: http://www.annualreviews.org/doi/10.1146/annurev.micro.112408.134215

118. Zhou Q, Ames P, Parkinson JS. Biphasic control logic of HAMP domain signalling in the Escherichia coli serine chemoreceptor. Mol Microbiol. 2011;80(3):596–611.

119. Kitanovic S, Ames P, Parkinson JS. Mutational analysis of the control cable that mediates transmembrane signaling in the Escherichia coli serine chemoreceptor. J Bacteriol. 2011;193(19):5062–72.

120. Park H, Im W, Seok C. Transmembrane signaling of chemotaxis receptor Tar: insights from molecular dynamics simulation studies. Biophys J [Internet]. 2011;100:2955. Available from: http://dx.doi.org/10.1016/j.bpj.2011.05.030

121. Wright GA, Crowder RL, Draheim RR, Manson MD. Mutational analysis of the transmembrane helix 2-HAMP domain connection in the Escherichia coli aspartate chemoreceptor Tar. J Bacteriol. 2011;193(1):82–90.

122. Adase CA, Draheim RR, Rueda G, Desai R, Manson MD. Residues at the cytoplasmic end of transmembrane helix 2 determine the signal output of the TarEcchemoreceptor. Biochemistry. 2013;52(16):2729–38.

123. Adase CA, Draheim RR, Manson MD. The residue composition of the aromatic anchor of the second transmembrane helix determines the signaling properties of the aspartate/maltose chemoreceptor tar of escherichia coli. Biochemistry. 2012;51(9):1925–32.

124. Zhou Q, Ames P, Parkinson JS. Mutational analyses of HAMP helices suggest a dynamic bundle model of input-output signalling m chemoreceptors. Mol Microbiol. 2009;73(5):801–14.

125. Egger L a, Park H, Inouye M. Signal transduction via the histidyl-aspartyl

phosphorelay. Genes Cells. 1997;2(3):167–84.

126. Forst SA, Roberts DL. Signal transduction by the EnvZ-OmpR phosphotransfer system in bacteria. Res Microbiol. 1994;145(5–6):363–73.

127. Hoch JA, Silhavy TJ, Stock AM, Robinson VL, Goudreau PN. Two-component signal transduction [Internet]. American society for Microbiology. 1995. p. 183–215. Available from: http://www.ncbi.nlm.nih.gov/pubmed/10966457%5Cnhttp://www.ncbi.nlm.nih.gov/pubmed/10966457%5Cnhttp://www.annualreviews.org/doi/pdf/10.1146/annurev.biochem.69.1.183

128. Mizuno T. His-Asp phosphotransfer signal transduction. Journal of Biochemistry. 1998. p. 555–63.

129. Forst S, Delgado J, Rampersaud A, Inouye M. In vivo phosphorylation of OmpR, the transcription activator of the ompF and ompC genes in Escherichia coli. J Bacteriol. 1990;172(6):3473–7.

130. Lan C, Igo MM. Differential Expression of the OmpF and OmpC Porin Proteins in Escherichia coli K-12 Depends upon the Level of Active OmpR Differential Expression of the OmpF and OmpC Porin Proteins in Escherichia coli K-12 Depends upon the Level of Active OmpR. 1998;180(1):171–4.

131. Russo FD, Silhavy TJ. EnvZ controls the concentration of phosphorylated OmpR to mediate osmoregulation of the porin genes. J Mol Biol. 1991;222(3):567–80.

132. Batchelor E, Silhavy TJ, Goulian M. Continuous control in bacterial regulatory circuits. J Bacteriol [Internet]. 2004;186(22):7618–25. Available from: http://www.ncbi.nlm.nih.gov/entrez/query.fcgi?cmd=Retrieve&db=PubMed&dopt=Citation&list_uids=15516575

133. Falke JJ. Piston versus Scissors: Chemotaxis receptors versus sensor his-kinase receptors in two-component signaling pathways. Structure [Internet]. Elsevier Ltd; 2014;22(9):1219–20. Available from: http://dx.doi.org/10.1016/j.str.2014.08.011

134. Unnerståle S, Mäler L, Draheim RR. Structural characterization of AS1-membrane interactions from a subset of HAMP domains. Biochim Biophys Acta - Biomembr. 2011;1808(10):2403–12.

135. Molnar KS, Bonomi M, Pellarin R, Clinthorne GD, Gonzalez G, Goldberg SD, et al. Cys-Scanning disulfide crosslinking and bayesian modeling probe the transmembrane signaling mechanism of the histidine kinase, PhoQ. Structure [Internet]. Elsevier Ltd; 2014;22(9):1239–51. Available from: http://dx.doi.org/10.1016/j.str.2014.04.019

136. Forst S, Delgado J, Inouye M. Phosphorylation of OmpR by the osmosensor EnvZ modulates expression of the ompF and ompC genes in *Escherichia coli*. Proc Natl Acad Sci U S A. 1989;86(16):6052–6.

137. Rampersaud A, Inouye M. Procaine, a local anesthetic, signals through the EnvZ

receptor to change the DNA binding affinity of the transcriptional activator protein OmpR. J Bacteriol. 1991;173(21):6882–8.

138. Gerken H, Charlson ES, Cicirelli EM, Kenney LJ, Misra R. MzrA: A novel modulator of the EnvZ/OmpR two-component regulon. Mol Microbiol. 2009;72(6):1408–22.

139. Boldog T, Hazelbauer GL. Accessibility of introduced cysteines in chemoreceptor transmembrane helices reveals boundaries interior to bracketing charged residues. Protein Sci [Internet]. 2004;13(6):1466–75. Available from: http://www.ncbi.nlm.nih.gov/entrez/query.fcgi?cmd=Retrieve&db=PubMed&dopt=Citation&list_uids=15133159

140. Zhou L, Lei XH, Bochner BR, Wanner BL. Phenotype microarray analysis of Escherichia coli K-12 mutants with deletions of all two-component systems. J Bacteriol [Internet]. 2003;185(16):4956–72. Available from: http://www.ncbi.nlm.nih.gov/entrez/query.fcgi?cmd=Retrieve&db=PubMed&dopt=Citation&list_uids=12897016

141. Groban ES, Clarke EJ, Salis HM, Miller SM, Voigt CA. Kinetic Buffering of Cross Talk between Bacterial Two-Component Sensors. J Mol Biol. 2009;390(3):380–93.

142. Siryaporn A, Goulian M. Characterizing cross-talk in vivo avoiding pitfalls and overinterpretation. Methods Enzymol [Internet]. 2010;471(10):1–16. Available from: http://www.ncbi.nlm.nih.gov/pubmed/20946839

143. Wang L, Quan C, Xiong W, Qu X, Fan S, Hu W. New insight into transmembrane topology of Staphylococcus aureus histidine kinase AgrC. Biochim Biophys Acta - Biomembr. 2014;1838(3):988–93.

144. Zaslaver A, Bren A, Ronen M, Itzkovitz S, Kikoin I, Shavit S, et al. A comprehensive library of fluorescent transcriptional reporters for Escherichia coli. Nat Methods. 2006;3(8):623–8.

145. Hsing W, Silhavy TJ. Function of conserved histidine-243 in phosphatase activity of EnvZ, the sensor for porin osmoregulation in Escherichia coli. J Bacteriol. 1997;179(11):3729–35.

146. Head CG, Tardy A, Kenney LJ. Relative binding affinities of OmpR and OmpR-phosphate at the ompF and ompC regulatory sites. J Mol Biol. 1998;281(5):857–70.

147. Feng X, Oropeza R, Walthers D, Kenney LJ. OmpR Phosphorylation and Its Role in Signaling and Pathogenesis. ASM News. 2003;69(8):390–5.

148. Chervitz SA, Falke JJ. Lock on/off disulfides identify the transmembrane signaling helix of the aspartate receptor. J Biol Chem. 1995;

149. Lee GF, Lebert MR, Lilly a a, Hazelbauer GL. Transmembrane signaling characterized in bacterial chemoreceptors by using sulfhydryl cross-linking in vivo. Proc Natl Acad Sci U S A. 1995;

150. Pakula AA, Simon MI. Determination of transmembrane protein structure by disulfide cross-linking: the Escherichia coli Tar receptor. Proc Natl Acad Sci. 1992;

151. Casadaban MJ, Cohen SN. Analysis of gene control signals by DNA fusion and cloning in Escherichia coli. J Mol Biol [Internet]. Academic Press; 1980 Apr 5 [cited 2018 Jan 30];138(2):179–207. Available from: https://www.sciencedirect.com/science/article/pii/0022283680902831?via%3Dihub

152. Guyer MS, Reed RR, Steitz JA, Low KB. Identification of a sex-factor-affinity site in E. coli as gamma delta. Cold Spring Harb Symp Quant Biol. 1981;45 Pt 1:135–40.

153. Siryaporn A, Goulian M. Cross-talk suppression between the CpxA-CpxR and EnvZ-OmpR two-component systems in E. coli. Mol Microbiol. 2008;70(2):494–506.

154. Cantwell BJ, Draheim RR, Weart RB, Nguyen C, Stewart RC, Manson MD. CheZ phosphatase localizes to chemoreceptor patches via CheA-short. J Bacteriol. 2003;185(7):2354–61.

155. Southern JA, Young DF, Heaney F, Baumgartner WK, Randall RE. Identification of an epitope on the P and V proteins of simian virus 5 that distinguishes between two isolates with different biological characteristics. J Gen Virol. 1991;72(7):1551–7.

156. Lai RZ, Bormans AF, Draheim RR, Wright GA, Manson MD. The region preceding the C-terminal NWETF pentapeptide modulates baseline activity and aspartate inhibition of Escherichia coli Tar. Biochemistry. 2008;47(50):13287–95.

157. Batchelor E, Goulian M. Robustness and the cycle of phosphorylation and dephosphorylation in a two-component regulatory system. Proc Natl Acad Sci U S A [Internet]. 2003;100(2):691–6. Available from: http://www.ncbi.nlm.nih.gov/pubmed/12522261%5Cnhttp://www.pubmedcentral.nih.gov/articlerender.fcgi?artid=PMC141058

158. Krogh A, Larsson B, Von Heijne G, Sonnhammer ELL. Predicting transmembrane protein topology with a hidden Markov model: Application to complete genomes. J Mol Biol. 2001;305(3):567–80.

159. Nyholm TKM, Özdirekcan S, Antoinette Killian J. How protein transmembrane segments sense the lipid environment. Biochemistry. 2007. p. 1457–65.

160. Hofnung M. A short course in bacterial genetics and a laboratory manual and handbook for Escherichia coli and related bacteria. Biochimie. 1993. p. 501.

161. Ausubel FM, Brent R, Kingston RE, Moore DD, Seidman JG, Smith JA, et al. Current Protocols in Molecular Biology [Internet]. John Wiley Sons New York N Y. 1994. 23 p. Available from: papers://10e8b09b-2029-4a89-baf0-b90acb9a6c30/Paper/p3768%5Cnpapers://10e8b09b-2029-4a89-baf0-b90acb9a6c30/Paper/p3810

162. Schneider CA, Rasband WS, Eliceiri KW. NIH Image to ImageJ: 25 years of image

analysis. Nature Methods. 2012. p. 671–5.

163. Blot S, Depuydt P, Vandewoude K, De Bacquer D. Measuring the impact of multidrug resistance in nosocomial infection. Current Opinion in Infectious Diseases. 2007. p. 391–6.

164. Kirby T. Europe to boost development of new antimicrobial drugs. Lancet [Internet]. Elsevier Ltd; 2012;379(9833):2229–30. Available from: http://dx.doi.org/10.1016/S0140-6736(12)60964-7

165. Delcour AH. Solute uptake through general porins. Front Biosci [Internet]. 2003;8:d1055-71. Available from: http://eutils.ncbi.nlm.nih.gov/entrez/eutils/elink.fcgi?dbfrom=pubmed&id=12700124&retmode=ref&cmd=prlinks%5Cnpapers2://publication/uuid/E456D04B-0A88-4E0C-94BC-34B728C25BD8

166. Nikaido H. Molecular basis of bacterial outer membrane permeability revisited. Microbiol Mol Biol Rev [Internet]. 2003;67(4):593–656. Available from: http://www.pubmedcentral.nih.gov/articlerender.fcgi?artid=309051&tool=pmcentrez&rendertype=abstract

167. Schulz GE. The structure of bacterial outer membrane proteins. Biochim Biophys Acta. 2002;1565(2):308–17.

168. Bryskier A. Antimicrobial agents: Antibacterials and antifungals. ASM Press. 2005;42–3.

169. Elliott E, Brink AJ, van Greune J, Els Z, Woodford N, Turton J, et al. In Vivo Development of Ertapenem Resistance in a Patient with Pneumonia Caused by Klebsiella pneumoniae with an Extended-Spectrum -Lactamase. Clin Infect Dis [Internet]. 2006;42(11):e95–8. Available from: https://academic.oup.com/cid/article-lookup/doi/10.1086/503264

170. Hernández-Allés S, Conejo MD, Pascual A, Tomás JM, Benedí VJ, Martínez-Martínez L. Relationship between outer membrane alterations and susceptibility to antimicrobial agents in isogenic strains of Klebsiella pneumoniae. J Antimicrob Chemother. 2000;46(2):273–7.

171. Jacoby GA, Mills DM, Chow N. Role of beta-lactamases and porins in resistance to ertapenem and other beta-lactams in Klebsiella pneumoniae. Antimicrob Agents Chemother. 2004;48(8):3203–6.

172. Kaczmarek FM, Dib-Hajj F, Shang W, Gootz TD. High-level carbapenem resistance in a Klebsiella pneumoniae clinical isolate is due to the combination of blaACT-1 ??-lactamase production, porin OmpK35/36 insertional inactivation, and down-regulation of the phosphate transport porin PhoE. Antimicrob Agents Chemother. 2006;50(10):3396–406.

173. Loli A, Tzouvelekis LS, Tzelepi E, Carattoli A, Vatopoulos AC, Tassios PT, et al. Sources of diversity of carbapenem resistance levels in Klebsiella pneumoniae

carrying blaVIM-1. J Antimicrob Chemother. 2006;58(3):669–72.

174. Martinez-Martinez L, Conejo MC, Pascual A, Hernandez-Alles S, Ballesta S, De Arellano-Ramos ER, et al. Activities of imipenem and cephalosporins against clonally related strains of Escherichia coli hyperproducing chromosomal β-lactamase and showing altered porin profiles. Antimicrob Agents Chemother. 2000;44(9):2534–6.

175. Mena A, Plasencia V, García L, Hidalgo O, Ayestarán JI, Alberti S, et al. Characterization of a large outbreak by CTX-M-1-producing Klebsiella pneumoniae and mechanisms leading to in vivo carbapenem resistance development. J Clin Microbiol. 2006;44(8):2831–7.

176. Forst SA, Delgado J, Inouye M. DNA-binding properties of the transcription activator (OmpR) for the upstream sequences of ompF in Escherichia coli are altered by envZ mutations and medium osmolarity. J Bacteriol. 1989;171(6):2949–55.

177. Utsumi R, Brissette RE, Rampersaud a, Forst S a, Oosawa K, Inouye M. Activation of bacterial porin gene expression by a chimeric signal transducer in response to aspartate. Science. 1989;245(4923):1246–9.

178. Szurmant H, Bunn MW, Cho SH, Ordal GW. Ligand-induced conformational changes in the Bacillus subtilis chemoreceptor McpB determined by disulfide crosslinking in vivo. J Mol Biol. 2004;344(4):919–28.

179. Cheung J, Hendrickson WA. Structural Analysis of Ligand Stimulation of the Histidine Kinase NarX. Structure. 2009;17(2):190–201.

180. Moore JO, Hendrickson WA. Structural Analysis of Sensor Domains from the TMAO-Responsive Histidine Kinase Receptor TorS. Structure. 2009;17(9):1195–204.

181. Yaku H, Mizuno T. The membrane-located osmosensory kinase, EnvZ, that contains a leucine zipper-like motif functions as a dimer in Escherichia coli. FEBS Lett [Internet]. Federation of European Biochemical Societies; 1997;417(3):409–13. Available from: http://dx.doi.org/10.1016/S0014-5793(97)01329-X

182. Forst S, Comeau D, Norioka S, Inouye M. Localization and membrane topology of EnvZ, a protein involved in osmoregulation of OmpF and OmpC in Escherichia coli. J Biol Chem. 1987;262(34):16433–8.

183. Bass RB, Butler SL, Chervitz SA, Gloor SL, Falke JJ. Use of Site-Directed Cysteine and Disulfide Chemistry to Probe Protein Structure and Dynamics: Applications to Soluble and Transmembrane Receptors of Bacterial Chemotaxis. Methods in Enzymology. 2007. p. 25–51.

184. Oropeza R, Calva E. The cysteine 354 and 277 residues of Salmonella enterica serovar Typhi EnvZ are determinants of autophosphorylation and OmpR phosphorylation. FEMS Microbiol Lett. 2009;292(2):282–90.

185. Cai SJ, Khorchid A, Ikura M, Inouye M. Probing catalytically essential domain orientation in histidine kinase EnvZ by targeted disulfide crosslinking. J Mol Biol. 2003;328(2):409–18.

186. Dunnill P. The Use of Helical Net-Diagrams to Represent Protein Structures. Biophys J. 1968;8(7):865–75.

187. Careaga CL, Falke JJ. Structure and dynamics of Escherichia coli chemosensory receptors. Engineered sulfhydryl studies. Biophys J. 1992;62(1):209–19.

188. Balaji VN, Mobasser A, Rao SN. Modification of protein stability by introduction of disulfide bridges and prolines: Geometric criteria for mutation sites. Biochem Biophys Res Commun. 1989;160(1):109–14.

189. SRINIVASAN N, SOWDHAMINI R, RAMAKRISHNAN C, BALARAM P. Conformations of disulfide bridges in proteins. Int J Pept Protein Res. 1990;36(2):147–55.

190. Leatham-Jensen MP, Frimodt-Møller J, Adediran J, Mokszycki ME, Banner ME, Caughron JE, et al. The streptomycin-treated mouse intestine selects Escherichia coli envZ missense mutants that interact with dense and diverse intestinal microbiota. Infect Immun. 2012;80(5):1716–27.

191. Adediran J, Leatham-Jensen MP, Mokszycki ME, Frimodt-Møller J, Krogfelt KA, Kazmierczak K, et al. An escherichia coli nissle 1917 missense mutant colonizes the streptomycin-treated mouse intestine better than the wild type but is not a better probiotic. Infect Immun. 2014;82(2):670–82.

192. Monzel C, Unden G. Transmembrane signaling in the sensor kinase DcuS of *Escherichia coli* : A long-range piston-type displacement of transmembrane helix 2. Proc Natl Acad Sci [Internet]. 2015;112(35):11042–7. Available from: http://www.pnas.org/lookup/doi/10.1073/pnas.1507217112

193. Goldberg SD, Clinthorne GD, Goulian M, DeGrado WF. Transmembrane polar interactions are required for signaling in the Escherichia coli sensor kinase PhoQ. Proc Natl Acad Sci U S A [Internet]. 2010;107(18):8141–6. Available from: http://www.pnas.org/content/107/18/8141.long

194. Forst SA, Delgado J, Inouye M. DNA-binding properties of the transcription activator (OmpR) for the upstream sequences of ompF in Escherichia coli are altered by envZ mutations and medium osmolarity. J Bacteriol. 1989;

195. Hernández-Allés S, Conejo MD, Pascual A, Tomás JM, Benedí VJ, Martínez-Martínez L. Relationship between outer membrane alterations and susceptibility to antimicrobial agents in isogenic strains of Klebsiella pneumoniae. J Antimicrob Chemother. 2000;

196. Adler M, Anjum M, Andersson DI, Sandegren L. Combinations of mutations in envZ, ftsI, mrdA, acrB and acrR can cause high-level carbapenem resistance in Escherichia coli. J Antimicrob Chemother. 2016;71(5):1188–98.

197. Foo YH, Gao Y, Zhang H, Kenney LJ. Cytoplasmic sensing by the inner membrane

histidine kinase EnvZ. Progress in Biophysics and Molecular Biology. 2015.

198. Ghosh M, Wang LC, Ramesh R, Morgan LK, Kenney LJ, Anand GS. Lipid-Mediated Regulation of Embedded Receptor Kinases via Parallel Allosteric Relays. Biophys J. 2017;

199. Goulian M. Two-component signaling circuit structure and properties. Current Opinion in Microbiology. 2010.

200. Jung K, Fried L, Behr S, Heermann R. Histidine kinases and response regulators in networks. Curr Opin Microbiol [Internet]. Elsevier Ltd; 2012;15(2):118–24. Available from: http://dx.doi.org/10.1016/j.mib.2011.11.009

201. Misra R. Modulators of The Bacterial Two-component Systems Involved in Envelope Stress, Transport, and Virulence. Stress and Environmental Regulation of Gene Expression and Adaptation in Bacteria. 2016. p. 1055–64.

202. Hessa T, Meindl-Beinker NM, Bernsel A, Kim H, Sato Y, Lerch-Bader M, et al. Molecular code for transmembrane-helix recognition by the Sec61 translocon. Nature. 2007;

203. Wright GA, Crowder RL, Draheim RR, Manson MD. Mutational analysis of the transmembrane helix 2-HAMP domain connection in the Escherichia coli aspartate chemoreceptor Tar. J Bacteriol. 2011;

204. Bass RB, Butler SL, Chervitz SA, Gloor SL, Falke JJ. Use of Site-Directed Cysteine and Disulfide Chemistry to Probe Protein Structure and Dynamics: Applications to Soluble and Transmembrane Receptors of Bacterial Chemotaxis. Methods in Enzymology. 2007.

205. Gushchin I, Melnikov I, Polovinkin V, Ishchenko A, Yuzhakova A, Buslaev P, et al. Mechanism of transmembrane signaling by sensor histidine kinases. Science (80-). 2017;

206. Unnerståle S, Mäler L, Draheim RR. Structural characterization of AS1-membrane interactions from a subset of HAMP domains. Biochim Biophys Acta - Biomembr. 2011;

207. Gushchin I, Gordeliy V. Transmembrane Signal Transduction in Two-Component Systems: Piston, Scissoring, or Helical Rotation? BioEssays. 2018.

208. Falke JJ, Hazelbauer GL. Transmembrane signaling in bacterial chemoreceptors. Trends in Biochemical Sciences. 2001.

209. Parkinson JS, Hazelbauer GL, Falke JJ. Signaling and sensory adaptation in Escherichia coli chemoreceptors: 2015 update. Trends in Microbiology. 2015.

210. Hwang E, Cheong H-K, Kim S-Y, Kwon O, Blain KY, Choe S, et al. Crystal structure of the EnvZ periplasmic domain with CHAPS. FEBS Lett [Internet]. 2017;591(10):1419–28. Available from: http://doi.wiley.com/10.1002/1873-3468.12658

211. Upadhyay AA, Fleetwood AD, Adebali O, Finn RD, Zhulin IB. Cache Domains That are Homologous to, but Different from PAS Domains Comprise the Largest Superfamily of Extracellular Sensors in Prokaryotes. PLoS Comput Biol. 2016;12(4):1–21.

212. Mise T. Structural Analysis of the Ligand-Binding Domain of the Aspartate Receptor Tar from Escherichia coli. Biochemistry. 2016;55(26):3708–13.

213. Bi S, Pollard AM, Yang Y, Jin F, Sourjik V. Engineering Hybrid Chemotaxis Receptors in Bacteria. ACS Synth Biol. 2016;5(9):989–1001.

214. Lehning CE, Heidelberger JB, Reinhard J, Nørholm MHH, Draheim RR. A Modular High-Throughput in Vivo Screening Platform Based on Chimeric Bacterial Receptors. ACS Synth Biol. 2017;6(7):1315–26.

215. Groisman EA. The Pleiotropic Two-Component Regulatory System PhoP-PhoQ MINIREVIEW The Pleiotropic Two-Component Regulatory System PhoP-PhoQ. J Bacteriol. 2001;183(6):1835–42.

216. Fass E, Groisman EA. Control of Salmonella pathogenicity island-2 gene expression. Curr Opin Microbiol. 2009;12(2):199–204.

217. Gunn JS, Miller SI. PhoP-PhoQ activates transcription of pmrAB, encoding a two-component regulatory system involved in Salmonella typhimurium antimicrobial peptide resistance. J Bacteriol. 1996;178(23):6857–64.

218. McPhee JB, Bains M, Winsor G, Lewenza S, Kwasnicka A, Brazas MD, et al. Contribution of the PhoP-PhoQ and PmrA-PmrB two-component regulatory systems to Mg2+-induced gene regulation in Pseudomonas aeruginosa. J Bacteriol. 2006;188(11):3995–4006.

219. Kim CC, Falkow S. Delineation of Upstream Signaling Events in the Salmonella Pathogenicity Island 2 Transcriptional Activation Pathway Delineation of Upstream Signaling Events in the Salmonella Pathogenicity Island 2 Transcriptional Activation Pathway. J Bacteriol [Internet]. 2004;186(14):4694–704. Available from: http://www.ncbi.nlm.nih.gov/entrez/query.fcgi?cmd=Retrieve&db=PubMed&dopt=Citation&list_uids=15231802

220. Yadavalli SS, Carey JN, Leibman RS, Chen AI, Stern AM, Roggiani M, et al. Antimicrobial peptides trigger a division block in Escherichia coli through stimulation of a signalling system. Nat Commun [Internet]. Nature Publishing Group; 2016;7:1–10. Available from: http://dx.doi.org/10.1038/ncomms12340

221. Gill DR, Pringle IA, Hyde SC. Progress and Prospects: The design and production of plasmid vectors. Gene Ther. 2009;16(2):165–71.

222. Silva-Rocha R, Martínez-García E, Calles B, Chavarría M, Arce-Rodríguez A, De Las Heras A, et al. The Standard European Vector Architecture (SEVA): A coherent platform for the analysis and deployment of complex prokaryotic phenotypes.

Nucleic Acids Res. 2013;41(D1):666–75.

223. Martínez-Garćía E, Aparicio T, Goñi-Moreno A, Fraile S, De Lorenzo V. SEVA 2.0: An update of the Standard European Vector Architecture for de-/re-construction of bacterial functionalities. Nucleic Acids Res. 2015;43(D1):D1183–9.

224. Balzer S, Kucharova V, Megerle J, Lale R, Brautaset T, Valla S. A comparative analysis of the properties of regulated promoter systems commonly used for recombinant gene expression in Escherichia coli. Microb Cell Fact. 2013;

225. Danino T, Prindle A, Kwong GA, Skalak M, Li H, Allen K, et al. Programmable probiotics for detection of cancer in urine. Sci Transl Med. 2015;

226. Piñero-Lambea C, Bodelón G, Fernández-Periáñez R, Cuesta AM, Álvarez-Vallina L, Fernández LÁ. Programming controlled adhesion of E. coli to target surfaces, cells, and tumors with synthetic adhesins. ACS Synth Biol. 2015;

227. Ganesh I, Ravikumar S, Yoo IK, Hong SH. Construction of malate-sensing Escherichia coli by introduction of a novel chimeric two-component system. Bioprocess Biosyst Eng. 2015;38(4):797–804.

228. Ganesh I, Ravikumar S, Lee SH, Park SJ, Hong SH. Engineered fumarate sensing Escherichia coli based on novel chimeric two-component system. J Biotechnol [Internet]. Elsevier B.V.; 2013;168(4):560–6. Available from: http://dx.doi.org/10.1016/j.jbiotec.2013.09.003

229. Selvamani V, Ganesh I, Maruthamuthu M kannan, Eom GT, Hong SH. Engineering chimeric two-component system into Escherichia coli from Paracoccus denitrificans to sense methanol. Biotechnol Bioprocess Eng. 2017;22(3):225–30.

230. Ravikumar S, Ganesh I, Maruthamuthu MK, Hong SH. Engineering Escherichia coli to sense acidic amino acids by introduction of a chimeric two-component system. Korean J Chem Eng. 2015;32(10):2073–7.